Universitat Autònoma de Barcelona

Immunotherapy against HER2-positive breast cancers

Rocío Vicario

Universidad Autónoma de Barcelona

Immunotherapy against HER2-positive breast cancers

PhD Thesis

Rocío Vicario

Barcelona, 2016

Title: Immunotherapy against HER2-positive breast cancers

PhD Thesis

Rocío Vicario

Dr. Joaquin Arribas Lopez — Director

Rocío Vicario — PhD Student

PhD program in Biochemistry, Molecular Biology and Biomedicine

Department of Biochemistry and Molecular Biology

Universidad Autónoma de Barcelona (UAB)

Barcelona, 2016

A mamá y papá, Sole, Maru y Bauti

Octa, Lean

A mis abuelos, al abuelo

A toda mi familia marplatense

A mis amigos/familia de BCN

A los de la facu (G-M)

A mis amigas de toda la vida (A, L, M, C, V, M)

A mi compañero de equipo favorito, Yasir

Table of contents

Summary: Twenty percent of breast tumors are characterized by the overexpression of the receptor tyrosine kinase HER2, due to amplification of the gene, either within the chromosome (HSR) or outside as extrachromosomal entities (DM). Little is known about the clinical outcome or role in therapy resistance associated with these patterns of amplification. Furthermore, a proportion of HER2+ patients also express carboxyl terminal fragments of HER2, p95HER2. More than half of the patients do not respond to the current available anti-HER2 therapies. It is not yet known whether p95HER2 can be a therapeutic target. Therefore this dissertation is focused on the study of resistance to HER2-therapies and the development of new therapies for the treatment of p95HER2/HER2+ tumors.

In this work we address whether the pattern of HER2 amplification impacts therapeutic response. We show that ~30% of HER2-positive tumors show amplification in DMs but respond equally to trastuzumab as HSR tumors. The number of DMs containing HER2 is maintained upon therapy resistance, even when the acquisition of resistance is concomitant with loss of HER2 protein expression. Thus, loss of DMs containing HER2 is not a likely mechanism of resistance to anti-HER2 therapies.

In this thesis we also evaluate p95HER2 as a target for immune therapy for p95HER2/HER2+ patients. We present a T cell bispecific antibody (p95-TCB) that binds p95HER2 and CD3e, a subunit of the T cell receptor (TCR) present on T lymphocytes. Simultaneous binding of p95-TCB to tumor and T cells leads to T-cell activation, secretion of cytotoxic granules, and tumor cell lysis. In pre-clinical models we showed that p95-TCB increases immune cell infiltration and promotes tumor regression. Compared to classical HER2-TCB, p95-TCB has the potential advantage of sparing normal tissues with low HER2 expression from undesired killing.

In summary, this work rules out the role of DMs as clinical predictors to anti-HER2 therapy, and describes a novel bispecific antibody that recruits immune cells to p95HER2/HER2+ tumors and consequently counteracts tumor growth.

Resumen: El 20% de los tumores mamarios sobre expresan el receptor de tirosina quinasa HER2, debido a su amplificación génica, tanto dentro de los cromosomas (HSR) como fuera ellos (DM). Se sabe muy poco acerca de la respuesta clínica o el rol en resistencia a terapias de estos patrones de amplificación. Por otro lado, un porcentaje de pacientes HER2+ expresa fragmentos carboxyl-terminales de HER2, p95HER2. Mas de la mitad de pacientes HER2+ no responde a las terapias disponibles. Hasta el momento, se desconoce si p95HER2 puede ser un blanco terapéutico. En este trabajo estudiaremos resistencias a terapias anti-HER2 y desarrollaremos nuevas terapias para el tratamiento de tumores p95HER2/HER2+.

En esta tesis, evaluamos si el patrón de amplificación tiene impacto en la respuesta terapéutica. Mostramos que el ~30% de los tumores HER2+ tienen amplificación en DM pero responden a la terapia de la misma manera que los HSR. El número de DM se mantiene cuando se desarrolla resistencia a la terapia, incluso si se pierde expresión proteica de HER2. Por lo tanto, la perdida de DM no parece ser un mecanismo de resistencia a terapias anti-HER2.

Por otro lado, también evaluamos si p95HER2 puede ser un blanco para inmunoterapia. Presentamos un anticuerpo bi-especifico de células T (p95-TCB) que se une a p95HER2 en la célula tumoral y a CD3e, miembro del receptor de células T, presente en linfocitos T. La unión simultanea a la célula tumoral y a la célula T induce la activación de la célula T, la secreción de gránulos citotóxicos y la lisis de la célula tumoral. En modelos pre-clínicos, mostramos que p95-TCB aumenta la infiltración de células T y promueve la regresión tumoral. Comparado con HER2-TCB, p95-TCB tiene la ventaja de discriminar las células normales con baja expresión de HER2 previniendo efectos colaterales.

En resumen, este trabajo descarta a los DMs como predictores de respuesta a terapias anti-HER2, y describe un nuevo anticuerpo bi-especifico que recluta y active células inmunes a los tumores p95HER2/HER2+ y como consecuencia la regresión de los mismos.

Abbreviations

ADCC antibody dependent cell cytotoxicity

APC antigen-presenting cells such **DC** dendritic cells

CD45,3 , 4, 8 cluster of differentiation

CTF c-terminal fragment

CTLA-4 Cytotoxic T-Lymphocyte Associated Protein 4

DISH dual-in-situ hybridization

DM double minutes

Dox Doxycycline

EGF Epidermal growth factor

EGFR Epidermal growth factor receptor

ER estrogen receptor

ERK1,2 extracellular signal-regulated kinase 1,2

Fab antigen binding fragment

FACS Fluorescence-activated cell sorting

FcR Fc receptor

FDA Food and Drug Administration

FFPE Formalin-Fixed Paraffin-Embedded

GVHD Graft vs Host Disease

GZMB Granzyme B

HER/ErbB 1-4 Human epidermal growth factor receptor/avian erythroblastosis oncogene B 1-4

HGF Hepatocyte Growth Factor

HSC Human Hematopoietic Stem Cells

HSR Homogeneously staining regions

IFN interferon

IGF-1 Insulin-like growth factor-1

IgG Immunoglobulin G

IHC immunohistochemistry

IL-2 Interleukin 2

INPP4B inositol polyphosphate-4-phosphatase

LPBCs Lymphocyte-Predominant Breast-Cancer

MAPK Mitogen-activated protein kinase

MDSC myeloid derived suppressor cells

MEK1,2 Mitogen/Extracellular signal-regulated Kinase

MHC major histocompatibility complex

Myc avian myelocytomatosis viral oncogene cellular homolog

NK natural killer

NSCLC Non-Small Cell Lung Cancer

PBMC Peripheral Blood Mononuclear Cells

pCR pathological complete response

PCR polymerase chain reaction

PD-1 Programmed cell death protein 1

PD-L1 Programmed cell death protein 1ligand

PDX Patient-Derived Xenografts

PI3K phosphatidylinositide 3-kinases

PI3K Phosphatidylinositol 3-kinase

PR progesterone receptor

PTEN phosphatase and tensin homolog

RAF Rapidly accelerated fibrosarcoma

RTK receptor tyrosine kinase

shRNA short hairpin RNA

TCR T cell Receptor

TIL Tumor-Infiltrating Lymphocyte

TNBC Triple Negative Breast Cancer

UCB Umbilical Cord Blood

Introduction

1. Breast Cancer: heterogeneous disease with different cell components

1.1 Breast cancer subtypes

Breast cancer is the second most common cancer in the world and the most frequent cancer among woman. It is also the fifth cause of death from cancer overall, with 450,000 deaths attributed to this disease per year world-wide (Globacan). The most important risk factors include genetic predisposition, exposure to estrogens and obesity among others [1]. The fundamental discoveries of hormone receptors and growth factor receptors in breast cancer have shaped oncology and the current understanding of how cancers rely on growth-promoting systems, which has proven critical for targeted therapy development and clinical-decisions for patient treatment. However, breast cancer is a heterogeneous disease with a wide range of different outcomes [2] [3, 4].

With the use of immunohistochemistry (IHC) and more recently genetic characterization based on mRNA, copy number alterations and somatic mutations, breast cancer can be subdivided into four major distinct pathological tumor types (Fig. 1) [3]. Two of them, are hormone receptor positive groups, which expresses the estrogen receptor (ER) and/or progesterone receptor (PR). They are referred as luminal-like due to the high expression of genes expressed by breast luminal cells and can be sub-classified in luminal-A and luminal-B based on proliferation rate as measured by the percentage of Ki67, being higher in the luminal-B subtype [5]. The two hormone receptor negative tumor types are characterized by expression of genes related to basal cells and they include: human epidermal growth factor receptor 2 (HER2 or ERBB2)-positive group, which overexpresses HER2 detected by IHC or fluorescence in-situ hybridization (FISH); and the Triple Negative Breast Cancer (TNBC) group, which is negative for ER, PR, and HER2 and has positive staining with basal keratins. Different therapeutic alternatives exist for each breast cancer subtype. Luminal-like tumors receive endocrine therapy, accompanied by chemotherapy in the case of the Luminal-B type. HER2+ patients receive chemotherapy in combination with anti-HER2 therapy

(commented below in section 3) and, for the triple negative population; chemotherapy is the main alternative [1].

A correlation between the molecular subtype and clinical prognosis reveals that TNBCs and HER2+ tumors have worse prognosis compared with the luminal-like tumors [6] [7].

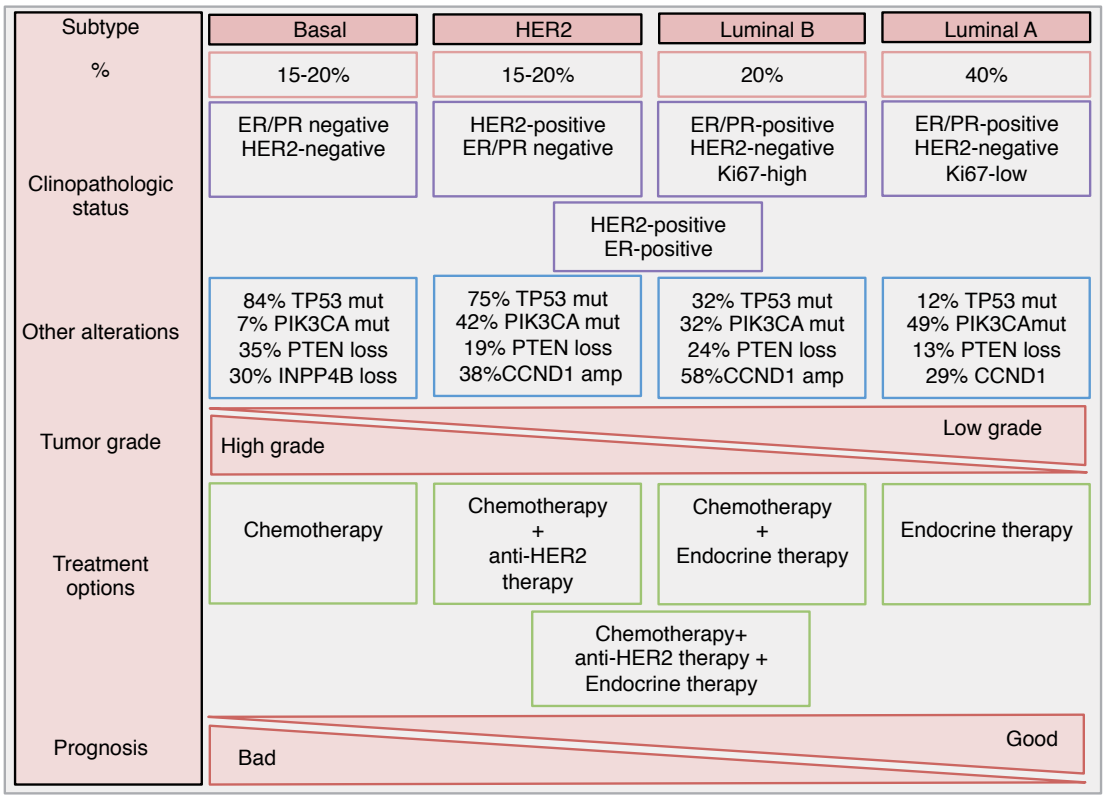

Figure 1: Breast Cancer Subtypes and their distinctive features. ER: estrogen receptor; PR: progesterone receptor.

More recent comprehensive studies on the molecular characteristics of breast cancers revealed a wide diversity in the array of genomic alterations in the different subtypes (Fig. 1) [4]. In general terms, TNBCs and HER2 have a higher mutational load compared to luminal tumors (Fig. 2) [4, 8, 9]. Between 70 and 80% of these two types of cancer carry mutations in TP53 gene that codifies for p53 protein, and point mutations and amplifications in members of the

phosphatidylinositol 3-kinase (PI(3)K) pathway, such as PI3K itself, PTEN and INPP4B. In addition, TNBC are enriched in patients with BRCA1 mutations, a protein involved in DNA repair and associated with hereditary breast cancers [4]. As expected, HER2+ subtype is genetically characterized by focal amplification of 17q12, which carries ERBB2 gene. This large study on 500 tumors reveled that within the HER2 enriched, two different subtypes could be distinguish: the so called HER2E, where they detected a significantly higher expression of other Receptor Tyrosine Kinases [10], other genes located in the HER2 amplicon and mutations in TP53. On the other hand, luminal-HER2 subtype showed a higher expression of luminal type of genes and less frequency of TP53 mutations [4]. This confirms that even within a subtype there is a great level of heterogeneity. Nevertheless, it is important to note that when measuring the number of mutations per mega base, compared with other types of cancers, such as melanoma, Non-Small Cell Line Carcinoma (NSCLC) and gastric cancer, breast cancer displays less alterations and is therefore not considered a hypermutated disease [9].

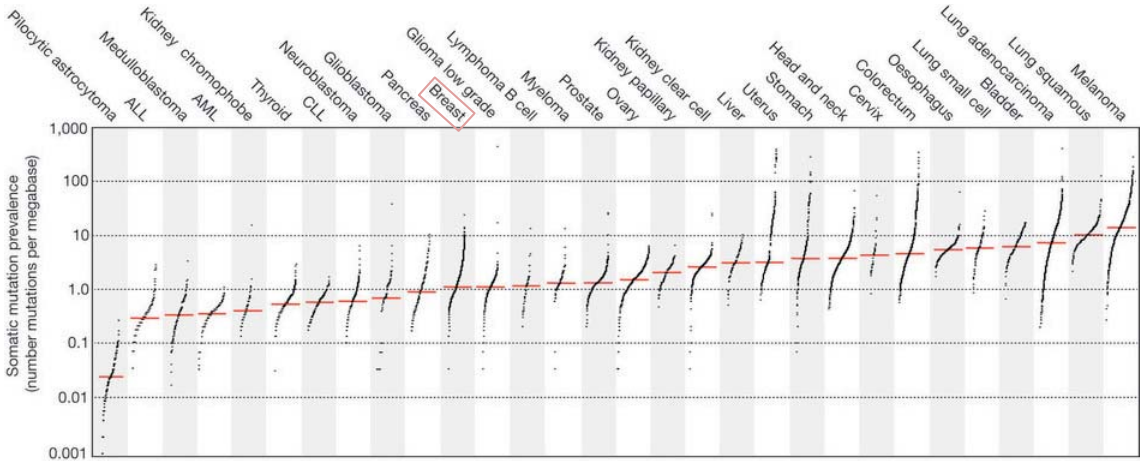

Figure 2: Somatic mutation prevalence in different cancers. Every dot represents a sample and the red line the median number of mutations per mega base. (From Alexandrov, 2013 #1422).

In summary, breast cancer tumors vary in their expression profiles and sensitivities to therapies. It is becoming clear that while certain primary features distinguish tumor subtypes, several layers of tumor biology exist that may ultimately impact

clinical outcomes. Furthermore, tumor biology also consists of numerous cell-types all of which are now appreciated as directly contributing to cancer cell growth and survival.

This work will focus on HER2+ tumors that account for approximately 20% of all breast tumors [11].

1.2 Breast cancer and the immune system

1.2.1 Immune infiltration and breast cancer prognosis

Cancer is not a cell-autonomous disease, but instead is intimately connected to the tumor microenvironment, which contributes to the evolution and progression of the disease. One main component of tumor microenvironment together with endothelial cells and fibroblasts is the immune cell-infiltrate. For breast cancer, there is a compelling amount of evidence showing that the immune system plays a crucial role not only in the evolution but also in the treatment of this disease [12]. In fact, there are a number of efforts put towards further understanding whether this impacts the classification of breast tumors, by not only evaluating the molecular profile of the neoplastic cells but also of the stromal tissue surrounding the tumor. For instance, Staaf and colleagues divided HER2+ patients into three clusters, one of which is characterized at the molecular level by high expression of immune related genes [13]. The immune compartment of the breast tumor microenvironment contains both myeloid and lymphoid cells, which includes the Tumor-Infiltrating Lymphocytes [14]. When evaluated by IHC staining, TILs are observed in the stromal compartment, adjacent to the tumor tissue, and/or in the intratumoral compartment, in direct contact with the malignant cells [15]. However, the fibrotic stroma surrounding the tumor is considered as part of the tumor, therefore the stromal TILs are evaluated as part of the whole tumoral immune infiltrate [15]. Usually, stromal TILs are observed in higher numbers compared to intratumoral TILs, and are a more reliable predictive biomarker.

The percentage of TILs in the different subtypes of breast cancer vary in frequency, with TNBC having the higher infiltration, 20-25% of immune infiltrate,

HER2+ approximately 15% and Luminal A and B 10% [12].

Not only are TILs a defining feature of breast cancers, but also they are associated with clinical outcomes. In TNBCs, higher levels of TILs at diagnosis are associated with decreased distant recurrence, and in early HER2+ breast cancer, higher percentage of TILs is associated with increased therapy benefit [16]. In the neo-adjuvant setting, TILs are predictors of an increase in pathological complete response (pCR) in both TNBC and HER2+ tumors [17, 18]. Interestingly, it has been reported that the presence of more than 50-60% of TILs in the tumor stroma (tumors termed Lymphocyte-Predominant Breast-Cancer, LPBCs) is predictive of higher pCRs compared to lower infiltrated tumors, independently of whether the tumors are classified at the molecular level as HER2 or TNBC [17] [18]. Therefore the characteristics of the immune cells within breast tumors have a strong impact in the progression of the disease.

1.2.2. The anti-cancer immune response

Lymphocytic infiltration of tumors occurs because cancer cells are recognized by the immune system as “non-self” due to antigen presentation, via the major histocompatibility complex (MHC) class I, of antigens that can arise from mutated proteins (neo-antigens, antigens that are absent in the normal human genome) or non-mutated proteins with aberrant expression [19] [20].

The burden of mutational load in a tumor has can particularly have an effect on the immune infiltration. In principle, tumors with higher mutational loads have higher probabilities of generating neo-antigens that can lead to higher immune recognition [20]. However, as mentioned previously, while some breast subtypes have more mutational loads than others, breast cancers in general do not contain high mutational loads as compared to other cancers (Fig. 2) [9].

The immune response against tumors involves many components of the immune system, from which T cells are probably the most potent mediators [21] (Fig. 3). The anti-tumor immune response mediated by T cells involves a series of steps illustrated in Figure 3. At the tumor site, antigen-presenting cells (APC) such as

dendritic cells (DC) take up tumor antigens and present them on MHC class II and I to T cells, resulting in T-cell activation and proliferation. T effector cells then migrate to the tumor site through the circulating system, assisted by the secretion of chemokines that orchestrate trafficking of the immune cells. Once in the tumor, CD8+ cells recognize cancer cells through an interaction between the T cell Receptor (TCR) and the antigen bound MHC I presented by the tumor cell. The TCR complex is formed by the $\alpha\beta$ heterodimers that are responsible for the antigen recognition, and the CD3 molecules involved in the intracellular signaling. The $\alpha\beta$ chains are formed by gene rearrangements and differ between individuals. The CD3 chains, ε,ζ,δ and γ are non-polymorphic and contain the intracellular activation motifs that will trigger signaling activation (Fig. 4). The interaction between the antigen and the T cell leads to T cell activation and killing of tumor cells by the release of lytic components such as Granzyme B that cause disruption of the cell membrane and activation of the apoptotic pathway. Activated T cells commonly express CD69, and early activation marker and CD25, a late activation marker.

CD4+ T cells only recognize antigens presented by the MHC class II. Therefore they don't recognize antigens presented directly by the tumor cells. However, they cooperate in the activation and proliferation of CD8+ positive cells through the secretion of a vast number of activating cytokines, including IL-2 and IFNgamma [22].

The priming of T cells may occur in lymph nodes as well as within the tumor stroma in organized tertiary lymphoid structures [23]. The killing of the cancer cells promotes the release of more antigens that ultimately potentiate the immune response [19].

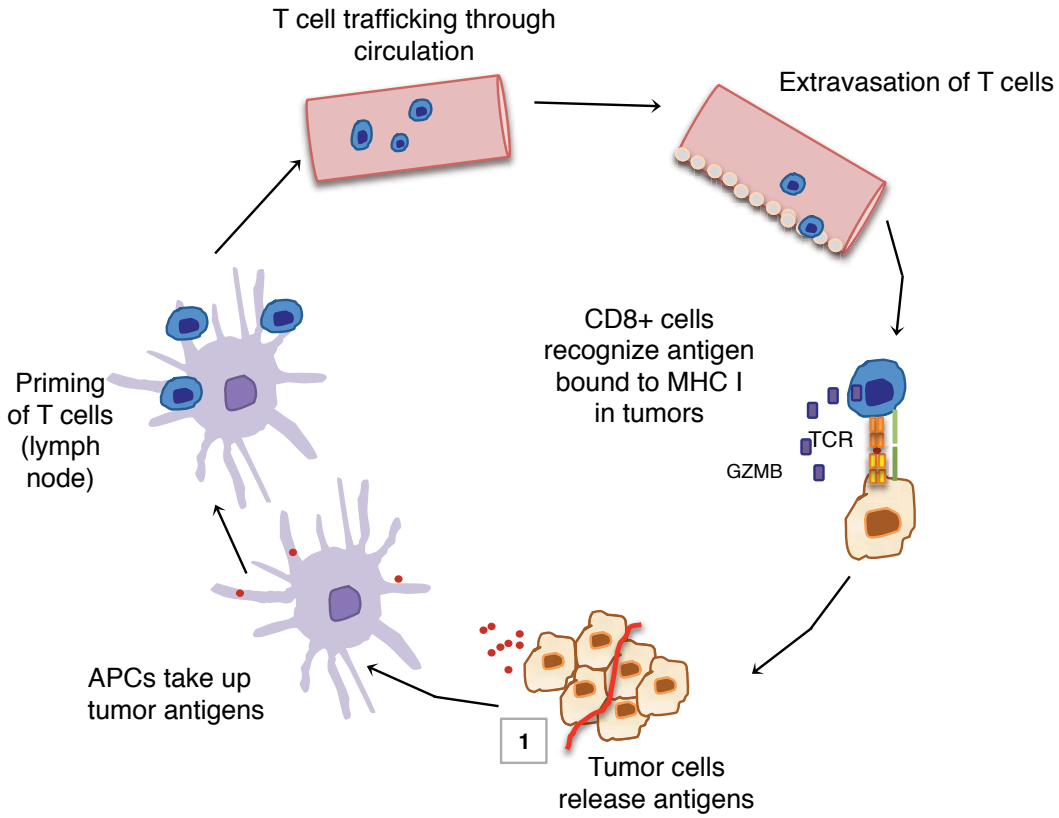

Figure 3: T cells are the main mediators of the anti-cancer immune response. Tumors release tumor antigens that are captured by APC and presented by MHC class I and II to T cells. T effector cells migrate through the blood vessels to the tumor site where the recognition of TCR and the specific tumor antigen presented by MHC class I takes place, triggering the cytotoxic effect of the T cell to release Granzyme B to lysate the tumor cell. APC: Antigen Presenting Cell; GZMB: Granzyme B; TCR: T cell receptor (Adapted from [19]).

Antigen presenting cells and T cells not only interact through the TCR and MHC, but also between receptors and ligands present in both. For instance, CD28 binds to CD80 and CD86 on the APC propagating the co-stimulatory signal and enhancing the secretion of cytokines such as IL-2 increasing T cell activation (Fig. 4). Ultimately, the amplitude of the T cell response against the tumor cell and the type of immune response mounted is the result of a balance between co-stimulatory signals and inhibitory signals [22].

However, T cells encounter numerous suppressive mechanisms along this process, which limit their ability illicit an anti-tumor immune response [24]. For

instance, the presentation of antigens by the DCs in a toleraizing manner; stimulation of regulatory T cells and myeloid derived suppressor cells (MDSC) that oppose antitumor response; post-translational modifications in attractant chemokines important for the trafficking of the T cells to the tumor site among others [23, 24]. A now druggable immune suppressive mechanism also exists, which targets the activation of immune checkpoints such as PD-1/PDL1 and CTLA-4 (Fig. 4). In normal cells, these pathways are crucial for maintaining self-tolerance and modulating the duration and amplitude of physiological immune responses but in the tumor microenvironment they act as immune response suppressors.

CTLA-4 is an inhibitory receptor present mainly in activated CD8+ and CD4+ cells [25]. It functions through counteracting the effects of the co-stimulatory receptor CD28, also expressed on T cells. CTLA-4 binds with higher affinity to CD80 and CD86, present on APCs, down modulating the amplitude of T cell activation [25]. Ipilimumab, an antibody against CTLA-4 has already been approved by the FDA for the treatment of melanoma.

PD1, another immune checkpoint receptor, is induced when T cells become activated. When it binds to its ligands, PD1 inhibits intracellular kinases that are involved in T cell activation. PD1 ligands, PDL1 and PDL2 are upregulated on the tumor cell surface, and PDL1 is the most common ligand in solid tumors. Blocking antibodies for the PD-1/PD-L1 axis have been already approved for the treatment of several cancers, including NSCLC, melanoma and bladder cancer.

Importantly, many non-mutated overexpressed proteins that tumors express are also expressed by healthy tissues; therefore the immune system may have developed tolerance to them, meaning that it has been educated to recognize them as “normal” [23].

Finally not all tumor-produced antigens will generate a T cell response. Therefore, identifying ways to aid the anti-tumor immune response preventing the immune suppression may ultimately improve the progression of this disease.

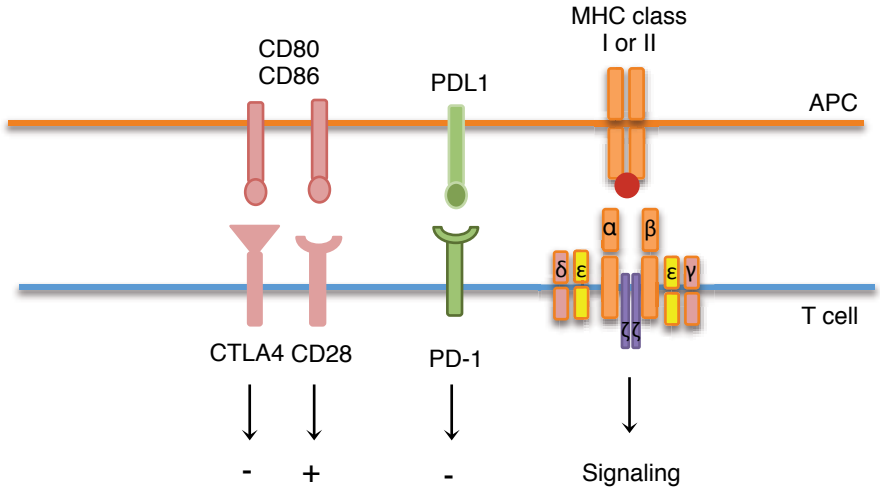

Figure 4: A balance between co-stimulatory and inhibitory signals determines the amplitude of the T cell response. The TCR complex is formed by the αβ heterodimers responsible for the antigen recognition, and the chains, ε,ζ,δ and γ that contain the intracellular activation motifs that will trigger signaling activation. CD28 binds to CD80 and CD86 propagating the co-stimulatory signal. CTLA-4 counteracts these effects by binding with higher affinity to CD80 and CD86. When PD1 binds to its ligands, PDL1 or PDL2, it inhibits intracellular kinases that are involved in T cell activation. APC: Antigen Presenting Cell; MHC: major histocompatibility complex.

2 HER2 positive breast cancers

2.1 HER2 a member of the Receptor Tyrosine Kinase Family

HER2 belongs to the receptor tyrosine kinase (RTKs) family type 1, together with EGFR (HER1), HER3 and HER4. Each receptor is composed of three main sections an extracellular domain, the transmembrane domain and the intracellular domain (Fig. 5). The extracellular domain is formed by domains I and III which are rigid β-helix/solenoid structures related to one another and serve as the primary ligand binding regions. Domains II and IV are cysteine-rich domains that contain a string of disulfide-bonded modules. The transmembrane domain links the extracellular region to the intracellular one that contains the tyrosine kinase domain [26].

The formation of dimers is essential for the activation of these transmembrane receptors. Dimerization can occur between different members of the family, heterodimers, or between the same members, homodimers. What triggers the

dimerization process is the binding of ERBB ligands to the domain I and III of the receptors, giving rise to a conformational change that opens the dimerization arm, in domain II. Inter-receptor domain IV contacts may also contribute to the dimerization process. In the absence of ligand, the dimerization arm from domain II forms auto-inhibitory interactions with domain IV and the extracellular region adopts the so-called “close” conformation. HER2 in particular does not have any known ligand and it exists in an open conformation, “ready” to dimerize with other members of the family [26, 27]. All the ligands have in common an EGF-like domain. Among the known ligands EGF, Amphiregulin (AR), Epigen/Epithelial Mitogen (EPGN) and the Transforming Growth Factor-α (TGF-α) specifically bind to HER1; Betacellulin (BTC), Heparin-Binding EGF (HB-EGF) and Epiregulin (EPR) bind to both HER1 and HER4; Neuregulins 1 and 2 bind to HER3 and HER4 and Neuregulins 3 and 4 bind to HER4 [26]. In general, HER ligands act over short distances as autocrine or paracrine growth factors [28].

The formation of dimers results in the phosphorylation of tyrosine residues in the C-terminal tail segments, which serve as docking sites adaptor proteins that trigger the activation of downstream signaling pathways, in particular the PI3K and Mitogen-Activated Protein Kinase (MAPK) pathway. The effect of HER signaling on the MAPK pathway involves the transcription of genes that drive cell proliferation and also migration and angiogenesis. On the other hand, the PI3K, via the activation of the serine-threonine kinase AKT, drives the expression of proteins involved survival and anti-apoptosis. HER1, HER2, and HER4 contain a competent kinase activity and can form heterodimer pairs with each other. HER3 contains an inactive kinase domain and its activity depends on forming heterodimers with other RTKs [28]. In fact, the heterodimer HER2-HER3 is thought to be the most transforming and mitogenic; the cytoplasmic tail of HER3 strongly activates the PI3K/AKT pathway, whereas HER2 powerfully signals through the ERK MAPK pathway, making it a very potent pair [28].

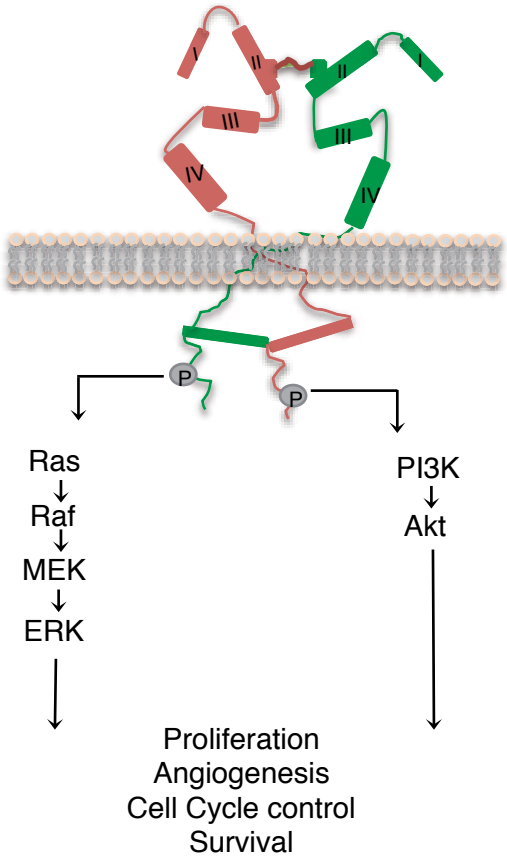

Figure 5: Schematic representation of a typical HER dimer. Ligand binding to domain I and III, triggers a conformational change that opens the dimerization arm in domain II triggering the formation of dimmers. Dimerization results in the trans phosphorylation of the C-terminal segments that triggers the activation of downstream signaling pathways leading to the modulation of several key cellular processes.

Due to the involvement of this receptor in pro-survival pathways, the aberrant overexpression of HER2, which results in constitutive receptor activation via the formation of dimers, is implicated in the development and progression of not only breast cancer but also gastric, lung, and ovarian cancer among others [29].

Additionally the activation of RTKs has not only been attributed to overexpression of the protein. Point activating mutations have been described for HER2 and HER3 [4] [30].

2.2 HER2 gene amplification

The increase in HER2 protein observed in breast cancers is the outcome of the amplification of a region located in chromosome 17 (17q12q21) that contains the ERBB2 gene. Gene amplification is likely initiated by DNA double-strand breaks and occurs only in cells endowed with the ability to progress through the cell cycle carrying damaged DNA. Although the mechanism(s) that lead to gene amplification remain(s) largely unknown, the final distribution of amplified DNA has been characterized in some detail (Fig. 6). Amplified DNA can form tandem arrays, as head-to-tail or head-to-head repeats, within a chromosome. These repetitions are cytologically visible as homogeneously staining regions (HSRs). Alternatively, amplified DNA can be stored in extra chromosomal entities called Double Minutes (DMs). These patterns of amplifications have been observed for MYCN (the gene that codifies for N-myc oncogene) in neuroblastomas, and for EGFR in gliomas, among others [31] [32]. How these two distinct patters arise is still under investigation. However many reports point to the episomal model in which the DNA segment is excised from an intact chromosome, circularized, and amplified by mutual recombination and then, in the case of HSR, integrated into the genome [32].

While HSR amplicons follow the same fate as the rest of chromosomal regions during mitosis, DMs do not contain centromeres, do not bind the mitotic spindle and, thus, are likely not distributed evenly between daughter cells. [31]. In line with this, previous reports have shown that MYCN DMs in neuroblastoma cell lines segregate randomly during mitosis and that there is proliferative advantage for the cells receiving more copies [33]

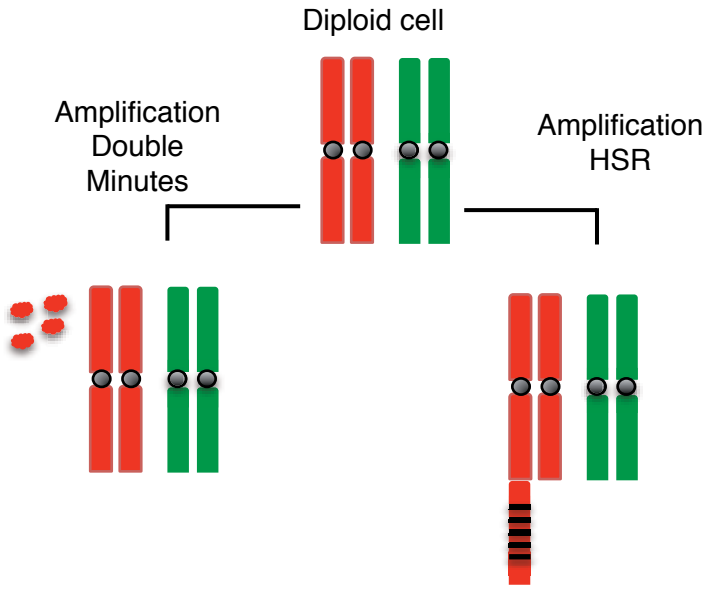

Figure 6: Schematic representation of the types of gene amplification. Amplified Overexpression of oncogenes, can result from gene amplification through the formation of extrachromosomal double minutes (DM) or intrachromosomal Homogeneously staining regions (HSR).

2.3 Carboxyl terminal fragments of HER2: p95HER2

A group of HER2 tumors express carboxyl terminal fragments of HER2. These truncated forms arise form by protease cleavage or by alternative initiation of translation of HER2 giving rise to forms located in the cytoplasm, or membrane-bound [34, 35]. Evidence published so far, show that the cytoplasmic fragments are inactive, while membrane-bound isoforms are active [36]. Shedding of the ectodomain of HER2, most likely carried out by the metalloprotease ADAM10 at a site proximal to the transmembrane domain, generates a 95- to 100-kDa p95HER2 membrane-anchored fragment (Fig. 7). Overexpression of this fragment promotes apoptosis in MCF7 cells (Bernadó Morales et al. unpublished). On the other hand alternative initiation of translation from two internal initiation codons located in the 611 and 678 position generates two p95HER2 fragments of 100 to 115 kDa and 90- to 95-kDa, also known as 611-C-terminal Fragment (611-CTF) (Fig. 7) (reviewed in (Arribas, 2011 #837). Part of this work will focus on the 611-CTF (from now on referred as p95HER2), a hyperactive form due to its ability to form

homodimers maintained by intermolecular disulfide bonds. Transgenic expression of this truncated form in the mouse mammary gland led to the development of aggressive tumors and a higher number of metastasis to the lung as compared to animals bearing tumors with full-length HER2 [36]. We have also reported that expression of high levels of p95HER2 leads to a fully penetrant senescence phenotype, characterized by a terminal cell proliferation arrest and a distinct secretory phenotype formed by pro-tumorigenic factors [37]. Further studies showed that the metalloproteinase ADAM17 contributes to the non-cell autonomous pro-tumorigenic effects of p95HER2-induced senescent cells [38].

Since part of the extracellular domain of HER2 is retained in p95HER2, a region that is masked in full-length HER2, several antibodies have been generated against p95HER2 (corresponding site in 611-CTF, but not 648-CTF) [39] [40]. The p95HER2 antibody generated in our laboratory recognizes the first 32 amino acids of the NH2 terminus of the isoform. We have used this tool to determine p95HER2 protein expression status in tumor specimens, finding that approximately 30% of HER2+ tumors express p95HER2 [39] [40]

Furthermore, according to to the levels of expression of 50 selected genes all the p95HER2/611CTF positive samples expressed high levels of HER2 mRNA and most of them (80.95%) belonged to the HER2- enriched subtype [41]. Therefore, expression of p95HER2 is most likely restricted to the tumoral tissue, compared to HER2 which expression is also found in other healthy tissues. Additionally, compared with tumors expressing only full-length HER2, p95HER2-positive tumors exhibit worse prognosis and a higher likelihood to metastasize [42, 43].

This distinct tumor marker, however, has so far not been evaluated as a therapeutic target.

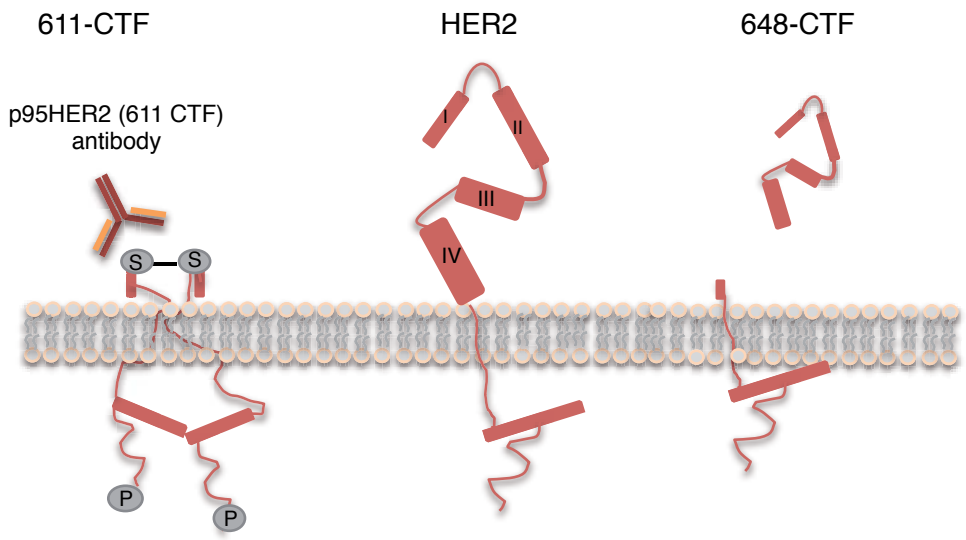

Figure 7: Carboxyl terminal fragments of HER2: alternative initiation of translation from methionine 611 gives rise to the 100-115 kDa fragment (611-CTF), a hyperactive form due to its ability to form dimers maintained by strong intermolecular disulfide bonds. Proteolytic cleavage in a site proximal to the transmembrane region gives rise to the 95-100-kDa isoform (648-CTF)

3. Therapies for HER2+ tumors and their mode of action

Accumulating evidence, over nearly 20 years from the approval of the first anti-HER2 drug (Trastuzumab; Herceptin) has proven that HER2 is a good therapeutic target. The prognosis of HER2+ patients has improved over the years thanks to the development of several successful anti-HER2 therapies. Currently, monoclonal antibodies and tyrosine kinase inhibitors are approved for the treatment of HER2+ breast cancers.

3.1 Monoclonal antibodies

The overexpression and availability of HER2 on the surface of cancer cells allows this receptor to be readily recognized by antibodies. Monoclonal antibodies targeting HER2 include trastuzumab; pertuzumab and chemotherapy conjugate forms such as trastuzumab-emtansine, T-DM1 (Fig .7).

Trastuzumab was the first monoclonal antibody developed and approved for

treatment of HER2+ breast cancers. It is a humanized IgG1 that binds the to an epitope on the domain IV of the HER2 receptor. The binding of trastuzumab to HER2 prevents the formation of ligand-independent HER2 dimers leading to a partial inhibition of downstream signaling that terminally promotes cell cycle arrest [29].

The first studies indicated that the clinical activity of trastuzumab was mostly due to the inhibition of intracellular signaling initiated by HER2, but accumulating evidence now show that the immune system activation contributes to the therapeutic effect of the antibody. Once trastuzumab binds to HER2 through the antigen binding fragment (Fab), it can be recognized by components of the innate immune system that contain Fc receptors, triggering antibody dependent cell cytotoxicity (ADCC) ((Arteaga, 2014 #11) [29]. The cells mediating this effect are most likely the macrophages and Natural Killer (NK) cells. In the seminal study describing the role of ADCC in trastuzumab efficacy it was shown that the effect of trastuzumab is diminished in mice deficient in the common γ chain (FcRγ–/–), lacking the activation Fcγ receptors FcγRI and FcγRIII [44]. In addition, it has been shown that polymorphisms in the FcR are associated with the clinical outcome of HER2+ breast cancer patients [45]. However, not only does the innate immune system appear to play a role in trastuzumab action, but studies also suggest that the adaptive immune system also contributes. Park and colleagues used a "mouse-trastuzumab" in immunocompetenet animals and showed that T lymphocytes also mediated response to Trastuzumab [46]. Furthermore, trastuzumab can induce the endocytosis of HER2, leading to its degradation and posterior peptide presentation via MHC class I to cytotoxic T cells. The role of the adaptive immune system in trastuzumab-based therapy is also supported by previously commented studies showing that there is an association between higher levels of TILs at diagnosis and increased trastuzumab based therapy benefit in HER2+ disease [16]. In this study the authors observed that each 10% increase in TILs was associated with 13% reduction in the relative risk of distant recurrence. In line with this finding, it has been suggested that a subset of HER+ patients with high TILs could benefit from trastuzumab alone, without the

combination of any cytotoxic agent, which is the standard of care [15]. Also, in a large early stage HER2+ clinical trial, mRNA analysis determined that the 4 out of the 6 more significant pathways associated with increase Relapse-Free Survival (RFS) following adjuvant trastuzumab were linked to the immune system [47].

To note, chemotherapy, which is included in the standard-of-care together with anti-HER2 therapy might also have a positive role in amplifying the immune response by inducing immunogenic cell death, a process in which tumor cells die in a way that they elicit the immune response against the tumor [12, 48].

TDM-1, trastuzumab-emtansine, is an antibody drug conjugate in which trastuzumab is covalently bonded with a microtubule polarization inhibitor, maytansinoid [49]. Apart from having equivalent effects as trastuzumab in terms of signaling inhibition and ADCC, when TDM-1 binds to HER2, both are internalized and degraded in the lysosome, releasing the DM1 and promoting the cell lysis [50, 51]. TDM-1 has been recently approved to treat advanced breast cancer.

Drug	Target/Mechanism	Approval
Trastuzumab	Binds domian IV. Inhibits ligand-independent dimmer of HER2, ADCC and adaptative immune response	HER2+ breast cancer, early and metastasic Standard of care
Pertuzumab	Binds domain II. Inhibits ligand-induced dimmers of HER2	HER2+ breast cancer, early and metastasic Standard of care
T-DM1	Binds domain IV. Same effects as trastuzumab plus microtubule inhibition followed by lysis	Metastasic breast cancer
Lapatinib	ATP competitive TKI	For patients that progressed to previous anti-HER2 therapy

Table 1: anti-HER2 therapies and mechanism of action

The more recently approved monoclonal antibody pertuzumab binds the heterodimerization domain II and inhibits ligand-induced HER2 containing dimers, including the potent HER2-HER3 heterodimers [52]. Since pertuzumab and trastuzumab bind different domains of HER2, they have proven to act in a synergic manner and are now the first line therapy together with chemotherapy for the treatment of HER2+ patients [53].

3.2 Tyrosine kinase Inhibitors

There are also inhibitors of the kinase activity of HER2. Lapatinib was the first small molecular inhibitor of HER2 to be approved by the Food and Drug Administration (FDA). It inhibits both HER2 and EGFR acting as an ATP competitor. [54]. The inhibition of the tyrosine kinase activity leads to the blocking of the PI3K/AKT and MAPK downstream signaling. Also, it has been reported that lapatinib stabilizes HER2 in the membrane, leading to an improved effect of trastuzumab through ADCC [55].

4 Anti-HER2 Therapy Resistance

Despite the remarkable effectiveness of anti-HER2 therapies, the response of patients to anti-HER2 therapies is very variable. Many tumors frequently become resistant to therapy and resume malignant progression [56]. Therefore, it is necessary to investigate resistance mechanisms to the therapies and identify biomarkers that can aid in identifying patients with probability of therapeutic response.

Therapy resistance can be intrinsic, meaning that the cancer does not respond to the therapy from the start of treatment, or can be acquired, referring to mechanisms of resistance that arise after the tumor responded to the treatment.

In terms ofSo far, most of the resistance mechanisms studied refer to trastuzumab, since it is the drug that has been in use for longer. However, many resistance mechanisms already described for this drug may also applied to T-DM1

and pertuzumab.

4.1 Alterations in signaling pathways downstream of HER2

Many resistance mechanisms are related to the capacity of trastuzumab to inhibit downstream signaling of HER2. As such, activating mutations in key members of the downstream signaling pathways can compensate the blockage of HER2 signaling by trastuzumab. For instance, overexpression of mutant PI3K has shown resistance to trastuzumab in pre-clinical studies [57]. Mutations in the PI3K gene (PIK3CA) or tumors that are null for PTEN, which antagonizes PI3K, have been associated with a poorer response to anti-HER2 therapy [58].

Increases in ligand levels for HER3 and EGFR, which lead to more HER2-dimer formation, have also been described as a mechanism of trastuzumab. In particular because it is thought that trastuzumab cannot block ligand induced HER2 heterodimers [59]. However, pertuzumab could compensate this effect. Lapatinib-induced HER2 inhibition can also cause a compensatory PI3K/AKT dependent upregulation of HER3 [60] leading to resistance.

Other RTKs, such as c-Met, appear to also be involved in trastuzumab and lapatinib resistance as well. c-Met is a cell surface receptor for the Hepatocyte Growth Factor (HGF) ligand, and its activation is sufficient to promote resistance through the activation of downstream signaling cascades, both in lapatinib and trastuzumab treatment [61]. Amplification of MET gene has been reported in a subset of non-trastuzumab responding patients [62]. Insulin-like growth factor-1 (IGF-1) receptor overexpression is also able to potently activate the PI3K/AKT pathway conferring resistance to trastuzumab [63]

Furthermore, alterations in the cell cycle progression in response to trastuzumab have been described to mediate resistance to therapy. Cells that became resistant upon chronic exposure to trastuzumab can aberrantly gain amplification in Cylcin E [64].

4.2 The role of the immune system in anti-HER2 therapy resistance

Resistance mechanisms associated with the effect of trastuzumab through the

immune system have been less studied, but are potentially just as relevant. For instance, Musolino and colleagues described that depending on what type of Fc polymorphism a patient carries, the response to anti-HER2 based therapy can be different [45]. Also, it has been reported that HER2+ tumors might be able to hide from the immune system by downregulating MHC class I expression [65]. This could lead to a poor recognition of cancer cells by cytotoxic lymphocytes and a poorer response to the anti-HER2 therapy. The downmodulation in MHC class I seem to be regulated at the transcriptional level [66]. Identifying the molecular mechanism governing transcriptional downregulation of MHC class I leading to immune escape response could help to restore this effect. Also, finding therapeutic options that are independent of MHC I presentation could be used as an alternative approach. Furthermore, HER2 is an antigen that is expressed in considerable levels in some tissues such as the cardiac tissue, and as such immune responses generated against this antigen can be restricted to lower-affinity interactions, which may lead to a poorer immune response as compared to that with neo-antigens, only expressed by tumors [20].

4.3 The type of HER2 amplification and its relation to anti-HER2 therapy resistance

Even though not described for HER2, the type of gene amplification (HSR or DMs, Fig. 6) may influence the effectiveness of HER-targeted therapies For example, many glioblastoma, the most common type of brain tumor, are characterized by the amplification in DMs of EGFR-vIII, a gene encoding a constitutively active form of EGFR [67]. Upon treatment with tyrosine kinase inhibitors, glioblastoma cells survive by losing DMs and, thus, down modulating the expression of EGFR-vIII [68]. Upon removal of the drug, resistant cells regain EGFR-vIII gene copies by re-accumulating DMs. Similar dynamic control of protein expression, through the elimination or accumulation of DMs, has been shown in different tumor models including cells with amplified Myc [69] or dihydrofolate reductase [70].

Preliminary results have shown that some patients with significant residual disease

after trastuzumab neoadjuvant therapy lose HER2 amplification and this was associated with poor RFS [71].

4.4 p95HER2-mediated resistance to anti-HER2 therapy

The presence of truncated forms of HER2, collectively known as p95HER2, has also been proposed as a mechanism of trastuzumab resistance. p95HER2 lacks the epitope to which trastuzumab binds, therefore it has been associated with resistance to trastuzumab as monotherapy (Fig. 7) [72]. More recently, our lab has reported that p95HER2 positive tumors are more sensitive to the combination of trastuzumab plus chemotherapy, via HER2 stabilization induced by chemotherapy in p95HER2/611CTF-positive cells [41].

5 Drug perspectives: new drugs and combinations

Due to the heterogeneity in response of HER2+ tumors and the above mentioned resistance mechanisms, new anti-HER2 drugs and new combination regimens are being studied both pre-clinically and in clinical trials. Furthermore, due to the previously mentioned evidence on the role of the immune system in the evolution and progression of breast tumors, many of these new approaches aim to promote the tumor immune response and overcome the immunosuppressive effects that the tumor microenvironment can present.

5.1 Engineered antibodies

The success of monoclonal antibodies as therapeutics for the treatment of different types of cancers has opened the door to the development of more complex antibody-based molecules. A number of bispecific and trispecific antibodies are currently under investigation for different malignancies, including breast cancer [73, 74]. These engineered antibody-based molecules are built to target an antigen present on the tumor cell and simultaneously a receptor present

on an immune cell. Hence, this forces the immune and tumor cells to be in close proximity to one another and aids in the cytolysis of the latter. Different formats of these antibodies are currently being developed, some of which are exemplified in Figure 8. For instance, the small bispecific antibody format BiTEs, which are bispecific T cell engagers are formed by two single-chain variable fragment molecules (scFv) fused by a linker. Others exhibit an IgG-like format (Fig. 8).

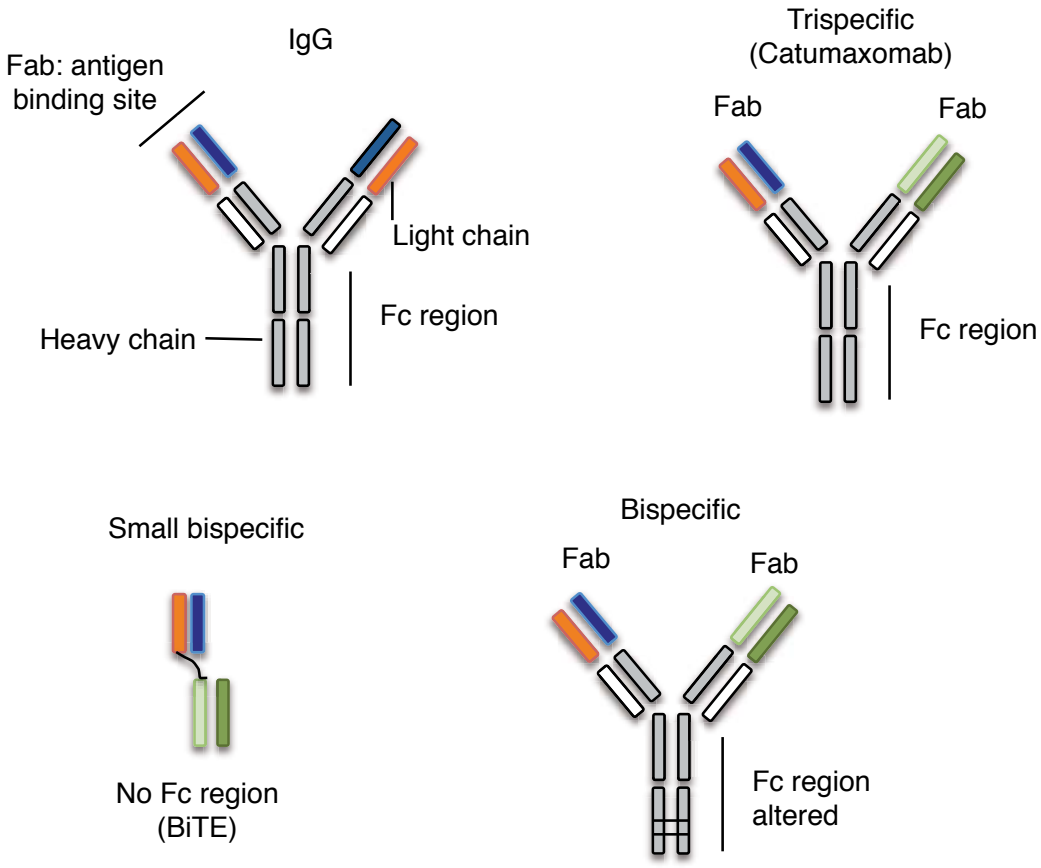

Figure 8: Schematic representation of some engineered antibody formats. IgG-like formats include: trispecific antibodies that display two different antigen binding arms and a competent Fc and bispecific that bear two different antigen binding domains and an inactive Fc domain. BiTEs, are small molecules that engage T cells and are formed by two scFV molecules connected by a linker.

The immune cell of preference as target for the development of these molecules, are the T cells that include the cytotoxic T cells (CD8+), one the most potent

effector cells of the immune system. The engagement of CD3 an invariant and activating member of the TCR and the antigen on the tumor cell triggers T cell activation and destruction of the tumor cell [75]. This process mimics the immunological synapse and is independent of MHC presentation. Due to the fact that these T cell engaging antibodies have high potency, the selection of the appropriate tumor antigen is challenging because many of the known tumor antigens are also expressed by healthy tissues [75]. This could lead to off-target T cell activation and undesired toxicities.

Antibody engineers have to overcome important challenges. These molecules tend to have poor stability, low titers, high immunogenicity and low half-life [74]. The BiTE format antibodies for instance, has such a short half-life that it needs to be administered by continues infusion [76]. On the other hand, IgG-like format antibodies, with a competent Fc, have much higher half-lives, but toxicity issues due to the effect of innate immune cells that can be recognized through the Fc domain limiting their applicability.

Blinatumomab (BiTE format), was the first FDA approved (December 2014) bispecific antibody for the treatment of refractory B cell acute lymphocytic leukemia, and it is designed to bind CD19 on B cells and CD3 on T cells [77]. Catumaxomab (trispecific format) which binds anti-epithelial cell adhesion molecule (EpCAM) and CD3, was also approved for local administration in malignant ascites [78]. For solid tumors, bispecific antibodies targeting carcinoembryonic antigen, CEA, and CD3 have shown promising results in pre-clinical models and are currently being tested in clinical trials [79]. In the field of RTKs, the HER2 targeting ertumaxomab, a trispecific antibody that binds CD3 present on the surface of T cells, HER2 on cancer cells and Fcγ type I/III receptor-positive immune cells, has been tested in phase II clinical trials showing promising results [80]. More recently, a HER2 bispecific antibody that targets HER2 and CD3 on T cells has also been developed [81], but was demonstrated in pre- clinical studies to induce tumor cell lysis even when HER2 levels were very low. This point should be of concern since many tissues in the body, such as the cardiac tissue, express considerable levels of HER2 and will therefore result in unwanted therapy

mediated toxicities. This is particularly clear even for trastuzumab itself, where heart failure occurs in approximately 4% of the patients and other cardiac dysfunction occur in 3 to 18% of patients due to therapy [82].

Therefore, despite promising advances being made with antibody based therapies, caution must be taken to design new therapies with lowered toxicities and at the same time provide the benefit of greater target inhibition than what has been achieved with early generation therapies.

5.2 Anti-HER2 therapies plus immune checkpoint inhibitors

As previously mentioned, the presence of T cell lymphocytes within the tumor microenvironment can induce the expression in tumor cells of immune checkpoints that can limit the effect of T cells. This is the case for PD-1/PDL1 and CTLA-4 [15]. Antibodies against these immune checkpoints have been generated and proven to be effective in different cancers.

In particular for HER2+ tumors pre-clinical evidence demonstrated a synergy between anti-PD1 therapy and trastuzumab [83]. Currently, a clinical trial is ongoing to treat patients that progressed to trastuzumab with trastuzumab plus anti-PD-1 antibodies (PANACEA NCT02129556). In the same line, Müller and colleagues showed that the combination of T-DM1 with anti–CTLA-4/PD-1 led to tumor regression in pre-clinical models [84], supporting the argument that immune function is not fully engaged during monotherapy treatments.

6 Models to study breast cancer

In order to advance our knowledge of breast cancer and to evaluate the effect of new therapies, it is necessary to find suitable models that recapitulate the disease. Still, all available models have their strengthens and limitations however none fully mimic all the aspects of the disease.

Breast cancer cell lines have been the most widely used models to study breast

cancer [85]. They are easy to manipulate and to propagate. Moreover, there is currently a large panel of cell lines which genomic, transciptomic and drug sensitivity data available [86]. Additionally, many breast cancer cells can grow as xenografts in immunocompromised mice, allowing the study of tumor processes *in vivo*.

Genetically modified mouse models have also contributed to the understating of breast cancer biology. In particular for the discovery of oncogene and tumor suppressor genes. Advances in genetic engineering have allowed controlling the timing and location of the transgene expression [87]. These immunocompetenet animals have also been crucial for the study of basic aspects of tumor immunology.

More recently, Patient Derived Xenografts, PDXs, have emerged as a powerful tool to study tumor biology and therapeutic effect of drugs. For breast cancer, orthotropic PDX models are developed by implantation of a tumor piece directly obtained from biopsies or surgical resection into the mammary fat pad of immunocompromised animals. It has been well documented that PDXs display similar characteristics, histologically and genetically, to the original tumor [88]. Moreover, this similarity is maintained throughout tumor passaging [89]. Importantly, they recapitulate drug sensitivity as observed in patients, and are more faithful predictors of therapeutic response that cell line models. PDX tumors have polyclonal cell populations, which better resembles human tumor heterogeneity, whereas cell lines lack this heterogeneity and are instead a homogenous population [89]. Therefore, PDXs could represent a powerful tool to study clonal evolution upon treatment and reflect human cancer more appropriately.

One major disadvantage for the *in vivo* study of human cell line-based tumors or PDX models is that they must be grown in immunodeficient animals. The current advances in immunotherapies have underscored the need to develop more complex models without the limited innate immune systems of “immunodeficient” mouse models, such as is the case with athymic nude mice which contain NK

cells, monocytes and macrophages, and in NOD/SCID mice that only have functional macrophages and monocytes. One option is to reconstitute the human immune system into the recipient mouse generating the so-called humanized mouse models.

A major breakthrough that allowed the generation of these sophisticated models was the introduction of mutation of IL2*ry,* the IL-2 receptor gamma chain, in the NOD/SCID background. This mutation disables cytokine signaling [90]. Therefore, these mouse strains bearing IL2rg mutation lack T, B and NK cells and have a reduced function of macrophages and dendritic cells. Depending on the genetic background and which specific mutation the IL2*ry* has, there are three principal strains: NSG, NOG and BRG [91]. There are reports that show that these mouse strains are different in their ability to support the engraftment of functional human immune systems, being NSG and NRG mice the ones that support higher levels than BRG ones [92].

Reconstitution of the human immune system into these animals can be achieved by different methods, and depending on the question being addressed and the advantages and disadvantages of each model, one method may be more suitable than the other (Fig. 9)

Injection of Peripheral Blood Mononuclear Cells (PBMC) obtained from human donors gives rise to a rapid engraftment of the human cells. The majority of these cells are T cell lymphocytes, which expand rapidly in the mice. The experimental window in this setting is approximately four weeks due to the development of Graft vs Host Disease (GVHD). This is a severe complication that develops in patients that receive allogeneic bone marrow transplantation. Mice suffer from weight loose, ruffled fur and hunched posture. Therefore due to ethical reasons experiments have to be terminated once the animals start developing the symptoms. Despite this experimental drawback, PBMC reconstitution model allows addressing questions quickly and is useful for testing therapies that rely on T cell function.

A more sophisticated method for humanizing mice is through the engraftment of

Human Hematopoietic Stem Cells (HSC-CD34+). HSC can be obtained from several different tissues including adult blood, previous mobilization with G-CSF; Umbilical Cord Blood (UCB) and Fetal Liver [93].

Mice need to be either irradiated or treated with a myeloablative chemotherapeutic agent to eliminate the bone marrow of the mice and favor the engraftment of CD34+ cells.

This model allows an experimental window as large as the lifespan of the animal due to the fact that human T and B cells that develop in the animal undergo negative selection during differentiation, and are therefore tolerant of the mouse host. Furthermore, the engraftment of these progenitors supports the development of most of the human immune cells lineages. The achievement of a good level of circulating human leucocytes (huCD45) takes approximately 16 weeks. One disadvantage, however, is that not all of human immune cell populations seem to have a full maturation or function. T cells develop in the thymus; accumulate mainly in the spleen and they follow a normal differentiation pathway and selection for mouse MHC molecules. The functionality of these cells is still controversial. B cells also develop normally and are the first ones to appear in blood circulation. NK cells develop but in a very low percentage compared to human. In terms of the myeloid compartment, monocytes, dendritic cells and granulocytes differentiate correctly but their frequencies are very low.

To overcome these drawbacks, more complex mouse strains are being developed in order to favor the development and function of all the lineages. For instance, a triple transgenic NSG mice-expressing IL-3/GM-CSF/SCF engrafted with human HSC display increased levels of myeloid cells, specifically dendritic cells.

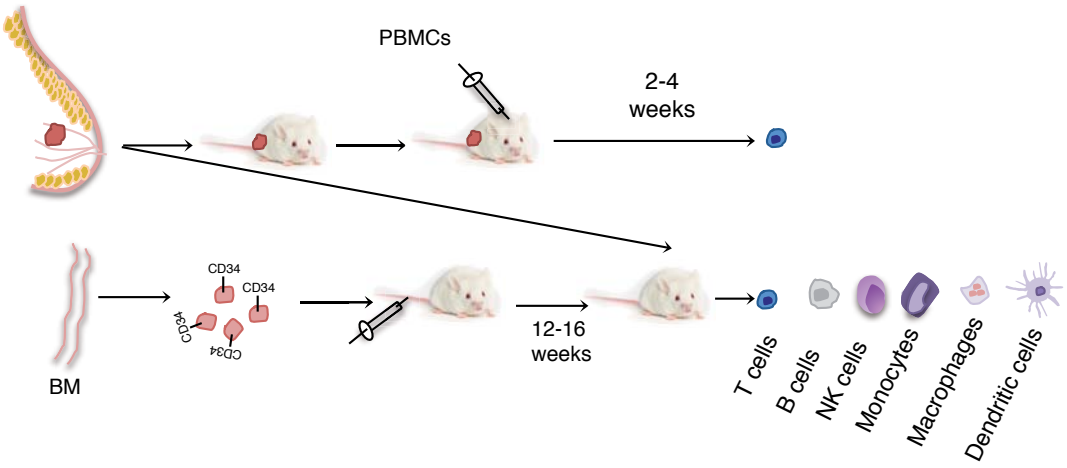

Figure 9: Schematic representation of the development of a mouse model carrying a PDX and human immune system. PBMC: Peripheral-Blood-Mononuclear-Cells; BM: Bone-Marrow; NK: Natural Killer

An ever more sophisticated version of the HSC model is the BLT (Bone Marrow-Liver-Thymus) in which human fetal liver and autologous thymus fragments are co-implanted under the renal capsule of the immunodeficient mouse, together with human HSCs isolated from the same donor. Therefore the T cells are “educated” to recognize the donors antigens as self. This model is technically very challenging and the access to the tissues required is very limited.

When these models are used to evaluate the effects of therapeutic agents in tumor growth, depending on the type of model chosen, the steps to follow to generate these models may differ (Fig. 9). In the case of the PBMC transfer model, due to the rapid expansion of T cells once injected in the mice, the tumor has to be preferentially engrafted before the immune cells. On the other hand, in the CD34+ based models, due the slow development of the immune system (16 weeks), it is more likely that the tumor will be implanted after the injection of the CD34+ cells, depending on the growth rate of the tumor,

All mouse models present limitations. The selection of the accurate model depends both on the question that needs to be addressed as well as the time frame you have to perform the experiments.

Hypothesis and Objectives

The result part of this thesis is divided into two main sections. Each is arranged with its own hypothesis and objectives.

Section 1: "Patterns of HER2 Gene Amplification and Response to Anti-HER2 Therapies"

Background

HER2 is amplified in 20-25% of breast tumors. Genes can be amplified in two different patterns, extrachormosomally as Double Minutes (DMs) or within the chromosome (HSR). DMs do not have centromeres and may not segregate evenly during cell division.

Hypothesis

We hypothesize that tumor heterogeneity and resistance to anti-HER therapy can arise more quickly in the setting of DM amplification, where there is much greater opportunity for diverse cell populations to form quickly and be selected for.

Objectives:

1. Define the patterns of HER2 amplification in cell lines, Patient-Derived Xenografts (PDX) and patient clinical samples.

2. Evaluate the effect of the pattern of amplification on the response to anti-HER2 therapies.

3. Study the effect of anti-HER2 therapy on the HER2 amplicon *in vivo* and in *vitro*.

Section 2: "p95-TCB, a T Cell bispecific antibody that targets a truncated form of HER2"

Background

p95HER2 is expressed in 30% of HER2+ tumors and its expression is associated with elevated HER2 levels present in the tumoral tissue. There are currently antibodies that detect specifically this truncated for of HER2.

Hypothesis

We hypothesize that due to the restricted expression of p95HER2 in tumoral tissue this tumor-specific antigen could be used to target with bispecific antibodies to aid in the recruitment of immune cells to promote cytotoxic killing of HER2+/p95HER2+ cancer cells.

Objective:

1. Develop p95HER2 bispecific antibody

2. Evaluate the *in vitro* effect of p95-TCB antibody towards multiple cell-lines

3. Determine the safety profile of p95-TCB antibody in low HER2 expressing cells

4. Study the *in vivo* effect of p95-TCB antibody towards PDX and cell-line xenografts in humanized mouse models

Materials and Methods

Antibodies

Antibodies for Western Blot: Primary antibodies: HER2 (c-erbB-2) (CB11) (Mouse monoclonal), (#MU134-UCE, BioGenex). Anti-GAPDH antibody (Rabbit monoclonal), clone EPR6256 (#ab128915, Abcam), Cyclin D1 (Rabbit monoclonal), clone 92G2 (#2978, Cell Signaling Technology), p21 (#Ab-11CP74, NeoMarkers). All used at 1:1000 dilutions. Secondary antibodies: ECL Rabbit IgG, HRP-linked whole Ab (from donkey, #NA934-1ML) and ECL Mouse IgG, HRP-linked whole Ab (from sheep, #NA931). All secondary antibodies for western blot were used at 1:2000 dilution (all Amersham GE Healthcare)

Antibodies for Flow Cytometry: huCD45-PE, clone HI30, (#304008); msCD45AF488, clone 30-F11 (#103122); huCD3Percpcy5.5, clone UCHT1 (#300430); CD8 PE-Cy7, clone SK1 (#344712); CD4BV421, clone OKT4 (#317434); APC anti-human CD25, clone BC96 (#302610); FITC anti-human CD69, clone FN50, (#310904), (all from BioLegend). hu-CD34-AF488, clone 581 (#60013AD.1, Stem Cell Technologies). All used at 1:300 dilutions

Antibodies for immunohistochemistry: HercepTest (#K5207, Dako). p95-HER2 was detected by an antibody generated in house as previously described [39]. anti-CD8 (Rabbit Monoclonal) clone SP57 (#5937248001,Ventana, Roche). Anti-Human Cytokeratin (Monoclonal Mouse), clones AE1/AE3 (#M3515, Dako)

Plasmids

All HER2 constructs were derived from a cDNA clone identical to the published sequence gi:183986. HER2 was cloned into pQCXIH vector (Clontech, Mountain View, CA, USA). HER2 deletion constructs were generated (CBM cite 178) as follows; p95HER2-611 cDNA was generated by cloning the HER2 sequence starting at M611 into pLEX-MCS (#: OHS4735, Thermo, Catalog). p95HER2-611(M611A) was generated as previously described [34] and cloned into pQCXIH vector. For MCF7 cells, p95HER2 sequence was cloned into pENTR1A Dual Selection Vector from Invitrogen, using BglII/BamHI (5') and NotI (3') restriction sites, and used as the Entry vector to introduce the sequence into the Destination vector pInducer20-Neo-Luc (#44012, Addgene) using GateWay LR reaction.

Briefly, short-hairpin sequence for targeting p21 mRNA (NM_000389) was removed from pGIPZ CDKN1A shRNA from Open Biosystems-Thermo Scientific (RHS4430-200281172 clone V3LHS-322234) using XhoI and MluI restriction enzymes, and inserted into the same sites of pTRIPz vector (Open Biosystems, Thermo Scientific) using standard cloning techniques.

Cell lines

HCC1954, MDA-MB-453, SkBr3, BT474, MCF7 and MCF10A cells were from ATCC-LGC Standards. SkBr3 and BT474 and MCF7 were maintained in Dulbeccos's minimal essential medium:F12 (DMEM:F12) (1:1) (#21331-046, Gibco-LifeTechnologies). HCC1954 in RPMI 1640 (#61870-044, Gibco-LifeTechnologies) and MDA-MB-453 in Leibovitz's L-15 (#21083-027, Gibco-LifeTechnologies)**.** MCF10A cells were maintained in DMEM:F12 supplemented with 9 µg/ml of insulin (#I9278, Sigma), 0,5 µg/ml of Hydrocortisone (#H0888, Sigma) and 18 ng/ml of EGF (#E9644, Sigma). All media was supplemented with 10% fetal bovine serum (FBS) (#10270-106, Gibco-LifeTechnologies) and 1% L-Glutamine (#M11-004, PAA Laboratories-GE Healthcare). Cardiomyocyte (# CMC-100-110-00, iCell Cardiomyocytes, Cellular Dynamics) were cultured according to the supplier's instructions. Briefly, freshly thawed cardiomyocytes were seeded in human fibronectin coated plates in the suppliers plating medium. After 48h were cells 2x washed with the maintenance medium and fresh maintenance medium was added to the cells. The maintenance medium was replaced every 2-3 days and cells were cultivated in a humidified cell culture incubator at 37°C/5 % CO_2.

MCF10A cells

MCF10A cells stably expressing Vector, p95HER2, HER2 or the combination was performed by retroviral and lentiviral infection. Briefly, retroviral infection was produced by the transfection of Phoenix packaging cells with pQCXIH or pQCXIH-HER2 using Lipofectamine 2000 (#11668-027, Invitrogen). Medium from 15 cm plate was collected and filtered with 0.45µm PVDF filters (Millipore) and passed to

a 15cm plate with MCF10A cells at 50% confluence. Cells were selected with hygromycin (100 µg/ml; #10687-010, Gibco). For the lentiviral infection of pLEX or pLEX-p95HER2, TLA-HEK-293T packaging cell line was transfected with pMD.G2 (Addgene) and pPAX2 (Addgene) packaging vectors, in addition to the corresponding lentiviral vectors, using standard calcium phosphate transfection protocol. Lentiviral supernatants produced were collected and filtered with 0.45µm PVDF filtered. Medium from 15cm plate was collected and filtered with 0.45µm PVDF filters (Millipore) and passed to a 15cm plate with MCF10A cells at 50% confluence, using 8 µg/ml polybrene [94], infection medium was removed after 6 hours. Cells were selected with puromycin (1 µg/ml; Puromycin; #P7255, Sigma-Aldrich)

MCF7-p95HER2 shp21

MCF7 were obtained from ATCC-LGC Standard and were maintained at 37ºC and 5% CO_2 within Dulbeccos's minimal essential medium: F12 (DMEM: F12) (1:1) (#21331-046, Gibco-Life Technologies, Rockville, MD, USA) supplemented with 10% fetal bovine serum (FBS) (#10270-106, Gibco-Life Technologies) and 1% L-glutamine (#M11-004, PAA Laboratories-GE Healthcare, Pasching, Austria). MCF7 TetOn-p95HER2 cell line was generated by lentiviral transduction of pInducer-p95HER2. Polyclonal population was selected and maintained with 200*µ*g/ml Geneticin. MCF7 double TetOn for p95HER2 and shp21 or p95HER2 and sh-nt cell lines were generated by lentiviral transduction of the previously generated MCF7 TetOn-p95HER2 with pTRIPz-shp21 or pTRIPz-empty vector. Polyclonal population was selected for at least 48h with 1 µg/ml Puromycin, double resistant population maintained with 200 *µ*g/ml Geneticin and 1 *µ*g/ml Puromycin.

Proliferation assay

Proliferation was analyzed by cell counting. Briefly, $1x10^5$ cells per well were seeded in 96-well plates. At the indicated times: 0 (10h was counted as time 0), 24h, 48h, 72h and 144h cells were detached with trypsin-EDTA and viable cells

were determined by trypan blue dye exclusion and counted on a Neubauer-chamber.

Animal research

The study was performed in accordance with European Community Standards of Care and Use of Laboratory Animals. Approval was granted for the animal experiments by the Vall d'Hebron University Hospital Care and Use Committee.

Tumor samples

Human breast tumors used in this study were from biopsies or surgical resections at Vall d'Hebron University Hospital, Barcelona and Hospital Clinico Universitario, Valencia (Spain) and were obtained following institutional guidelines. The institutional review boards (IRB) at Vall d'Hebron Hospital and Hospital Clinico de Valencia provided approval for this study in accordance with the Declaration of Helsinki. Written informed consent for the performance of tumor molecular studies was obtained from all patients who provided tissue.

Patient-derived xenografts (PDX)

For Breast Cancer PDXs, fragments of patient samples were implanted into the number four fat pad of the mice. 17 ß-estradiol (1 µM) (#E8875-1G,Sigma-Aldrich) and Baytril was added to drinking water. NOD.CB17-*Prkdc*^{scid} (NOD/SCID) and NOD.Cg-*Prkdc*^{scid} *Il2rg*^{tm1Wjl}/SzJ (NSG) were purchased from Charles River Laboratories (Paris, France). PDX models 288, 289 and 290 corresponded to HBCx-13B, HBCx-41and HBCx-5, respectively, and were established at Institut Curie. Tumor xenografts were measured with calipers every 3 times a week, and tumor volume was determined using the formula: (length x width^2) x (pi/6). Body weight was monitored twice a week.

Establishment of cell cultures from PDXs

For the establishment of cell cultures derived from PDXs, tumors were excised and cut into the smallest pieces possible with scalpel, incubated for 30 minutes with collagenase IA (Sigma-Aldrich, #C9891-1G,), washed and resuspended in DMEM:F-12, 10% FBS, 4 mmol/L L-glutamine, Penicillin/Streptomycin (#P4333-Gibco), 10 mM HEPES (# sc-286961, Santa Cruz Biotechnology,) and 1.75 µg/ml Amphotericin B (#15240062, Gibco) for 6 hours. Then, medium was carefully removed and changed to 10%-supplemented Mammocult human medium (#5620, StemCell Technologies) with Penicillin/Streptomycin and 10 mM HEPES.

DISH / Determination of HER2 amplification patterns

The INFORM HER2 Dual ISH DNA Probe Assay was used on 5-µm sections using the BenchMark XT Staining Platform [95-4422, Ventana Medical Systems]. All samples were processed following the FDA-approved protocol. Samples with >70% of the cells with a DM (small dispersed dots distributed throughout the nucleus) or HSR (tightly clustered dots in discrete regions of the nucleus) patterns were classified accordingly. Cases not falling into these categories because Samples with >70% of the cells with a DM (small dispersed dots distributed throughout the nucleus) or HSR (tightly clustered dots in discrete regions of the nucleus) patterns were classified accordingly. Cases not falling into these categories because of the presence of both HSR and DM patterns in the same sample were classified as mixed. Two teams including certified pathologists blindly assessed the pattern of HER2 amplification in the series of samples from patients treated with neoadjuvant trastuzumab and adjuvant trastuzumab. The HER2/centromere 17 probe signal ratio was determined based on the quantification of 20 cells in at least two different fields, as recommended in ASCO/CAP 2013 guideline [96].

DISH or Metaphase Spreads on cells treated with colchicine

Cells grown to 85% confluence were treated with 100 ng/ml of colchicine (#15210-040, Gibco) for 18 hours, trypsinized and pelleted. Then, cell pellets were stained by DISH or treated with a hypotonic solution (0.075 M KCl) at 37 ^{0}C for 15 minutes. After the hypotonic treatment, cells were treated with ice-cold fixative (1:3 acetic acid: methanol). Metaphase spreads were obtained by dropping fixed cells onto slides. Slides were air-dried overnight and then stained with Giemsa.

Immunohistochemistry

Tumor samples were fixed in 4% formaldehyde (#2529311315, Panreac) and then paraffin included. Stainings were performed on 5 μm paraffin cuts in a Dako Autostainer Plus machine (Dako) according to the manufacturer's instructions. Certified pathologists evaluated HER2 protein expression by H-score. Scoring 3+, 2+, 1+ was performed following the ASCO/CAP recommendations [96]. 3+ indicates a strong complete membrane staining in >10% % of the cells; 2+ indicated weak to moderate complete membrane staining in >10% of the cells; 1+ indicates barely perceptible staining detected in >10% of tumor cells with incomplete membrane staining. When a sample scored 2+, FISH/DISH is performed to rule out if its HER2 amplified or not, a determine the sample as HER2 positive or negative.

RTqPCR

For copy number variation, DNA was isolated from FFPE tumors or cell pellets with QIAamp DNA FFPE Tissue Kit (#51304, QIAGEN) following manufacturer's instructions. Nucleic acid concentrations were quantified using Nanodrop spectrophotometer (ND-1000, Thermo Scientific) and associated software ND-1000 3.8.0. Ten ng of DNA were run in a Applied Biosystems 7900HT using ErbB2 TaqMan Copy Number Assays (Hs00641606_cn) and RNase P TaqMan Copy Number Reference Assay (4403326). Each sample was assayed in quadruplicate. BT474 and MCF7 DNA were used as control for HER2-amplified and non-amplified cell respectively. Relative copy number was calculated with Applied

Biosystems CopyCaller Software following manufacturer's instructions.

For RNA qPCR, RNA was isolated from FFPE tumors with ReliaPrep™ FFPE Total RNA Miniprep System (#z1002, Promega) following manufacturer's instructions. Nucleic acid concentrations were quantified using Nanodrop spectrophotometer (ND-1000, Thermo Scientific) and associated software ND-1000 3.8.0. 1µg RNA was retro-transcribed to cDNA using High capacity cDNA reverse transcription kit (#5468814, Applied Biosystems) following manufacturer's instructions. 50ng of cDNA were run in an Applied Biosystems 7900HT using TaqMan gene expression assays ERBB2 (HS01001580_m1) and GAPDH (Hs03929097_g1) CCND1 (Hs00765553_m1) from Applied Biosystems and Taqman Universal Master Master mix II, with UNG (#44440038, Applied Biosystems #44440038). Each sample was assayed in triplicate. Real Time PCR Data was analyzed using SDS v2.3 software (Applied Biosystems) following the 2ΔΔCt method. Briefly, average ΔCt calculated as (Assay_Ct)-(housekeeping GAPDH_Ct). Relative mRNA represented as mean ± SD of 2-ΔΔCt

Cell proliferation

Cells were plated and treated with lapatinib or T-DM1 at the described concentrations. At the indicated time points, cells were fixed by replacing the growth medium with 100 µl/well of 10% glutaraldehyde in phosphate-buffered saline (PBS) for 10 minutes at RT. After three washes with water, 100 µl of 0.1% crystal violet solution was added to each well and incubated 20 minutes. Plates were washed and air-dried, and 50 µl of 10% acetic acid was added to each of the wells. Optical Density (OD) was measured at 560 nm.

Western Blot

Protein extracts were obtained from cells washed with ice-cold 1xPBS and lysed in 20mM Tris-HCl pH7.4, 137mM NaCl, 2mM EDTA, 10% glycerol, 1% Nonidet P-40 supplemented with 5mM NaF (1M stock, Sigma #56521), 5 mM ß-

Glycerophosphate (#S6521, 1M stock, Fluka), 1mM Na3VO4 (#S65508, 250 mM stock, Sigma) and 40 µl/ml Complete EDTA-free Protease Inhibitor Cocktail Tablets (prepared according to manufacturer's instructions, Roche #11873 580 001). Protein extracts were clarified by centrifugation at 16,1x103rcf and quantified using DC protein assay reagents (Bio-Rad). Samples were mixed with loading buffer containing DTT (250mM Tris-HCl pH6.8, 10% SDS, 30% Glicerol, 0.5 mM 1.4-Dithiothreitol DTT (#10780984001, Roche), 0.2% Bromophenol blue) and incubated at 99ºC for 5 min before resolving proteins by SDS-polyacrylamide gel electrophoresis [97, Marcelin] and transferring them to nitrocellulose membranes. Membranes were blocked for 1h with 5% skim milk or 5% Bovine Serum Albumin (BSA) in Tris-buffered saline (TBS) 0.1% Tween-20 and incubated with primary antibodies o/n at 4ºC. Membranes were washed with TBS-Tween 0.1% and incubated with HRP-coupled secondary antibodies for 1h at RT. Proteins were detected by autoradiography upon addition of Immobilon western chemiluminescent HRP substrate (#WBKLS0500, Millipore). Western blots were quantified with ImageJ 1.42q software (NIH, USA)

Antibody binding by Flow Citometry

Cells were harvested with StemPro Accutase (#A11105-01, Invitrogen) and 400.000 were resuspended in 1xPBS, 2.5 mM EDTA, 1%BSA and 5%Horse Serum for 20 min p95-TCB was added at different concentrations for one hour. After a wash with PBS1x, an anti-human Alexa488 secondary antibody was added for 30 min. One wash with PBS 1x was performed and samples were acquired in a FACSCalibur flow cytometer (BD Biosciences).

PBMCs isolation

Peripheral blood mononuclear cells (PBMCs) were isolated from peripheral blood obtained from healthy donors through the Blood and Tissue Bank of Catalonia. Blood was diluted with 1xPBS, 2:1, and transferred to 50 ml tubes containing 15 ml Ficoll-Paque [70-1440-02, GE Healthcare]. Centrifugation was performed at

400g for 30 minutes with no breaks. The PBMC layer was collected, and centrifuged at 400g for 5 min with break. The pellet was resuspended in 20 ml of Red Blood Lysis buffer (# 00-4333-57,eBioscience) for 3 min at RT. Cells were centrifuged at 400g 5 min with breaks, washed twice with 1xPBS and counted.

Cytotoxicity assays

All target cells were harvested with StemPro Accutase (#A11105-01, Invitrogen), counted and seeded in 96 well flat bottom plates. Twenty-four hours later, PBMCs, isolated as previously described, were added to each well in a proportion 10:1 in RPMI 1640, 2%FBS. Antibodies serial dilutions were performed in RPMI 1640, 2% FBS medium and added to the Target/Effector containing wells. Wells containing only medium were present for the culture medium background control. Each target cell had maximum release and spontaneous release control wells containing only target cells. The assay also contained effector cell control wells, containing PBMCs and the different concentrations of antibodies. Each condition had triplicates. The plates were incubated for 48 h at 37ºC/5% CO_2 in humidified incubator. LDH release was determined with CytoTox 96 Non-Radioactive Cytotoxicity Assay (#G1780, Promega). Briefly, 45 min before the assay, 20 µl of lysis solution was added to the maximum release controls. After the 45 minutes each 96 well plate was centrifuged for 5 min at 420g and 50 µl of each supernatant was transferred to a new 96 well plate. 50 µl of CytoTox Reagent was added to each well and the plate was incubated for 30 min, at RT covered from light. Then 50 µl of the Stop solution was added and the absorbance was measured at 490 nm. Culture medium background was subtracted from each measure. The percentage of cytotoxicity was calculated as follow:

%Cytotoxicity = (Experimental abs. - Effector Spontaneous abs. –Target Spontaneous abs.) / (Target Maximum abs.-Target Spontaneous abs.)

Cytokine analysis

Fifty microliters from the tumor cell lysis assays supernatants were collected and transferred to a 96 well plate for Granzyme B, IFN-gamma and IL-2 detection with CBA Human Soluble Protein Flex Set (*#*558264, *BD Bioscience*). To prepare the standard curve, the standard spheres were pooled and reconstituted in a single tube. Serial dilutions were performed as recommended by the manufacturer. Standard curve and samples were incubated for one hour at RT, with 50 µl of the capture beads mix containing beads for each analyte to be detected. Then, 50 µl of the PE-detection reagent was added to each well and the plate was incubated for 2 hours at RT, protected from light. After one wash, the samples were acquired in a *LSR Fortessa using the* High Throughput Sampler,*(BD Bioscience). The analysis was performed with FCAP Array Software (BD Bioscience) following* manufacturer's instructions

T cell activation

After collecting supernatants for cytokine detection and LDH release as previously described, the rest of was discarded and the PBMCs were resuspended in 1xPBS, 2,5 mM EDTA, 1%BSA and 5%Horse Serum. Twenty minutes later, samples were centrifuged and cells were incubated fro 45 min with the following antibody mix: CD4-BV421 and CD8-PE-Cy7, CD25-APC, CD69-FITC at 1:300. After a wash with1xPBS, samples were acquired in a *LSR Fortessa (BD Bioscience). Data was analyzed in FlowJo software.*

Humanization with PBMCs

MCF7-p95HER2-shp21 were resuspended 1:1 in PBS: Matrigel matrix (BD #356237, Bioscience) and were orthotopically injected into NSG mice ($3x10^6$ cells /mouse; 100µl/animal). Tumors were implanted as previously described. When tumors reached an average size of 150-200 mm^3, NSG mice were intraperitoneally injected with 20 $x10^6$ PBMCs resuspended in 200 µl of 1xPBS. For MCF7-p95HER2-shp21, at this point, doxycycline was added to the drinking water (1g/L) (25g/L sucrose were added to the water solution to compensate doxycycline solution flavor). Tumor xenografts were measured with calipers every 3 times a

week, and tumor volume was determined using the formula: (length x width^2) x (pi/6). Body weight was monitored twice a week.

Immune cell Infiltration in tumors

At the end of the in vivo studies, tumors were weighed and then excised. To generate single cell suspensions, tumors were cut into small pieces and passed to a 50 ml falcon containing 50µl collagenase IA (100 mg/ml) and 50 µl of DNAse (2 mg/ml) in 5 ml of media RPMI. This mixture was incubated at 37º for 1 hour with rotation. The mixture was filtered in a 100-µm-cell strainer (#352360, Corning) and centrifuged for 5 min at 400 g. Then, red blood cell lysis was performed and after a wash with PBS1x the cells were resuspended in 1xPBS, 2.5 mM EDTA, 1%BSA and 5% Horse Serum for 20 min. After the blocking the cells were stained with msCD45, huCD45, huCD3, huCD4 and huCD8 for 1 h. Samples were acquired in a *LSR Fortessa and analyzed with FlowJo software.*

Statistical analysis

All statistical analysis was performed in GraphPad Prism version 5.0 software.

Results: Section 1

“Patterns of HER2 Gene Amplification and Response to Anti-HER2 Therapies”

---

1. Distinct HER2 amplification patterns

1.1. HER2 amplification patterns in breast cancer cell lines

Gene amplification can give rise to two distinct patters depending if the amplification occurs within the chromosome or extrachormosomally. In order to know if HER2 distinct amplification patterns can be evaluated by by dual-in-situ hybridization (DISH), we performed this technique in four HER2-amplified breast cancer cell lines: BT474, SkBr3, MDA-MB-453 and HCC1954. Cells were treated or not with colchicine, a microtubule polymerization inhibitor. As seen in the chromosome spreads shown in Figure 10 (upper panels), this compound arrests the cells in metaphase, when the chromatin is tightly condensed allowing the observation of distinct dispositions of amplicons. The results showed two distinct HER2 amplification patterns: tightly clustered dots in discrete regions or many small-dispersed dots distributed throughout the nucleus (Fig. 10, middle panels). The first, also known as Homogeneously Staining Region (HSR), corresponds to tandem gene amplification; the second pattern is consistent with gene amplification in Double Minutes (DM). Analysis of interphase cells showed a pattern similar to that observed in metaphase cells (Fig. 10, lower panels), indicating that HER2 gene amplification patterns can be identified through this technique even in regular cycling cells.

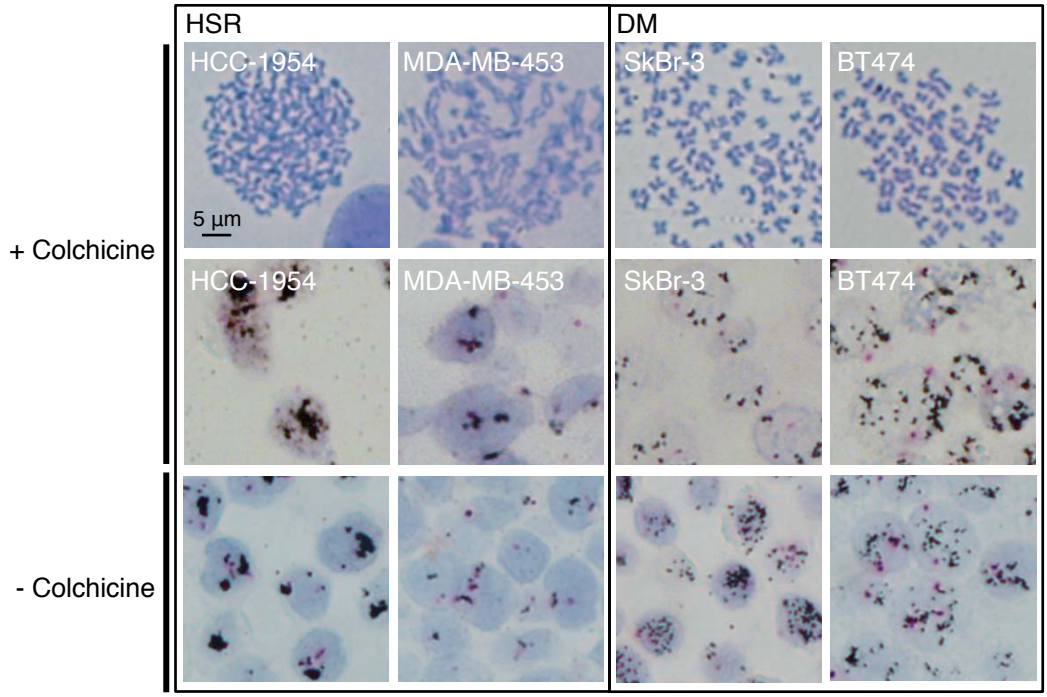

Figure 10: HER2 gene amplification patterns in different breast cancer cell lines. The indicated cell lines were treated with 100 ng/ml of colchicine for 18h and metaphase spreads (top panels) or HER2 DISH staining (middle panels) were performed. As a control, HER2 DISH was also performed on untreated cultures of the same cell lines (lower panels).

1.2. HER2 amplification patterns in Patient-Derived Xenografts

We next evaluated the amplification pattern of HER2 in a panel of HER2 positive Patient-Derived Xenografts (PDXs) developed in our laboratory. These tumors come from biopsies or surgical resections of breast cancer patients that are rapidly implanted in NOD/SCID animals. Once grown, the tumors were excised and confirmed HER2 positive by immunohistochemistry following the ASCO/CAP guidelines where 3+ indicates a strong complete membrane staining in > 10% of the cells (Fig. 11B). This was further confirmed by Western Blot were HER2 protein can be detected in al HER2+ PDX and BT474 and not in MCF7 and a TNBC PDX (Fig. 11A). Tumor samples in FFPE were analyzed by DISH, revealing the presence of six HSR and three DM models (Fig. 11B, C). The amplification ratio (HER2/CEP17) is obtained by dividing the amount of HER2 amplicon by the amount of chromosome 17 probe (Fig. 11B).

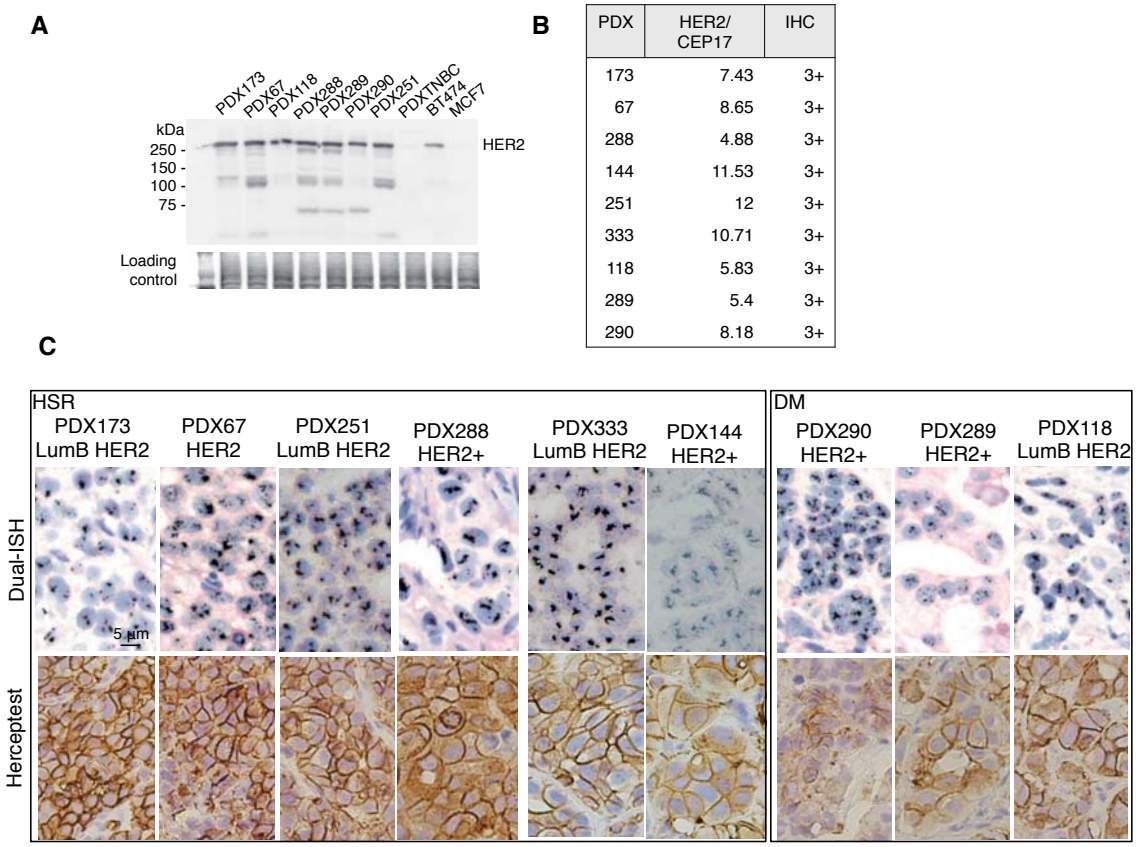

PDX	HER2/ CEP17	IHC
173	7.43	3+
67	8.65	3+
288	4.88	3+
144	11.53	3+
251	12	3+
333	10.71	3+
118	5.83	3+
289	5.4	3+
290	8.18	3+

Figure 11: HER2 gene amplification patterns in breast cancer PDXs. PDX obtained from biopsies or surgical resections of breast cancer patients were confirmed HER2 positive by Western Blot (A) and Immunohistochemistry (C). Samples were analyzed by HER2 DISH and the pattern of gene amplification (C) as well as the ratio HER2/CEP17 (B) were determined.

In order to validate these patterns observed in FFPE PDX samples, we generated primary cultures of two of them, one PDX with HER2 amplification following an HSR pattern (PDX67) and one with DM (PDX118) amplification. We then treated primary cultures with colchicine and as shown in Figure 12, we confirmed the same pattern as observed in the PDX-tumor specimen, further demonstrating that the type of HER2 gene amplification pattern is identifiable in clinically relevant samples.

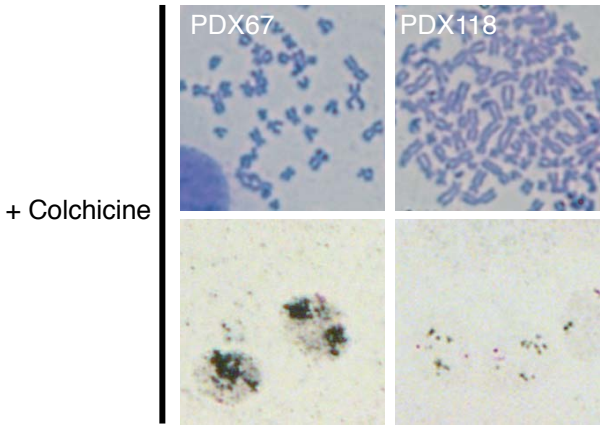

Figure 12: HER2 amplification pattern in cell cultures obtained from PDXs. Primary cultures from PDX67 (HSR) and PDX118 (DM) were treated with 100 ng/ml of colchicine and metaphase spreads (upper panels) or HER2 DISH (lower panels) were performed.

We conclude that, in breast cancers, HER2 is amplified both in HSR or DM patterns and that DISH technique applied to FFPE tumor samples allows to distinguish between these two forms of HER2 amplification.

2. HER2 amplification patterns and response to trastuzumab in clinical samples

2.1. HER2 amplification patterns and response to trastuzumab in neo-adjuvant setting

After demonstrating that the pattern of amplification can be determined by DISH in FFPE tumor samples, we analyzed 58 samples from patients affected by HER2-amplified tumors and treated with trastuzumab in combination with chemotherapy prior to surgical resection (neoadjuvant treatment). The results showed that 35% and 53% had pure DM and HSR patterns, respectively. We also detected tumors that contained both patterns and were considered mixed (12%) (Fig. 13A, B left graph). Thereafter, we established the cut-off to distinguish the different patterns as follows: samples with >70% of the cells with a DM (small dispersed dots distributed throughout the nucleus) or HSR (tightly clustered dots in discrete

regions of the nucleus) patterns were classified accordingly. Cases not falling into these categories because of the presence of both HSR and DM patterns in the same sample were classified as mixed. For example, samples with 40% and 60% of cells with DM and HSR patterns, respectively, were classified as mixed while samples with 20% and 80% of cells with DM and HSR patterns, respectively, were classified as HSR (Fig 13A).

Consistent with previous reports {Gianni:2010hn}, we observed that in our patient series treatment led to pathological complete response (pCR) in approximately 55% (Fig. 13B, right graph). Also the patients belonging to each amplification pattern had comparable markers in terms of age, histological subtype, histological grade, hormone receptor status and Ki67, suggesting that the main difference between the groups is the HER2 amplification pattern (Appendix Table 1). The percentage of pCR in the DM group (50%) was not statistically different from that of the HSR group (57%) (Fig 13B, right graph).

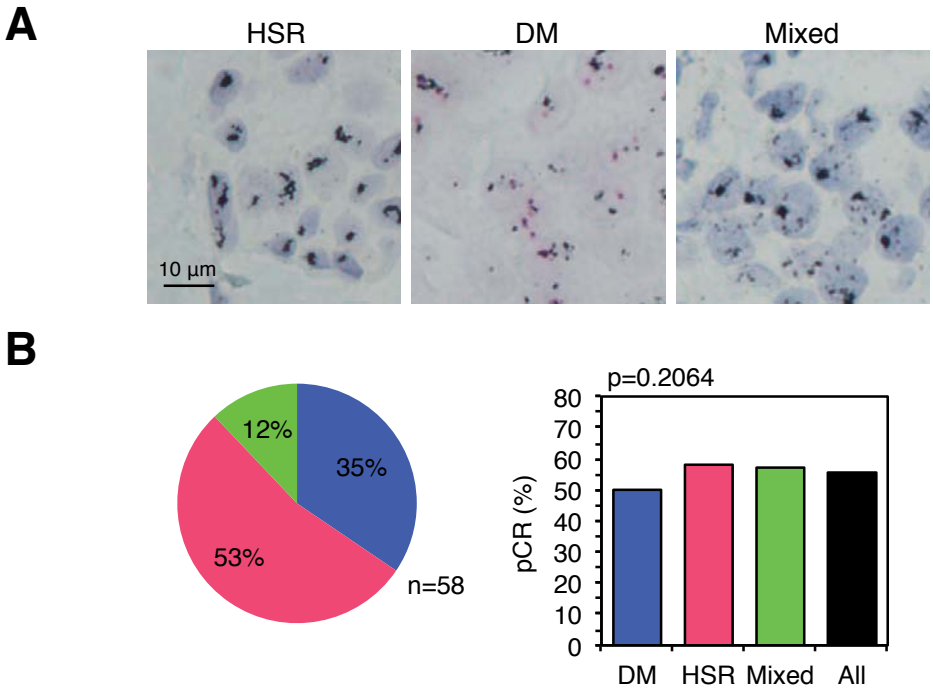

Figure 13: HER2 amplification patterns and response to trastuzumab in neoadjuvant setting. (A) Samples with >70% of the cells with a DM or HSR patterns were classified accordingly. Cases not falling into these categories because of the presence of both HSR and DM patterns in the same sample were classified as mixed. Representative examples are shown. (B) Left graph, percentages of the HER2 gene amplification patterns in tumors from a cohort of breast cancer patients treated with neoadjuvant trastuzumab. Right graph, pathologic complete response (pCR) rates according to the HER2 gene amplification pattern. *p* value shown was calculated by the two-sided Fisher's exact test.

Samples from 16 patients (8 with DM and 8 with HSR amplification) without pCR were amenable to analysis under pre- and post treatment. The average HER2 amplification ratios of the cases with DM, pre- and post-treatment, were 4.10 and 5.82, respectively (Fig. 14), arguing that the cases with DM that did not achieve pCR did not tend to lose HER2 gene copies. In contrast, the HER2 average amplification ratios of the pre- and post-treatment cases with HSR were 8.72 and 6.25, respectively (Fig. 14), Also, the pattern of amplification did not change with treatment in all cases but one, in which we observed a transition from HSR to DM (dotted line in Fig. 14 left graph).

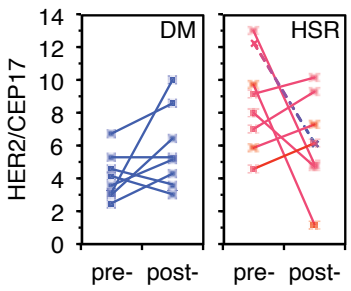

	DM		HSR	
	pre-	post-	pre-	post-
	6.8	8.6	13.1	4.9*
	5.3	5.4	12.3	6.2
	4.6	3.7	9.8	1.2
	4.2	4.7	9.1	10.2
	3.5	5.2	8	4.88
	3.1	10	7	9.3
	3	6.5	5.8	7.3
	2.7	4.3	4.68	6.1
Average	4.1	5.82	8.72	6.25
95% CI	0.82	1.53	2.07	1.95

Figure 14: HER2 amplification patterns pre- and post treatment. Paired samples, pre- and post-treatment with trastuzumab, from 8 tumors with DM and 8 with HSR amplifications, obtained from patients shown in Figure 13 without pCR, were analyzed by HER2 DISH and the ratio HER2/CEP17 was calculated and represented. Dotted line and * represents the only patient that changed the pattern. Note: Similar results were observed when we quantified only HER2 gene copies, arguing that the tendencies observed were not due to variations in the number of centromeres.

Thus, these results do not support our hypothesis that treatment with trastuzumab could result in loss of HER2 gene copies in tumors with DM amplification.

2.2. HER2 amplification patterns and response to trastuzumab in adjuvant setting

To extend these results, we analyzed the pattern of HER2 amplification in tumors from a cohort of patients (n=55) treated after surgery with trastuzumab-based therapy (adjuvant treatment). The proportion of patients displaying the different amplification patterns was similar to the one observed for the neoadjuvant patient series (Fig. 15, left graph). Also the patient and tumor characteristics of both DM and HSR groups were similar (Appendix Table 2). In agreement with the results in the neoadjuvant setting, the percentage of tumors with DM amplification that progressed was not significantly different from that of tumors with HSR amplification (Fig. 15, right graph).

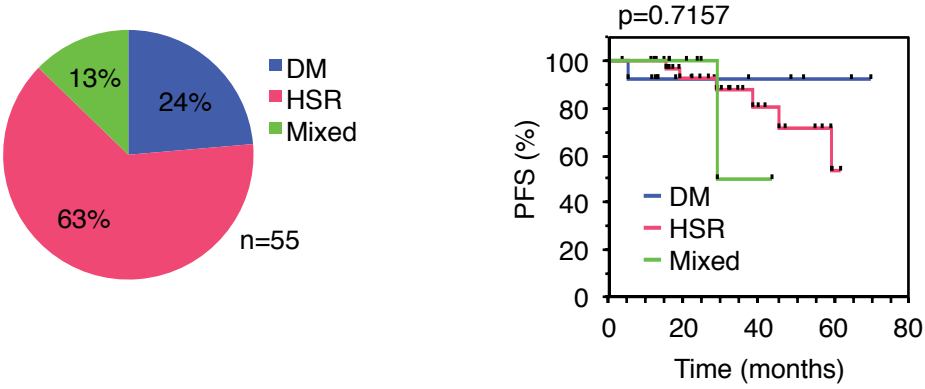

Figure 15: HER2 amplification patterns and response to trastuzumab in adjuvant setting. Patient samples from patients treated with trastuzumab in combination with chemotherapy after surgery were classified as shown in Figure 13. Left graph, percentages of the HER2 gene amplification patterns in tumors from a cohort of breast cancer patients treated with neoadjuvant trastuzumab. Right graph, disease-free survival (DFS) according to HER2 gene amplification pattern. *p* value shown was calculated by the Mantel-Cox test comparing the HSR and DM groups.

All together this finding indicates that amplification of HER2 in DM does not correlate with resistance to trastuzumab-based therapies, neither in adjuvant nor in neoadjuvant setting.

3. Resistance to anti-HER2 therapies *in vivo*

3.1. Acquisition of resistance to therapeutic anti-HER2 antibodies in PDXs

To characterize the acquisition of resistance to anti-HER2 therapies in tumors with HSR and DM amplification, we used PDX67 and PDX173 as HSR and PDX118 as DM models (Fig. 11). We treated these PDXs with trastuzumab and T-DM1. Among the HSR models, PDX173 was sensitive to both therapies (Fig. 16, right graph). On the other hand, PDX67 showed primary resistance to trastuzumab but sensitivity to T-DM1 (Fig. 16, left graph). Despite the continuous treatment of both tumors, no secondary resistances to the therapies arose.

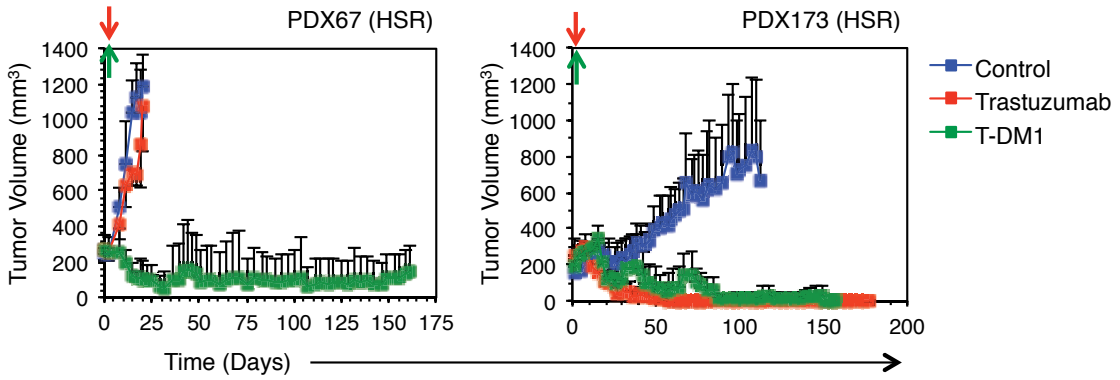

Figure 16: PDXs with HSR amplification and response to anti-HER2 therapies. PDX67, left graph, and PDX173, right graph, were implanted orthotopically into NOD/SCID mice (n = 8 per group). When tumors reached 200mm3 animals were treated or not with Trastuzumab (10 mg/kg, bi-weekly, i.p.) or T-DM1 (15 mg/kg, once every 3 weeks, i.v.). In the case of being sensitive to the drugs, animals were treated chronically. Tumor volumes were calculated using the formula: (length °— width2) °— (pi/6). Results are expressed as averages. Error bars correspond to 95% confidence intervals.

In the case of the DM tumor, PDX118, it was initially very sensitive to both trastuzumab and T-DM1 (Fig 17A), but after 75-125 days of continuous treatment, secondary resistances appeared (Fig.17B). In the trastuzumab group, the tumors of five out of six mice relapsed (Fig. 17B, TR stands for trastuzumab resistant). In the case of T-DM1, even though tumor shrinkage was observed upon treatment initiation, reducing the size to undetectable levels after two dosages (Fig. 17A), ~70 days after treatment only one tumor out of six regrew (Fig. 17B, TRD stands for T-DM1 resistance).

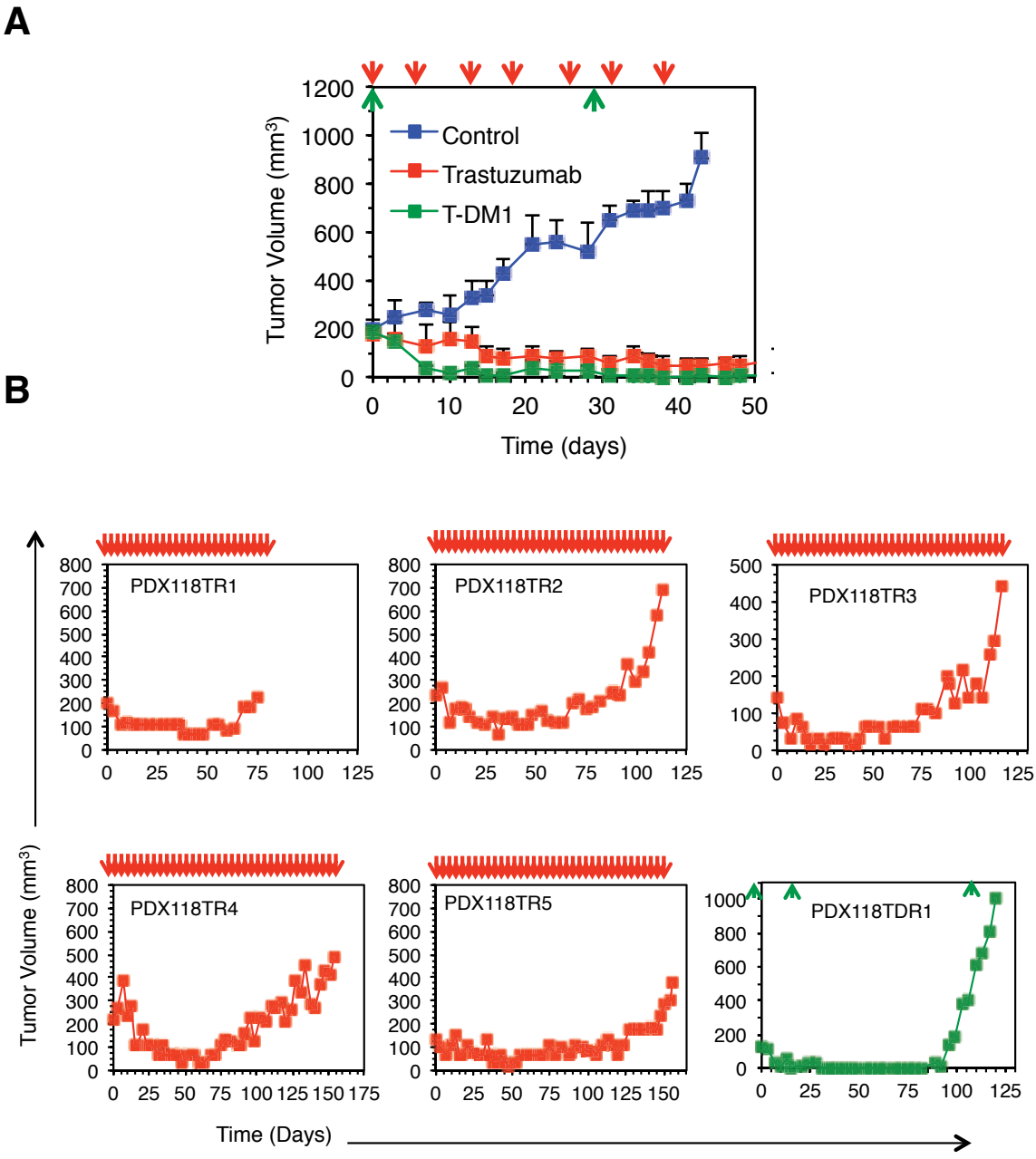

Figure 17. PDXs with DM amplification develop resistance to trastuzumab and T-DM1. PDX118, was implanted orthotopically into NOD/SCID mice (n = 6 per group). When tumors reached 200mm3, animals were treated or not with Trastuzumab (10 mg/kg, bi-weekly, i.p.) or T-DM1 (15 mg/kg, once every 3 weeks, i.v.). In the case of being sensitive to the drugs, animals were treated chronically. Tumor volumes were calculated using the formula: (length °— width2) °— (pi/6) and results are expressed as averages. A. Group average. B. Single animals. Error bars correspond to 95% confidence intervals

In order to confirm the resistances for both therapies, the re-growing tumors were passaged into new animals and treated again with trastuzumab or T-DM1 (Fig. 18).

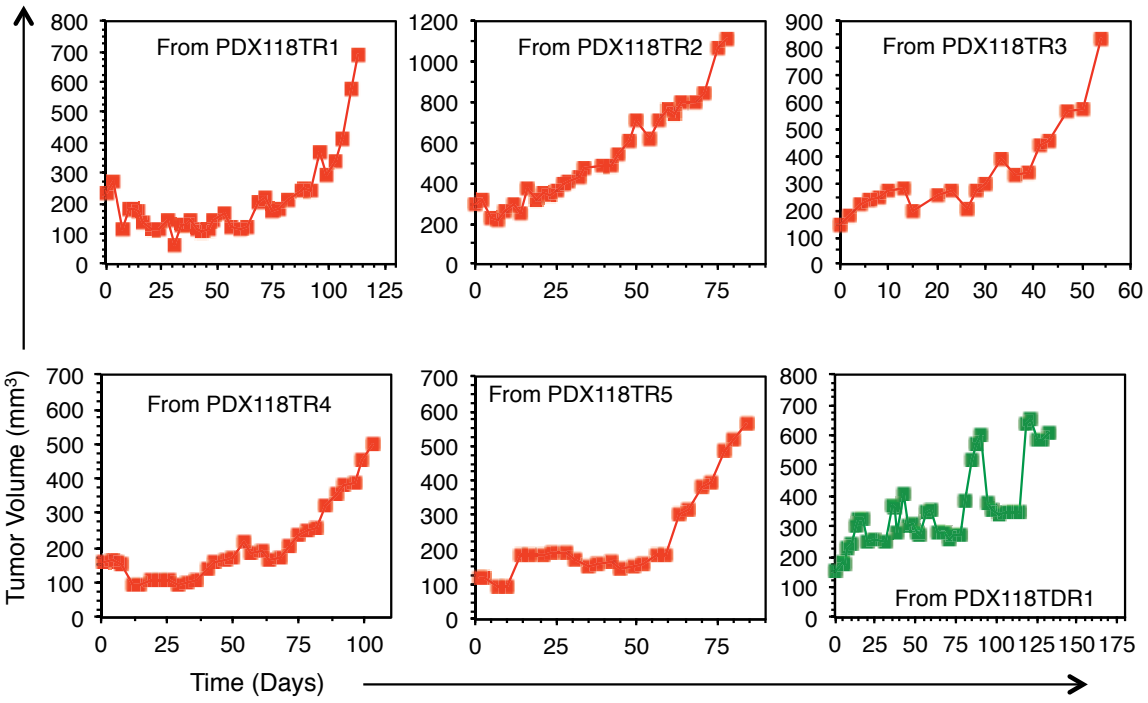

Figure 18: Validation of PDXs resistant to trastuzumab or T-DM1. Small pieces of the tumors that progressed after trastuzumab or T-DM1 treatment (Fig. 17) were orthotopically implanted into new NOD/SCID mice (n=6 per group) and treated again with Trastuzumab (10 mg/kg, bi-weekly, i.p.) or T-DM1 (15 mg/kg, once every 3 weeks, i.v.). TR: Trastuzumab resistant, TDR: T-DM1 resistant.

3.2. HER2 gene amplification and protein expression in resistant tumors

We then evaluated HER2 protein levels in the resistant tumors and observed that three out of five trastuzumab resistant tumors showed decreased expression of HER2 and the same was observed for T-DM1 resistant model (Fig. 19A, B). Thus, acquisition of resistance to anti-HER2 therapies in this model of DM amplification can be concomitant with loss of HER2 protein expression.

The HER2/CEP17 ratios indicated a similar level of amplification of HER2 in the parental and resistant tumors (Fig. 19A, B). We confirmed these data by a qPCR-based method (Fig. 19C) and concluded that the downregulation of HER2 protein in the trastuzumab and T-DM1 resistant tumors is not due to a decrease in HER2 gene copy number.

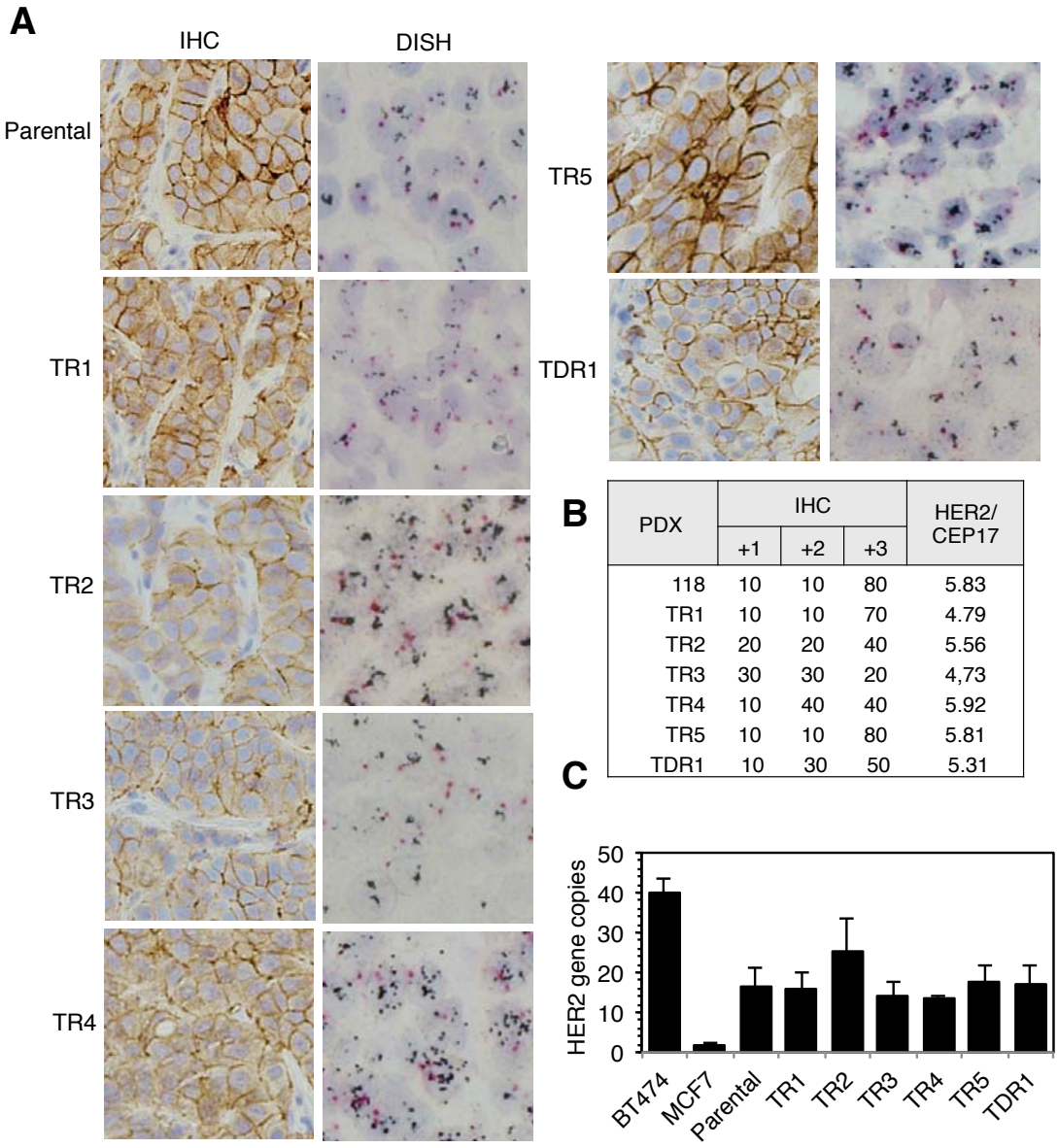

PDX	IHC			HER2/ CEP17
	+1	+2	+3	
118	10	10	80	5.83
TR1	10	10	70	4.79
TR2	20	20	40	5.56
TR3	30	30	20	4,73
TR4	10	40	40	5.92
TR5	10	10	80	5.81
TDR1	10	30	50	5.31

Figure 19: Analysis of HER2 protein levels and gene amplification in PDXs resistant to trastuzumab or T-DM1. (A) FFPE PDX samples from parental or resistant PDX118 tumors shown in Fig.17/18 were analyzed by IHC and DISH to evaluate HER2 protein and gene amplification, respectively. (B) H-score for HER2 and HER2/CEP17 from tumors in A. (C) DNA from FFPE samples was isolated and gene copy number was determined by qPCR with ErbB2 TaqMan Copy Number Assays. BT474 and MCF7 breast cancer cell lines were used as controls for HER2-amplified and not amplified samples, respectively. RNase P TaqMan Copy Number Reference Assay was used for normalization. Each sample was assayed in quadruplicate. Relative Copy number was calculated with Applied Biosystems CopyCaller Software. TR: Trastuzumab resistant, TDR: T-DM1 resistant.

4. Resistance to anti-HER2 therapies *in vitro*

The elimination of DMs carrying EGFR-vIII from glioblastoma cells can be achieved by specific tyrosine kinase inhibition {Nathanson:2014ik}. Therefore we tested the effect of lapatinib in the primary culture derived from the DM PDX, PDX118. Lapatinib impaired the proliferation of these cells (Fig. 20B, upper panels). Prolonged treatment of these cell cultures with increasing concentrations of the tyrosine kinase inhibitor led to the appearance of resistant cells (Fig. 20A and B middle and lower panels).

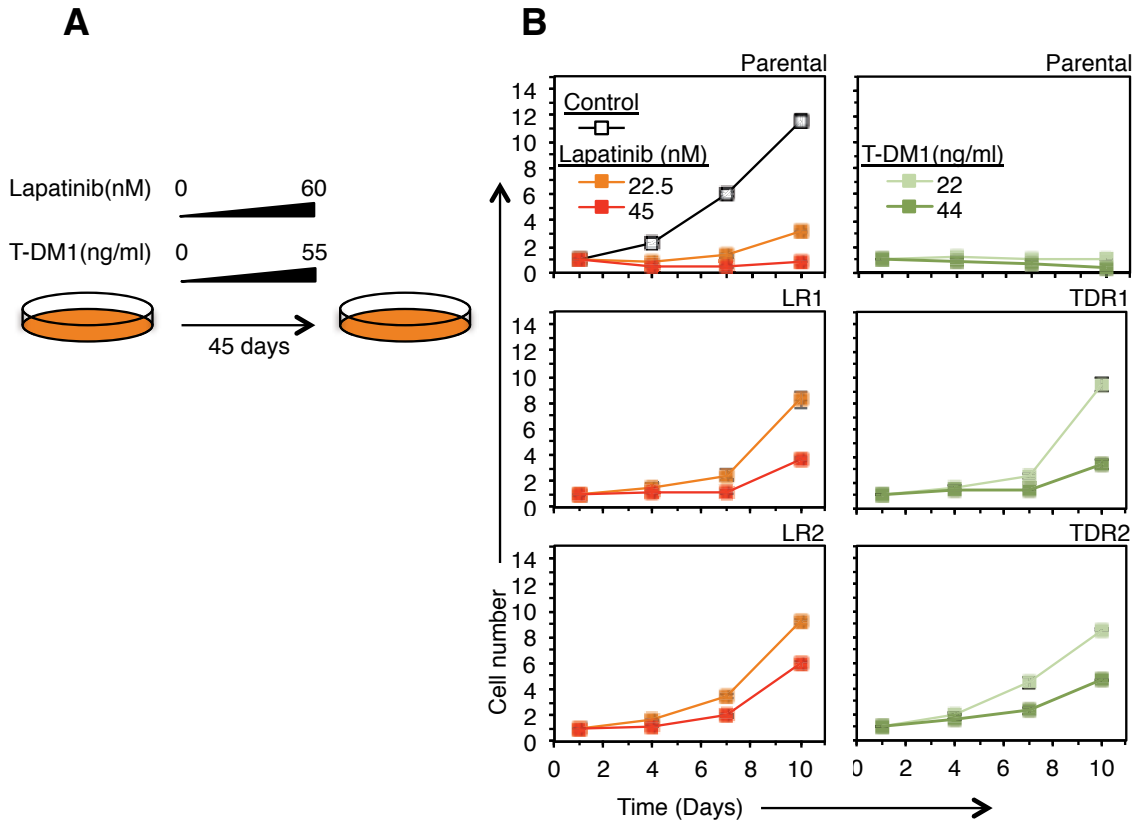

Figure 20: Generation of *in vitro* resistant cells to lapatinib and T-DM1 (A), Schematic showing the procedure to obtain cells resistant to anti-HER2 therapies *in vitro*. Cultures from PDX118 were treated with increasing concentrations of lapatinib or T-DM1 for 45 days. (B) Parental PDX118 cell cultures or cells selected in the presence of lapatinib or T-DM1 as shown in A, in two independent experiments, were plated in the presence of the indicated concentrations of the anti-HER2 drugs. At the indicated time points, cell proliferation was determined and normalized. The results were expressed as averages ± standard deviations. LR: Lapatinib resistant, TDR: T-DM1 resistant.

Analysis of two independent pools of lapatinib resistant cells showed a profound downregulation of HER2 protein by WB (Fig. 21A). However, quantification by qPCR confirmed the maintenance of HER2 gene copy number (Fig. 21B). Similar results were obtained with T-DM1 (Fig. 21A, B). Prolonged treatment *in vitro* with increasing concentrations of the antibody led to the appearance of resistant cells that showed a marked downregulation of HER2 (Fig. 20A, B and Fig. 21A). However, this HER2 protein downmodulation occurred without loss of HER2 gene copies (.. 21B).

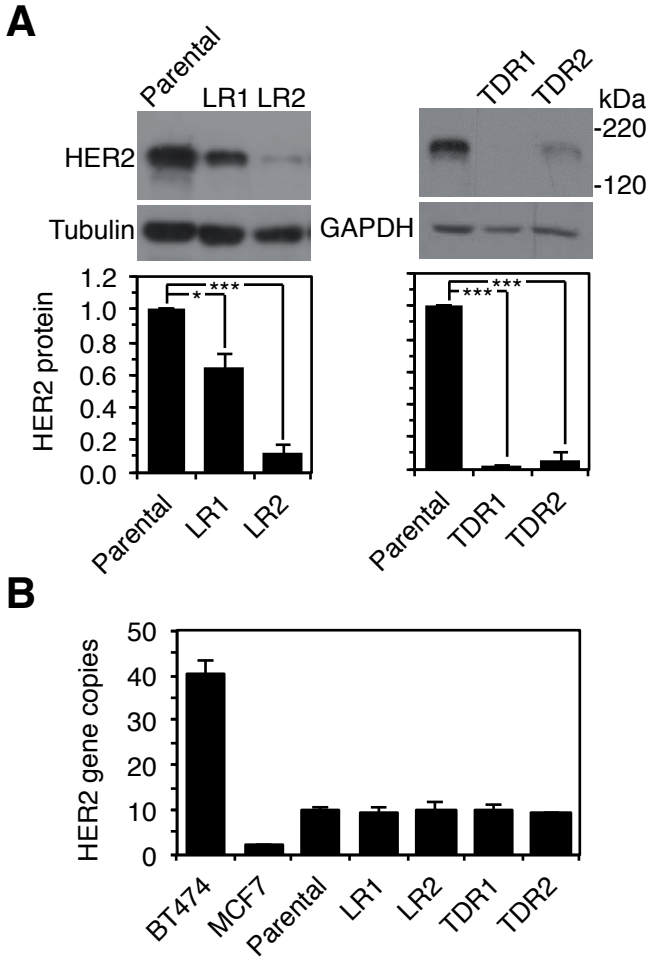

Figure 21: HER2 amplification pattern and gene copy number in cells resistant to lapatinib or T-DM. (A). The same cells as in Fig.20 were lysed and the cell lysates were analyzed by Western blot with antibodies against HER2 in three independent experiments. Representative results are shown. Blots were quantified and the results were expressed as averages ± standard deviations. *p* values shown were calculated by Student's t-test *, $p < 0.05$; ***, $p < 0.001$. (B) Gene copy number was determined by qPCR as described under Materials and Methods.

These results led us to conclude that acquired resistance of breast cancer cells to anti-HER2 therapies, even when concomitant with the loss of HER2 protein expression, is not due to the elimination of DMs encoding the receptor tyrosine kinase.

5. Characterization of Trastuzumab and T-DM1 PDX resistant models

After confirming in both, patient samples and PDX models, that the loss of DM copies was not a mechanism of resistance to anti-HER2 therapy, we decided to further characterize the PDX resistant models generated in this study to try to identify the resistance mechanism.

5.1. HER2 expression in resistant models

As seen in Figure 19, most of the resistant models lose in varying degrees the expression of HER2 even when retaining the HER2 gene copy number. Hence, we reasoned that the downmodulation of HER2 could be a consequence of a transcriptional or post-transcriptional mechanism. We performed qPCR analysis of HER2 transcript in these models, and observed that HER2 mRNA levels were slightly increased, suggesting that the downmodulation of HER2 was at the post-transcriptional level (Fig. 22)

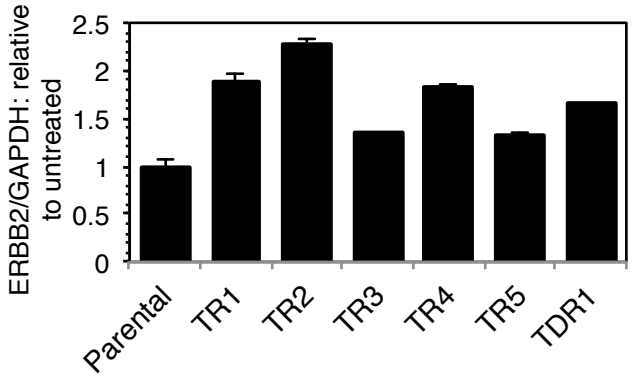

Figure 22: HER2 mRNA levels in trastuzumab and TDM-1 resistant models. RNA from resistant tumors was extracted and ERBB2 expression levels were determined by qPCR with TaqMan probes. GAPDH specific for human was used as control. Results are relativized to GAPDH and to parental tumors ERBB2 levels. TR: Trastuzumab resistant, TDR: T-DM1 resistant.

5.2. p95HER2 is not the cause of resistance

The presence of p95HER2 in HER2+ tumors is a cause of resistance to trastuzumab monotherapy [72]. This is a consequence of the inability of trastuzumab to bind to p95HER2. Even though not reported for T-DM1, this conjugated antibody binds to the same epitope as trastuzumab; it is likely that the same resistance mechanism applies to this drug. This prompted us to evaluate the presence of p95HER2 in our resistant PDX models. We carried out this by immunohistochemistry with an anti-p95HER2 antibody developed in the laboratory [39]. As seen in Figure 23, this HER2 isoform was not detected in our resistant models. Thus, the presence of p95HER2 is not the cause of the resistance to anti-HER2 therapy in this tumor.

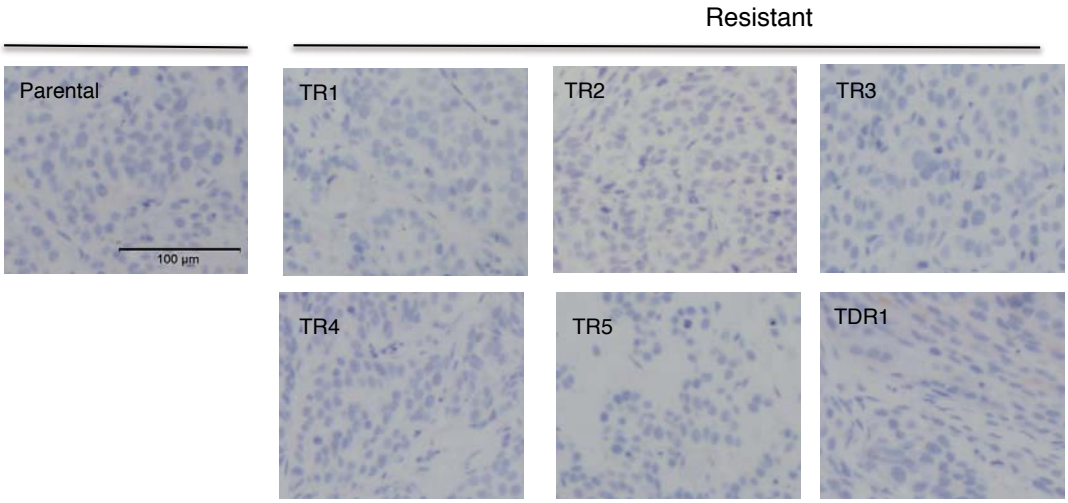

Figure 23: p95HER2 levels in trastuzumab and TDM-1 resistant tumors. Immunohistochemistry with an antibody that specifically recognizes p95HER2 was performed in trastuzumab and TDM-1 resistant models. TR: Trastuzumab resistant, TDR: T-DM1 resistant.

5.3. Genomic alterations in resistant models

We performed sequencing of 300 cancer related genes in the parental and the resistant PDX models (Appendix Table 3) to obtain information regarding copy number alterations and mutations in the resistant models compared to the parental tumor. Only a small number of alterations were detected. One of the interesting genomic alterations that arose in one of the resistant models (TR1) was the amplification of CCND1, the gene that codifies for Cyclin D1. It has been reported

previously that around 30% of HER2+ tumors have amplification in the CCND1 gene, however, its amplification as a result of trastuzumab resistance has not been reported [4]. On the other hand, Cyclin E has been previously associated with trastuzumab resistance [64]. Despite CCND1 copy number variation being slightly above normal (2.4), we decided to examine whether the amplification could be detected by fluorescent ISH (FISH) (Fig. 24A, upper images). The quantification confirmed a higher ratio CCND1/C11 (4.72) in the case of the resistant model. Despite this encouraging finding, when we checked mRNA and protein levels we did not detect an increase in Cyclin D1 with respect to the control (Fig. 24B, C). Also, immunohistochemical analysis of Cyclin D1 indicated that protein levels and pattern of expression was similar between parental and resistant tumors. (Fig. 24A, lower images). Thus, the amplification seen in the resistant model was not associated with an increase in protein level, indicating that this is not likely the mechanism of resistance in this model.

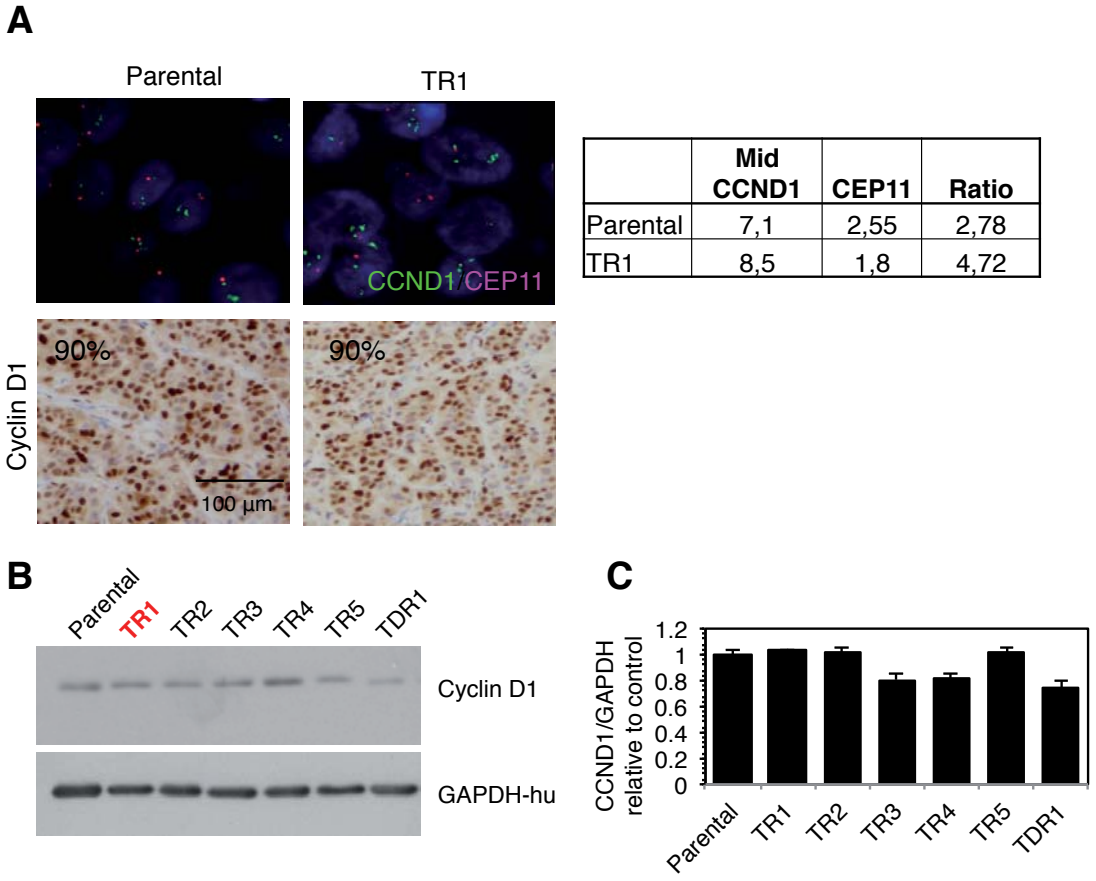

	Mid CCND1	CEP11	Ratio
Parental	7,1	2,55	2,78
TR1	8,5	1,8	4,72

Figure 24. Ciclyn D1 amplification, expression and protein levels in trastuzumab resistant model. (A). FISH analysis of CCND1 gene in TR1 and parental tumor. (B). Cyclin D1 protein levels were analyzed by Western Blot in lysates from trastuzumab and TDM-1 resistant models. (C). Cyclin D1 expression by TaqMan qPCR of trastuzumab and TDM-1 resistant models. GAPDH specific for human was used as control. Results are relativized to GAPDH and to parental tumors Cyclin D1 levels. TR: Trastuzumab resistant, TDR: T-DM1 resistant.

5.4. High activation of HER2 in TDR1 is not due to mutation of HER2 receptor

We also performed Receptor Tyrosine Kinase array in the resistant tumors to detect possible activation of other RTKs in response to the therapy. Despite the lowered HER2 levels shown in Figure 19, we were surprised to observe increased levels of pHER2 in T-DM1 resistant model (Fig. 25). Activating mutations in ERBB2 and ERBB3 have been described in the past [30, 98]. Therefore, we sequenced the entire HER2 gene by HaloPlex, but did not detect any mutation in HER2.

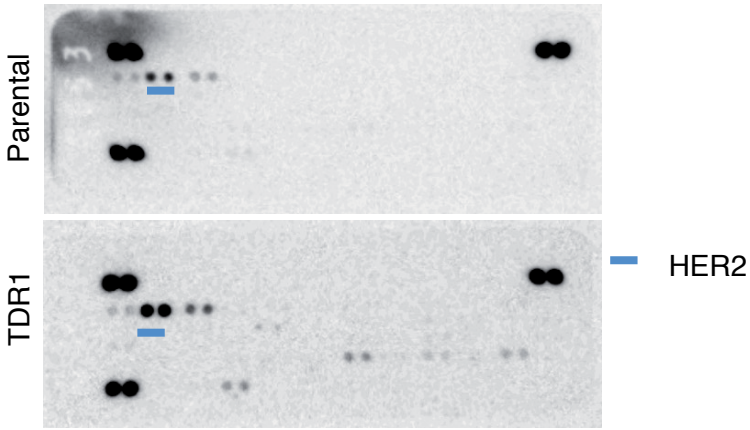

Figure 25: RTK analysis of parental and T-DM1 resistant tumor. RTK array was perfromed on lysates from parental and T-DM1 resitant tumor. Marked in blue and pHER2 levels TDR: T-DM1 resistant

In summary, we have shown that downmodulation of HER2 protein appears to be a post-translational mechanism. However, we have not been able yet to clarify the mechanism. In addition, no clear genetic alterations were observed in the resistant models compared to the parental one.

Results: Section 2

“p95-TCB, a T Cell bispecific antibody that targets a truncated form of HER2”

1.A T cell bispecific antibody targeting p95HER2 and CD3

p95HER2, a truncated form of HER2, present in 30% of HER2+ breast cancer is a protein which expression is associated with high levels of HER2 [41]. Therefore, it can only be detected in tumoral tissue and, compared to HER2 expression, at lower levels. Our laboratory and others have developed antibodies against this truncated form that allows the detection of this specific isoform in relevant clinical samples [39] [40]. Up to now, the potential use of these antibodies, as a therapeutic tool has not been assessed.

To increase the chances of p95HER2 antibodies of having a significant therapeutic effect, we engineered in collaboration with Roche pharmaceuticals, our p95HER2 antibody to become a T cell bispecific antibody (p95-TCB). The process was carried out in a similar fashion as described for other TCBs [79]. As mentioned previously in the introduction, T cell bispecific antibodies activate immune responses very potently, even at low antigen expression. Therefore p95HER2 resulted to be a very attractive tumor antigen to target with this technology due to its expression level and specificity. p95-TCB was designed to bind simultaneously p95HER2 present on tumor cells, and CD3ε, a subunit of the T cell receptor (TCR) present on T lymphocytes (Fig. 26). Importantly, the antibody has a mutated Fc domain and therefore is not able to bind innate immune cell components reducing the potential cross-linking between immune cells. Additionally, the use of an IgG isotype facilitates the purification and it improves the half-life.

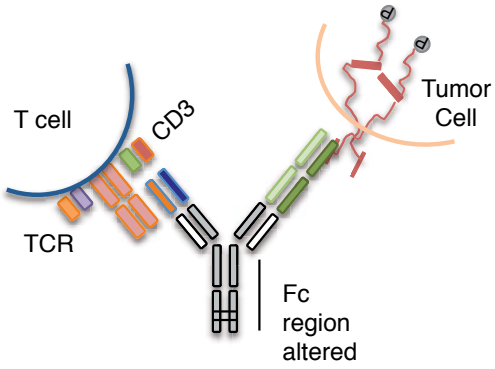

Figure 26: Schematic representation of p95-TCB. p95-TCB binds to CD3ε, part of the TCR, and to p95HER2 on tumor cells. Fc region is mutated

2. p95-TCB mode of action: in vitro assays

Antibody binding, T cell activation and tumor cell lysis assays were performed *in vitro* to evaluate the effect of p95-TCB on both tumor and T cells.

2.1 p95-TCB binds to CD3 and p95HER2 expressing cells

To determine whether the p95-TCB developed was able to bind to the CD3 receptor, we used Jurkat cells, an immortalized cell line of human T lymphocytes which maintains CD3 expression. This cell line is commonly used for studying T cell leukemia and T cell signaling. We observed that p95-TCB binds to Jurkat cells in a concentration dependent-manner (Fig 27A).

In order to evaluate the binding of the antibody to p95HER2, we used MCF10A cells, which were derived from benign proliferative breast tissue and are non-tumorigenic and negative for HER2 overexpression [99]. We stably expressed p95HER2 using a CTF-611 sequence, full-length HER2 or both concomitantly [36] (Fig. 27B). We detected that p95-TCB was able to bind significantly to p95HER2 expressing cells with or without concomitant HER2 expression, whereas the antibody exhibited little binding in HER2 only expressing cells (Fig. 27C).

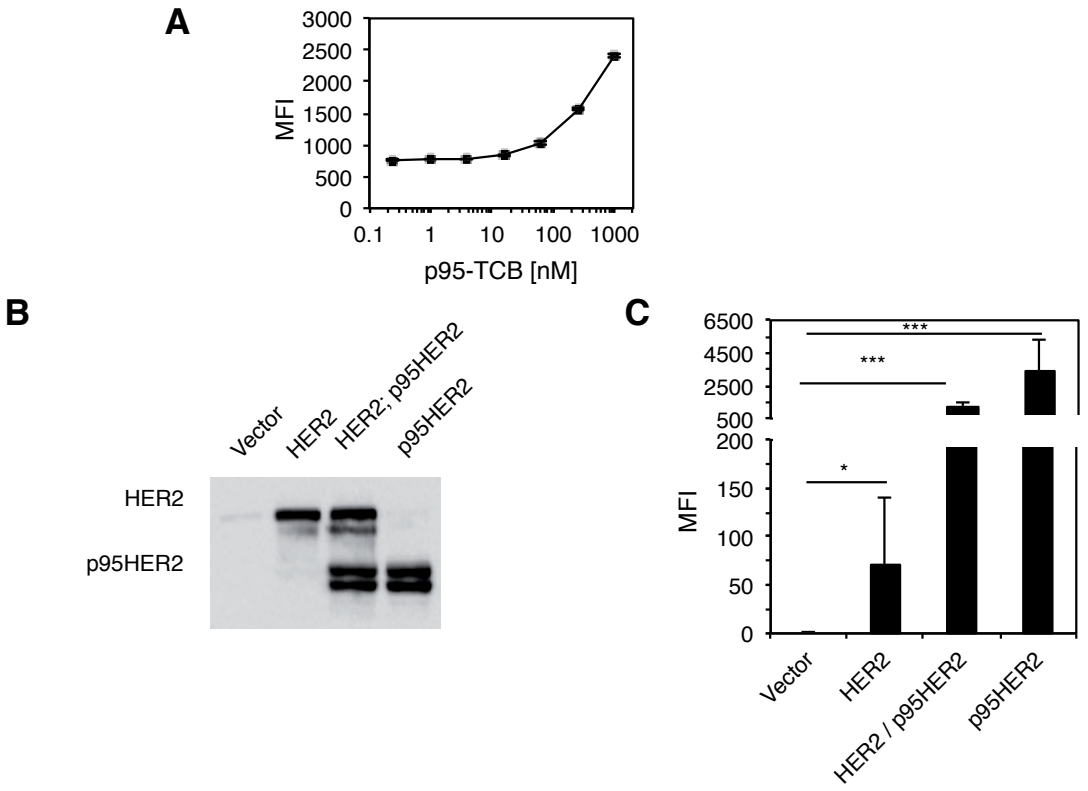

Figure 27: p95-TCB binding to CD3 and p95HER2 expressing cells. (A). Jurkat cells were incubated with increasing concentrations of p95-TCB. Binding was analyzed by flow cytometry using an Alexa 488-coupled anti-human secondary antibody. (B). Western Blot analysis of MCF10A cells stably transduced with Empty Vector, p95HER2, HER2, or both. (C) MCF10A cells were incubated with 2ug/ml of p95-TCB and binding of the antibody was analyzed by flow cytometry. MFI: median fluorescence intensity. Graphs represent the mean of three independent experiments. *p* values shown were calculated by Student's t-test *$p<0.05$, **$p<0.01$, ***$p<0.001$.

Notably, p95-TCB binding in HER2 expressing cells was significantly higher than cells transduced with the vector alone (Fig. 27C), suggesting either that p95HER2 antigen was being generated from alternative initiation of translation from the full-length HER2 or, that the antibody was binding non-specifically to HER2. In order to decipher which of the two possibilities was taking place, we generated MCF10A cells expressing full-length HER2 with a mutation in the methionine codon 611 (M611A), to prevent the generation of the 611-p95HER2 isoform (Fig. 28A). Importantly, MCF10A-HER2 and MCF10A-HER2 (M611A) displayed comparable levels of cell surface HER2 when analyzed by trastuzumab binding (Fig. 28B).

The presence of the mutant HER2 prevented the binding of p95-TCB in these cells, confirming that the p95-TCB antibody binds specifically to p95HER2 (Fig. 28B).

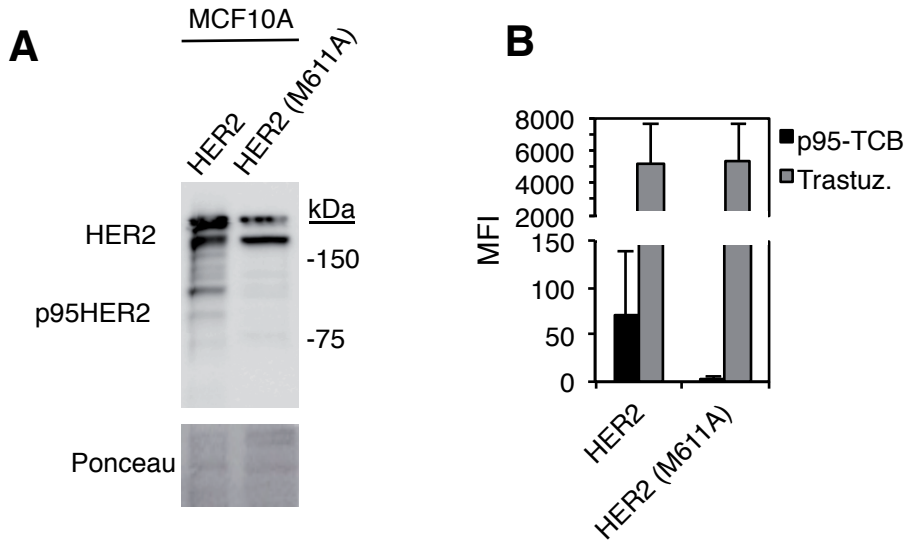

Figure 28: p95-TCB specific binding to p95HER2. (A). Western Blot analysis of MCF10A cells stably transduced with full length HER2 or with HER2 (M611A). (B). Cells in A were incubated with 2ug/ml of p95-TCB or trastuzumab and binding of the antibodies was analyzed by flow cytometry. MFI: median fluorescence intensity. Graphs represent the mean of three independent experiments. MFI: median fluorescence intensity.

Since endogenous levels of p95HER2 in tumor cells are lower than in cells ectopically overexpressing p95HER2, it was important to evaluate the capacity of p95-TCB to bind to endogenous p95HER2. Therefore we evaluated antibody binding in primary cultures from a p95HER2 positive and negative HER2+ breast cancer PDXs (Fig. 11 and Fig. 29A). We also used a TNBC PDX as negative control. We detected binding of p95-TCB to p95HER2 only in the case of cells derived from the p95HER2 positive PDX (Fig. 29B).

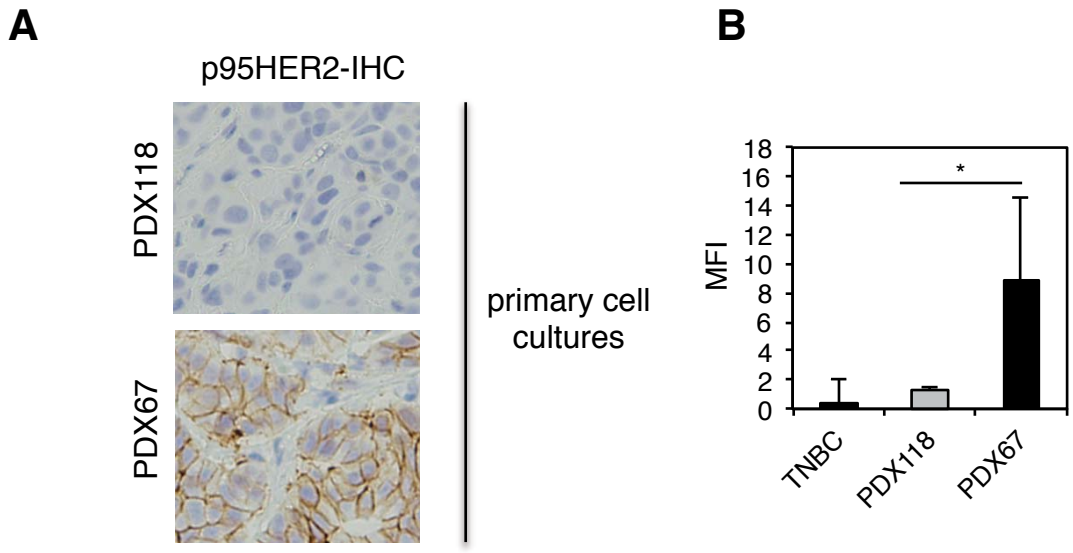

Figure 29: p95-TCB binding to endogenous p95HER2 in PDX cell lines. (A). Primary cultures derived from of a p95HER2 negative PDX (PDX118) and a p95HER2 positive PDX (PDX118) were generated. Cells were grown in culture, embedded in paraffin blocks as pellets and analyzed by IHC using p95HER2 32H2. (B). Cells derived from the primary cultures in A and cells derived from a TNBC PDX were incubated with 2 ug/ml of p95-TCB and binding of the antibody was analyzed by flow cytometry. MFI: median fluorescence intensity. Bar graph represents the mean of three independent experiments. *p* values shown were calculated by Student's t-test *p<0.05, **p<0.01, ***p<0.001.

All together these results confirm that p95-TCB binds specifically to both p95HER2-expressing cells and to CD3 positive T cells.

2.2 p95-TCB induces the activation of T cell lymphocytes in the presence of p95HER2 positive cells

Previous studies have shown that, upon binding to target and effector cells TCBs induce the activation of T cells [79, 100]. To evaluate if our antibody was activating T cells in a likewise manner, p95HER2 positive and negative cells were incubated in the presence of antibody and peripheral blood mononuclear cells (PBMCs) obtained from healthy donors. CD25 and CD69 activation markers on CD4 and CD8 T cells were assessed by flow cytometry. CD69 is the earliest glycoprotein

that appears on the cell surface upon activation of T cells. CD25 is the alpha chain of the IL-2 receptor and is also only present on activated T cells, a cytokine promoting T cell proliferation upon antigen recognition. Both activation markers are detected after high affinity interaction between the TCR and the antigen. A significant rise in the percentage of CD4 and CD8 cells expressing CD69 and CD25 was observed in PBMCs exposed to p95HER2 expressing MCF10A only in the presence of p95-TCB (Fig. 30A). Furthermore, T cell activation showed a p95-TCB concentration-dependent profile (Fig. 30A). Importantly, a significant induction of CD8+ CD69+ and CD8+ CD25+ cells by p95-TCB was observed only with the PDX67 cell-line that naturally expresses p95HER2, but not in the p95HER2 negative PDX118 which expresses full-length HER2 (Fig. 30B). As expected, due to the lower p95HER2 endogenous levels, the effect was seen at higher concentrations of antibody. Therefore, p95-TCB engagement of both CD3 on T-cell and p95HER2 on either MCF10A (overexpressed) or PDX cells (endogenous expression) triggers the activation of T cells.

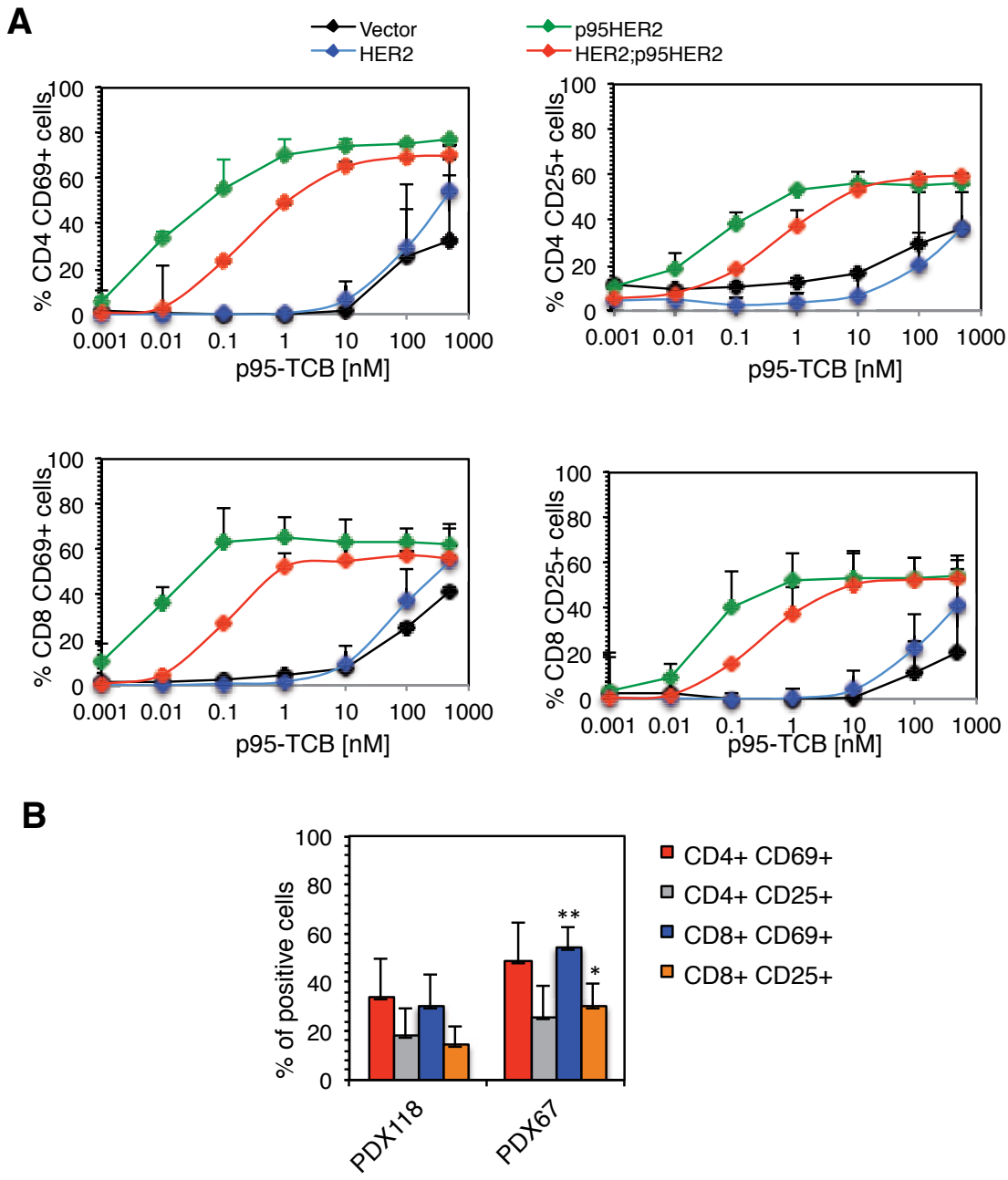

Figure 30: T cell activation induced by p95-TCB. (A) MCF10A cells were incubated with increasing concentrations of p95-TCB and with PBMCs in a ratio 10:1. After 48 h PBMCs were collected, stained for huCD45/CD8/CD4/CD69/CD25 and analyzed by flow cytometry. Graph represents the mean of three independent experiments and show the % of CD8 or CD4 positive for the activation markers CD25 or CD69. (B) PDX derived cells were treated as in A. Graph represents de activation at the higher concentration of p95-TCB 500 nM. *p* values shown were calculated by Student's t-test *$p<0.05$, **$p<0.01$.

As a further indication of T cell activation, we detected IL-2 and interferon gamma secretion in the culture supernatants of the T cell co-cultured with p95HER2-

expressing cells in the presence of p95-TCB (Fig. 31). These two cytokines are known to be secreted by activated T cells and induce their proliferation [101]. We also detected the enzyme contained within the cytotoxic granules of CD8+ T cells Granzyme B that is released by T cells to eliminate target cells (Fig. 31). The secretion of these cytokines was detectable only when T cells were incubated with the p95-TCB and p95HER2 positive cells but not with p95HER2 negative cells, both in the overexpressing MCF10 model (Fig. 31, right graph) as in the endogenous PDX67 model (Fig. 31, left graph). These results demonstrate that p95-TCB can functionally activate T-cells only in the presence of target-antigen expressing cells such as patient-derived breast cancer cells.

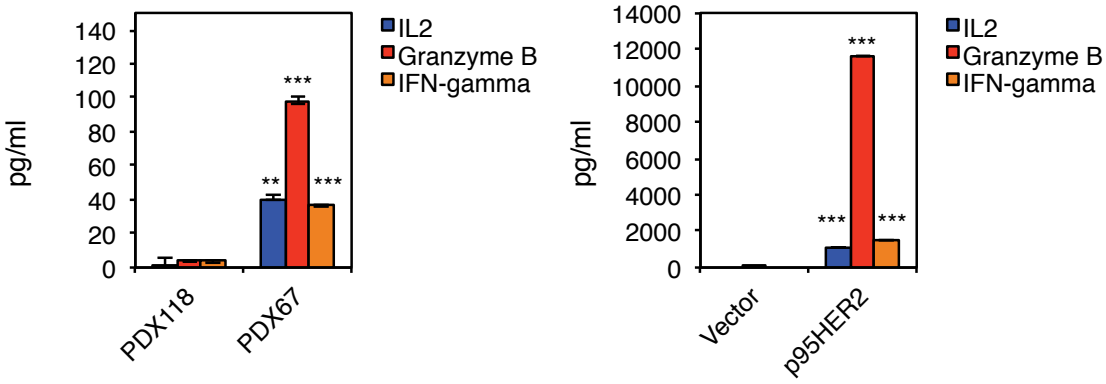

Figure 31: p95-TCB-induced the secretion of activating cytokines. Following the same scheme as in Figure 30, PDX-derived cell lines (left) or MCF10A transduced cells (right) were incubated with p95-TCB (500nM) and with PBMCs in a ratio 10:1. After 48 h supernatants were collected and cytokines were detected by flow cytometry. A representative graph of two independent experiments is shown. *p* values shown were calculated by Student's t-test $^{**}p<0.01$, $^{***}p<0.001$.

2.3 p95-TCB promotes the lysis of p95HER2 positive cells

Since p95-TCB induced the binding and activation of T cells only when incubated with p95HER2 positive cells, we next evaluated whether this resulted in tumor cell lysis. Cell lysis was assayed by the release of lactate dehydrogenase (LDH) enzyme from dead cells. We observed an antibody concentration-dependent killing of MCF10A cells expressing p95HER2, but not in full-length HER2 or control cells

(Fig. 32A). The same experiment was performed in the cell lines obtained from the p95HER2 positive and negative PDX67 and PDX118, respectively. Notably, at the highest concentration used, p95-TCB induced significant higher T-cell mediated killing of PDX67 tumor-derived cells compared to PDX118 cells (Fig. 32B).

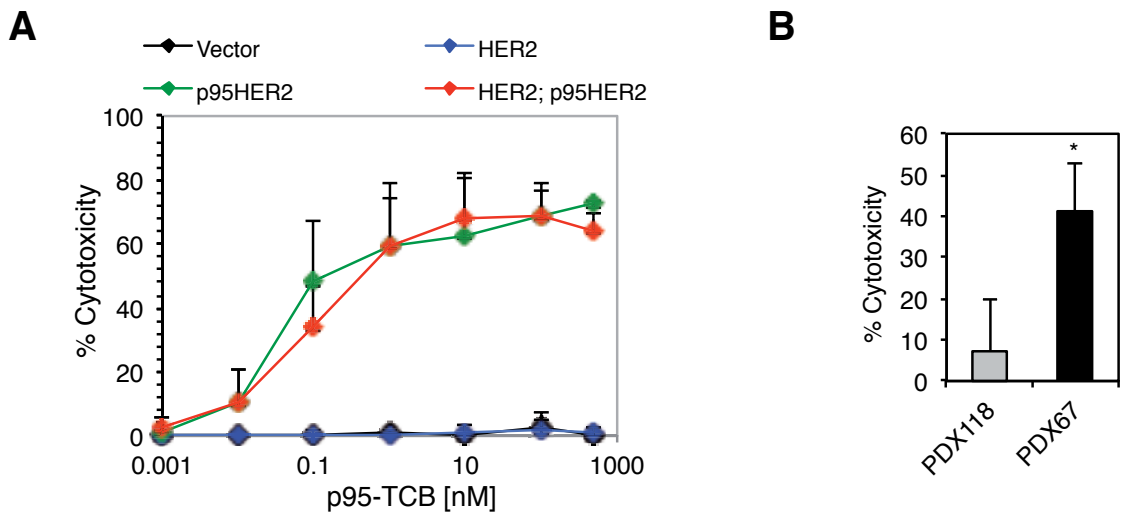

Figure 32: Tumor cell lysis induced by p95-TCB. (A) MCF10A cells were incubated with increasing concentrations of p95-TCB and with PBMCs in a ratio 10:1. After 48 h supernatants were collected and lysis was measured by LDH release. (B) PDX cell lines were treated as in A at a fixed concentration of 500 nM. Graph represents the mean of three independent experiments. *p* values shown were calculated by Student's t-test comparing PDX118 to PDX67. **p*<0.05.

All together these results demonstrate that p95-TCB is able to bind to p95HER2 positive tumor cells and to CD3 lymphocytes promoting the activation of the T-cells and the subsequent lysis of the tumor cell.

3. p95-TCB is a safe therapeutic option for HER2+ tumors

3.1 HER2 TCB lysates HER2 low expressing breast cancer cells

Bispecific antibodies targeting HER2 have also been developed [81]. It has been

reported that HER2-TCB is able to kill HER2+ cells at very low concentrations [81]. Importantly, that effect is also observed in low HER2 expressing cells. This raises very important safety concerns for this molecule as HER2 receptor is broadly expressed in healthy tissues. Therefore, in order to evaluate whether p95-TCB could represent a safe therapeutic option, we compared the efficacy of HER2-TCB and p95-TCB antibodies in breast cancer cell carrying different levels of HER2. We observed that HER2-TCB but not p95-TCB promoted the lysis of MCF10A cells, a cell line that is used as model for normal breast and is not considered positive for HER2 amplification/overexpression (Fig. 33A). When using MCF7 cells, which are a breast tumor cell line negative for HER2, we again detected cell killing with HER2-TCB but not with p95-TCB (Fig. 33A). To further examine the effect of both TCBs on HER2 negative cells, we measured T cell activation upon incubation of MCF10A cells with what has been reported a low antibody concentration (1nM). The evaluation of the percentage of CD4 and CD8 cells positive for CD25 and CD69, revealed high level of T cell activation only when MCF10A cells where incubated with HER2-TCB (Fig. 33B).

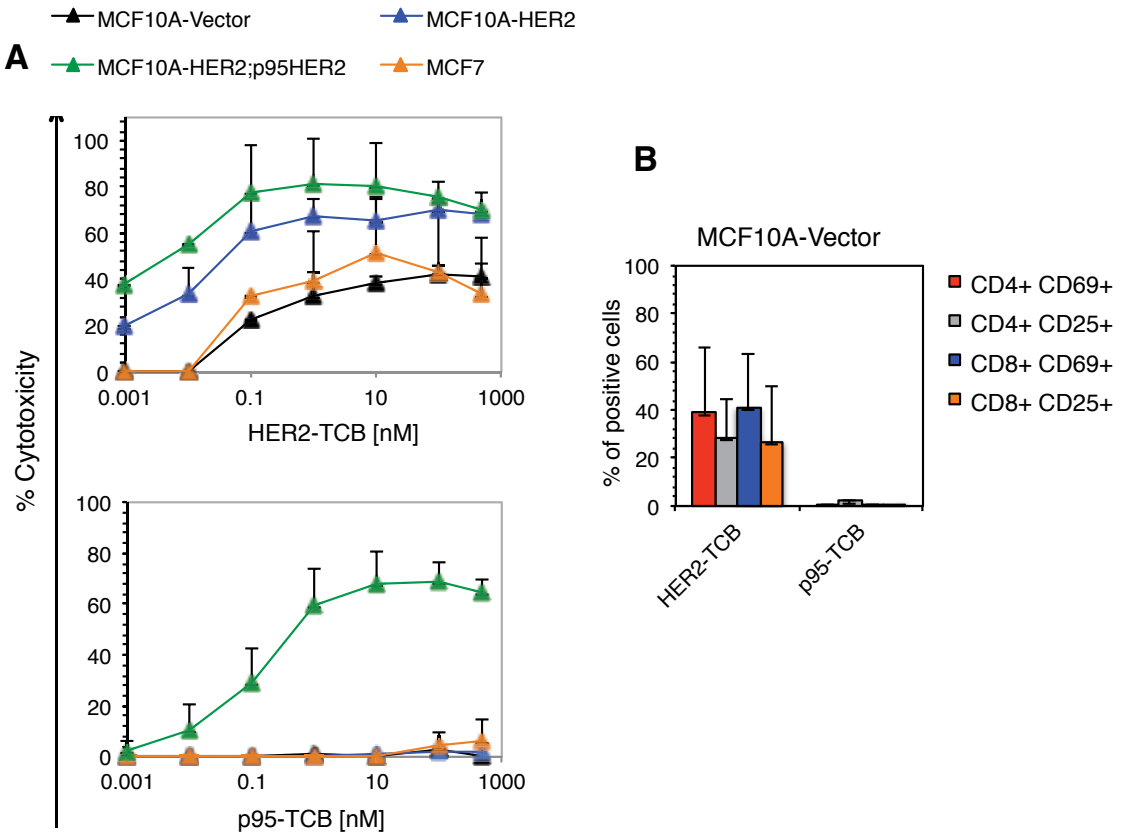

Figure 33: HER2-TCB and p95-TCB T cell activation and tumor cell lysis. (A) MCF10A cells and MCF7 cells were incubated with increasing concentrations of HER2-TCB or p95-TCB and with PBMCs in a ratio 10:1. After 48 h supernatants were collected and lysis was measured by LDH release. (B) PBMCs from MCF10A-Vector in A were collected, stained for huCD45/CD8/CD4/CD69/CD25 and analyzed by flow cytometry. Graph represents the mean of three independent experiments and show the % of CD8 or CD4 that are positive for the activation markers CD25 or CD69. Graph represents the mean of three independent experiments.

3.2 Cardio toxicity assay for HER2-TCB and p95-TCB

Some human tissues express low levels of HER2. Cardiac tissue is one of them and is in fact a major concern when oncologists use trastuzumab in patients with heart-related pathologies. Therefore, we decided to compare the effect p95-TCB and HER2-TCB in cardiomyocytes that express HER2 levels in a comparable level as that of MCF7 cells [102]. We detected an increased binding of HER2-TCB compared to p95-TCB on human cardiomyocytes (Fig. 34A). In the co-culture experiments with PBMCs, this was accompanied by an increase in the activation marker CD25 on both CD8 and CD4 T cells in the presence of HER2-TCB but not

of p95-TCB (Fig. 34B). Finally, we observed the lysis of the human cardiomyocytes when incubated with PBMCs and HER2-TCB but not p95-TCB (Fig. 34C).

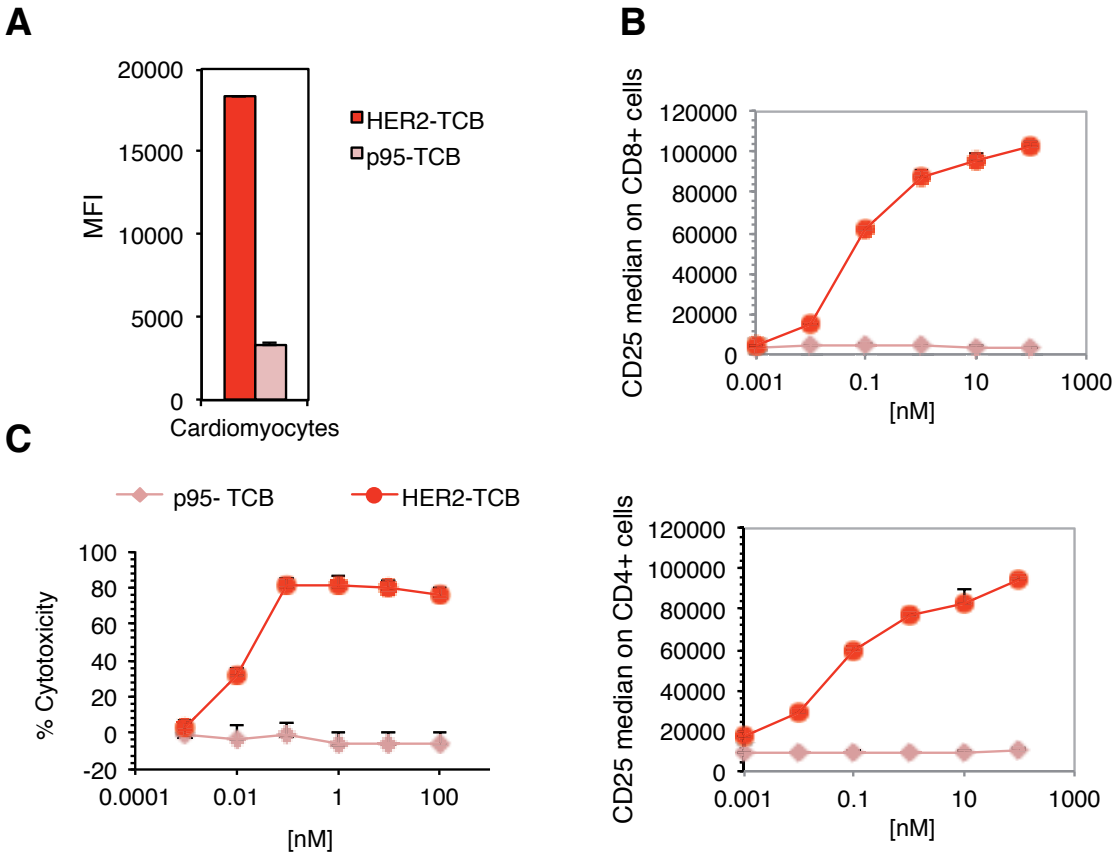

Figure 34: HER2-TCB and p95-TCB effect of human cardiomyocytes. (A) Human cardiomyocytes were incubated with 2ug/ml of HER2-TCB or p95-TCB and binding was analyzed by flow cytometry. (B) Cells in A were incubated with increasing concentrations of HER2-TCB or p95-TCB and with PBMCs in a ratio 10:1. After 48h supernatants cells were collected and stained for huCD45/CD8/CD4/CD69/CD25. (C) Supernatants from B were collected and lysis was measured by LDH release. Graph represents the mean of three independent experiments.

All together this data indicates that compared to classical HER2-TCBs, p95-TCB has the potential advantage of sparing normal tissues with low HER2 expression from undesired killing, making it a safer therapeutic option for the subset of patients to which is indicated.

4. p95-TCB pharmacokinetics

Bispecific antibody half-life is one of the main limitations of these therapeutic agents, since it limits the utilization of such short lasting molecules [75]. Therefore, we performed a pharmacokinetic study to evaluate the half-life of p95-TCB. Mice were administered the antibody intravenously and blood was extracted at different time points. Serum was analyzed by ELISA to specifically detect TCB levels. The half-life of p95-TCB was determined to be 4 days (Fig. 35).

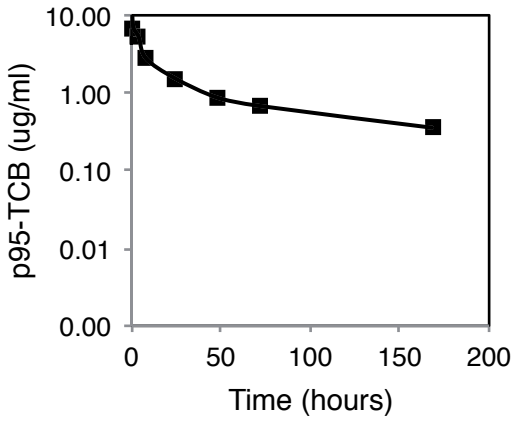

Figure 35: p95-TCB pharmacokinetics. p95-TCB was administered intravenously to mice and concentration of the TCB was measured by ELISA in mouse serum.

5. Effect of p95-TCB in tumor growth *in vivo*

After the in vitro evidence showing that p95-TCB was able to bind simultaneously to p95HER2 on tumor cells and to CD3 present on T cells, promote the activation of the later and subsequent lead to lysis of the tumor cells, we aimed to test the *in vivo* efficacy of the antibody in humanized mice bearing xenografts. The humanization model selected was the PBMC transfer model, an efficient setting to test therapies that rely mainly on T cell effect (see Introduction).

We first tested *in vivo* the effect of p95-TCB in an inducible system of p95HER2 on

MCF7 cells. Work from our lab has previously shown that the expression of high levels of p95HER2 (611-isoform) induces senescence in MCF7 cells [37]. This was confirmed in a Tet-on system where the expression of p95HER2 was induced by doxycycline (Fig.36 A. sh-NT, +Dox). In this cellular model, MCF7 expressing p95HER2 do not proliferate as compared to non-p95HER2 expressing ones (Fig. 36B left graph, +Dox vs -Dox) and exhibit an enlarged phenotype typical of senescent cells (Fig. 36C, sh-NT +Dox). More recently, we observed that silencing of p21, a key regulator of senescence, in MCF7-p95HER2 prevents the senescence phenotype (Bernado, et al. Unpublished). This is shown by the normal appearance of the cells (Fig. 36C, sh-p21 +Dox). The prevention of senescence allows MCF7-p95HER2-shp21 cells to proliferate in the same manner as MCF7 cells with no induction of p95HER2 expression (Fig. 36B, right graph +Dox vs -Dox).

Unfortunately, MCF10A cells used in the *in vitro* assays do not grow in mice. Therefore, MCF7-p95HER2-shp21 cells, that appear to behave as parental MCF7 cells and that are able to establish xenografts in mice, represent a good model to test the effect of p95-TCB *in vivo*. Furthermore, p95-TCB induced the killing of MCF7 only when expression of p95HER2 was induced by doxycycline (Fig. 36D).

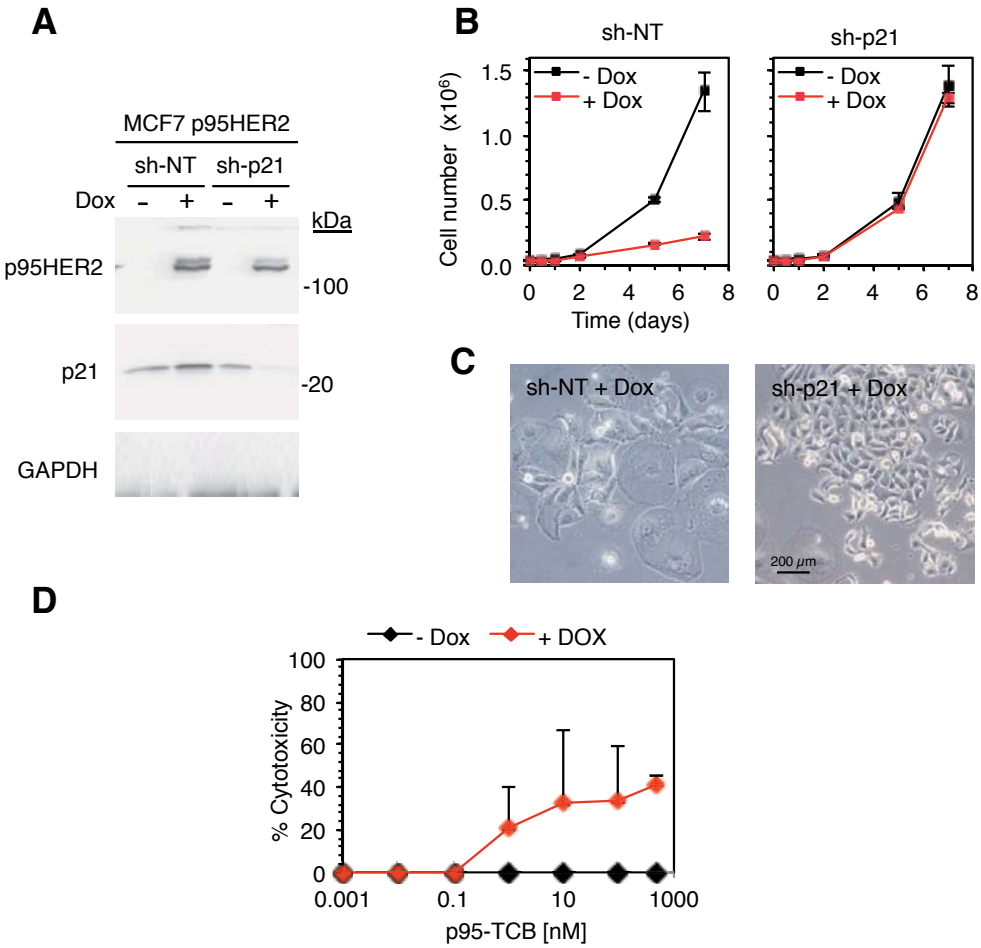

Figure 36: p95-TCB induces the killing of MCF7 Tet-Off p95HER2. (A) MCF7 Tet-On p95HER2 cells were transfected with vectors encoding control shRNAs or a shRNA targeting p21. Expression of p95HER2 in MCF7 cells in the presence of a proficient p21 leads to oncogene-induced senescence as determined by inhibition of cell proliferation (B) and a profound morphological change (C). (D) Cells in A were incubated with PBMCs in a proportion 10:1 and after 48 h supernatants were collected and lysis was measured by LDH release.

MCF7-p95HER2-shp21 were orthotopically injected in NSG mice and when tumors reached in average of 150-200 mm^3, mice were injected with PBMCs isolated from buffy-coats from healthy donors (Fig. 37). At this time point, p95HER2 expression was also induced by the addition of doxycycline to the drinking water of the animals. Treatment with vehicle or p95-TCB was initiated 2 days post PBMC injection and maintained bi-weekly until the end point of the experiment (Fig. 38A, arrow heads).

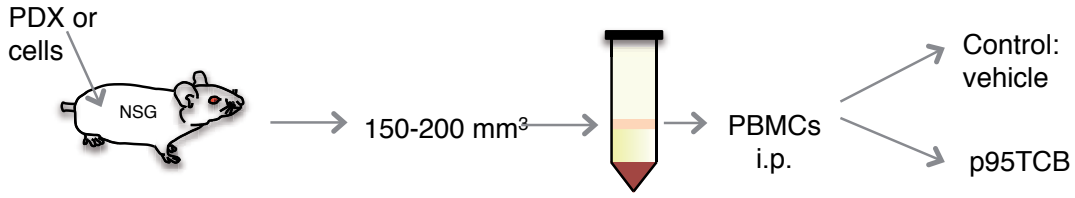

Figure 37: Experimental model to evaluate the in vivo efficacy of p95-TCB. Workflow followed for the in vivo assays. NSG mice were injected with MCF7 cells or PDX. When tumors reached 150-200 mm^3, mice were injected with $10x10^6$ PBMCs obtained from healthy donors and isolated by ficoll gradient centrifugation. 48 h post humanization with PBMCs, animals were administrated with vehicle or p95-TCB 1 mg/kg i.v. bi-weekly.

Two weeks after PBMC injection, we extracted blood from the animals to determine the levels of huCD45 in circulating blood. huCD45 was detected, indicating humanization, and no significant difference was observed between the animal groups used for treatment (Fig. 38B). Fifteen days after the beginning of the treatment we observed a significant anti-tumor effect of p95-TCB, resulting in a nearly complete regression of p95-TCB treated tumors and reduction in tumor weights (Fig. 38A, C). The late antitumor response was most likely due to the exponential expansion of PBMCs at this stage. Immunohistochemical staining in the small fibrotic pieces extracted at the end point of the experiment with an antibody that specifically stains human epithelial tissue (human cytokeratin) showed that no human epithelial tissue remained in p95-TCB treated tumors, whereas control group tumors were positive (Fig. 38D). The lack of human epithelial cells was further confirmed with the staining of p95HER2 (Fig. 38D).

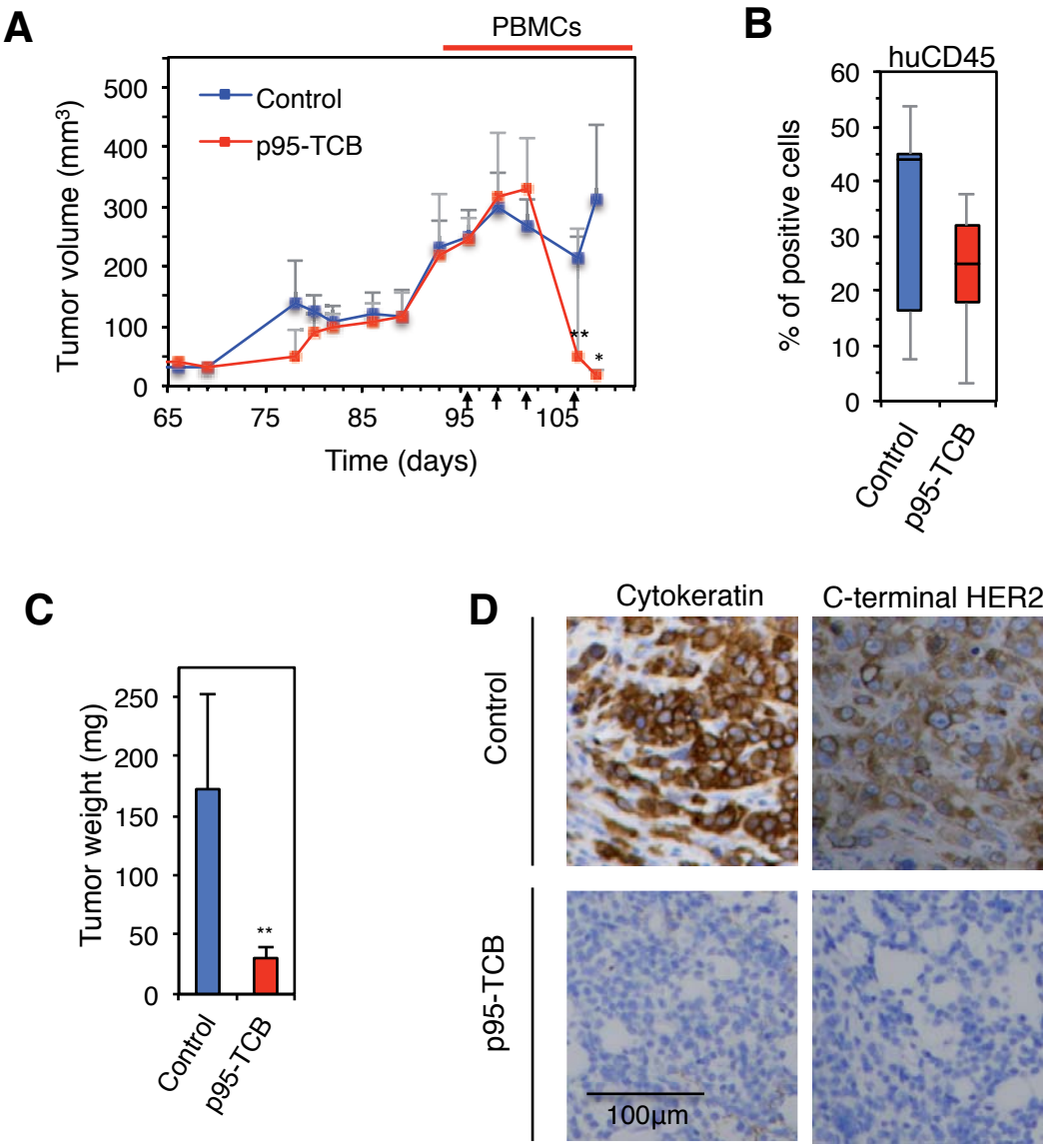

Figure 38: Effect of p95HER2-TCB on the growth of xenografts expressing p95HER2. (A). NSG mice (n=6 per group) were injected with 10^6 MCF7 Tet-On p95HER2-shp21 cells following workflow in Figure 37. (B) Two weeks post PBMC injection, blood was extracted and levels of human CD45 were analyzed by flow cytometry. Box plots show the percentage human $CD45^+$ cells in the mice. Lower and higher whiskers indicate 10^{th} and 90^{th} percentiles, respectively; lower and higher edges of box indicate 25^{th} and 75^{th} percentiles, respectively; the inner line in the box indicates 50^{th} percentile. (C) At the end of the experiment tumors were removed and weighed. (D) Tumors included in paraffin blocks and were analyzed by IHC for cytokeratin and p95HER2. Representative tumor from an animal from the control group and p95HER2 group is shown. The results are expressed as averages; error bars correspond to 95% confidence intervals. *p* values shown were calculated by Student's t-test *$p<0.05$, **$p<0.01$.

The use of PDX would allow us to test the effect of the TCB antibody in an animal model that better resembles a human tumor and, importantly, that carries endogenous levels of p95HER2.

Due to technical problems with PDX67, the p95HER2+ PDX from which the cell culture was established and used to test the *in vitro* effects of p95-TCB, we choose another PDX model positive for p95HER2 expression (PDX173) (Fig. 39A). PDX implantation and humanization of mice was performed following the workflow previously shown (Fig. 37) Levels of huCD45 in blood 15 days post-PBMC injection reveled a very homogenous degree of humanization in both groups with a mean between 15 and 20 % of huCD45 (Fig. 39C and representative FACS in Fig. 42). p95-TCB induced a significant reduction in both tumor volume and weight as compared with vehicle treated animals (Fig. 39D). Once again, anti-tumor response was observed in the last days of treatment, most likely due to the exponential expansion of PBMCs at this stage (Fig. 39B).

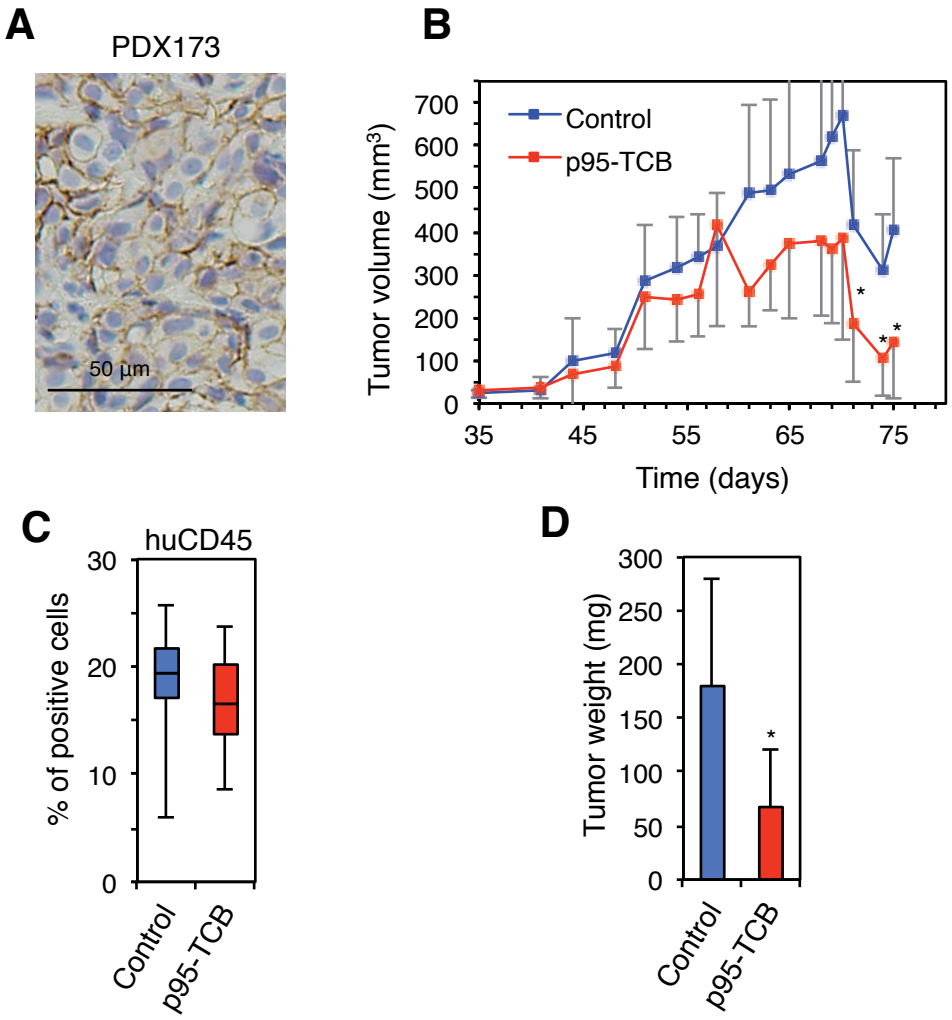

Figure 39. Effect of p95HER2 TCB on the growth of a PDX expressing p95HER2. (A) Analysis of the expression of p95HER2 by IHC in PDX173 used for the assay. (B) NSG mice (n=8 per group) were injected with PDX173 following workflow in Figure 37. (C) Levels of human $CD45^+$ were analyzed in blood by flow cytometry 15 days after PBMC injection. Lower and higher whiskers indicate 10^{th} and 90^{th} percentiles, respectively; lower and higher edges of box indicate 25^{th} and 75^{th} percentiles, respectively; the inner line in the box indicates 50^{th} percentile. (D) At the end of the experiment tumors were removed and weighted. The results are expressed as averages; error bars correspond to 95% confidence intervals. *p* values shown were calculated by Student's t-test *$p<0.05$.

In this *in vivo* study, residual tumoral tissue was remaining in the p95-TCB treated group. Therefore, we were able to analyze by both flow cytometry and immunohistochemistry whether p95-TCB increased the immune infiltrate within the tumors.

By flow cytometry, we observed a significant increase of total huCD3 and more specifically huCD8 in tumors of mice that received p95-TCB compared with the control group (Fig.40 and representative FACS Fig. 42). Notably, T cell infiltrate increased in tumors from p95-TCB treated animals up to 50%, a greater than 2-fold increase.

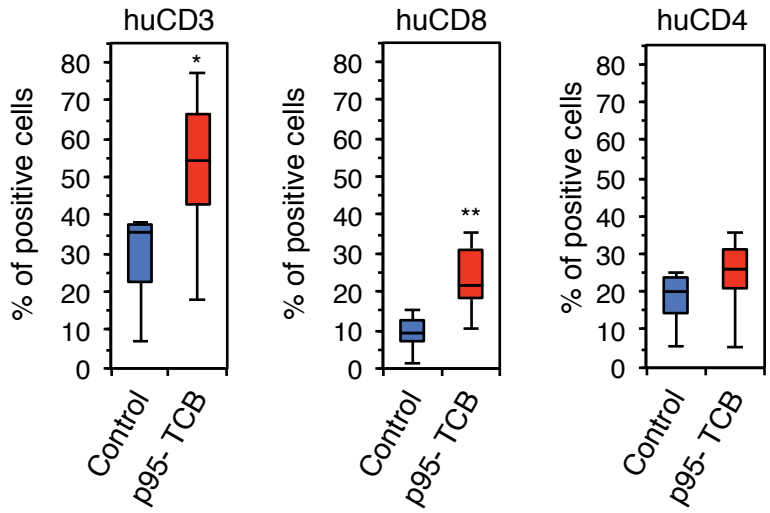

Figure 40: Effect of p95HER2 TCB in tumor T cell infiltration assessed by flow cytometry. At the end of the experiment shown in Fig. 39, tumor samples were disaggregated to single cells, stained with anti-human CD3, CD8 and CD4, and the number of positive cells quantified by flow cytometry. Box plots show the percentage of the cells positive for the indicated marker. Lower and higher whiskers indicate 10th and 90th percentiles, respectively; lower and higher edges of box indicate 25th and 75th percentiles, respectively; the inner line in the box indicates 50th percentile. *p* values shown were calculated by Student's t-test *$p <$ 0.05, **$p < 0.01$.

This was also confirmed by huCD8 immunohistochemical stainings, where we detected a significant increase of these cells in the p95-TCB treated group (Fig. 41). This was accompanied by a significant decrease in cytokeratin staining (Fig. 41). Interestingly, in the areas where we detected a higher number of CD8 T cells, we observed a concomitant reduction of tumoral tissue. Mouse stroma and necrotic tissue were most likely the remaining material in these samples that scored negative for human tumor.

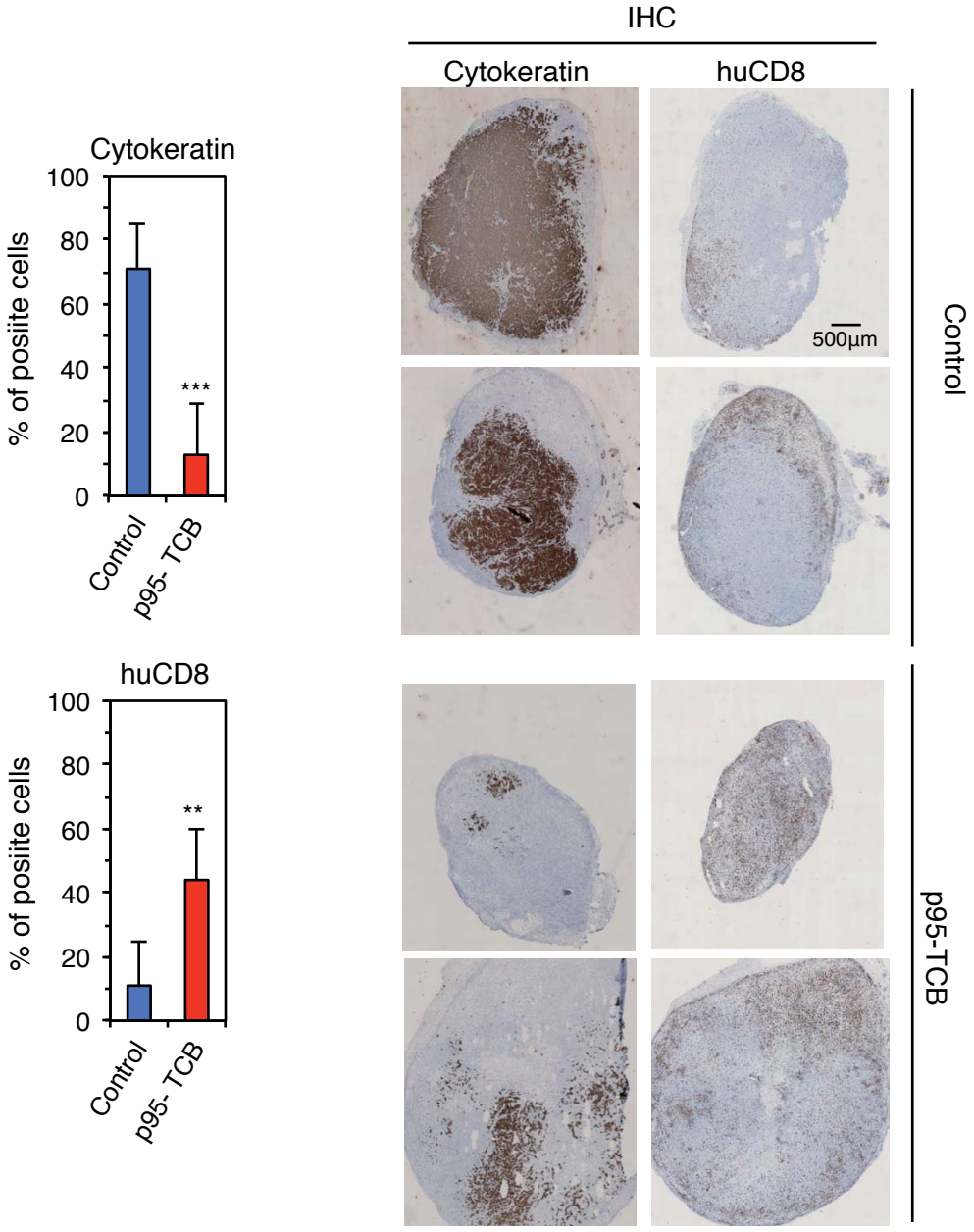

Figure 41: Effect of p95-TCB in T cell infiltration by immunohistochemistry. At the end of the experiment shown in Fig. 39, sagittal cuts of tumors embedded in paraffin were stained with anti-human cytokeratin and huCD8 antibodies and the % of positive cells were quantified. The results are expressed as averages; error bars correspond to 95% confidence intervals. *p* values were calculated using the two-sided Student's t test. **p*<0.05, ***p*<0.01, ****p*<0.001. A representative staining from each group is shown.

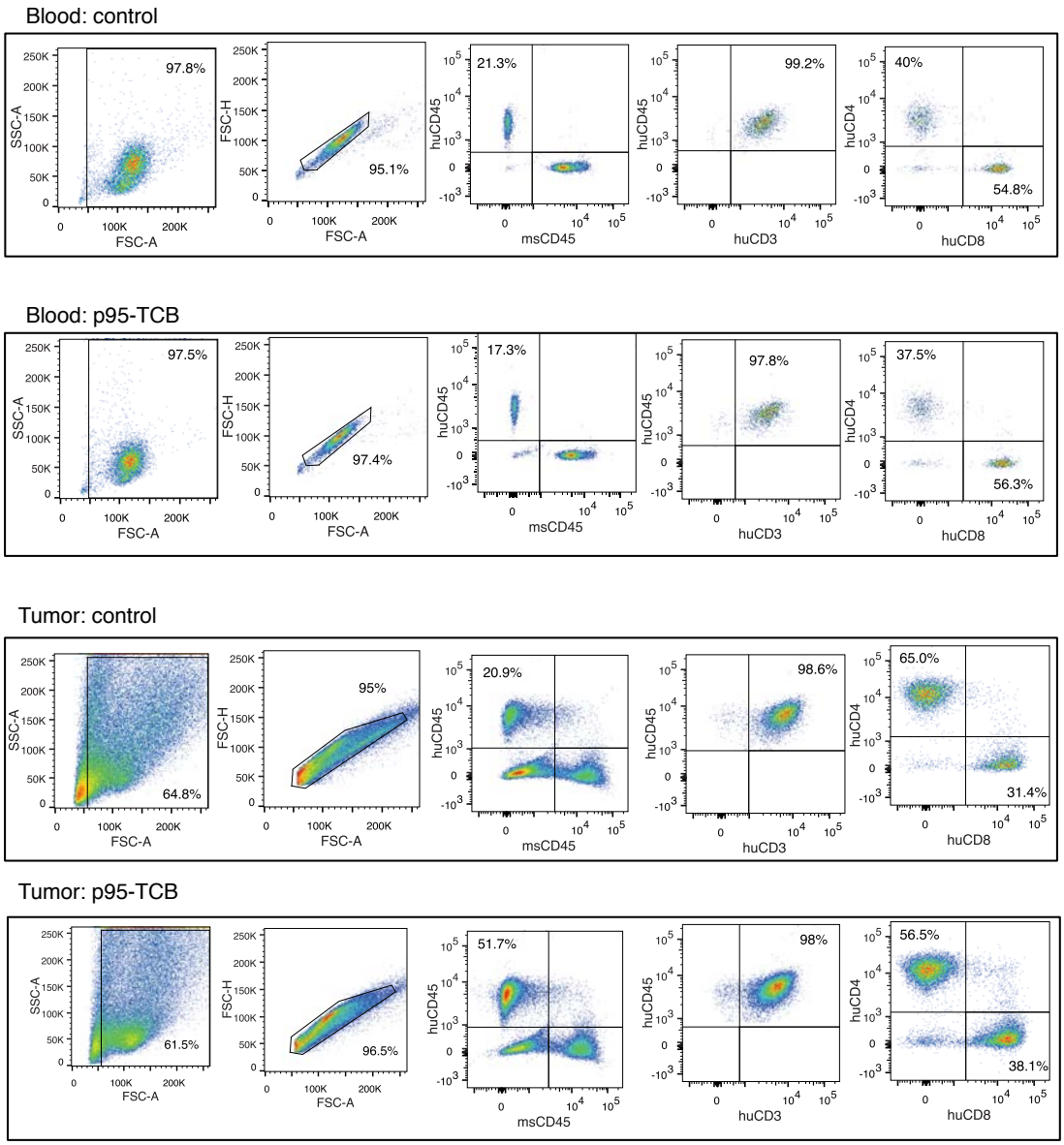

Figure 42. Representative flow cytometry analysis of blood and tumor samples from control and p95-TCB treated groups *in vivo* assays.

All together, these results indicate that p95-TCB induces T cell infiltration and ultimately reduction in tumor growth in p95HER2 positive tumors.

Discussion

The prognosis of patients with HER2+ tumors, which accounts for 20% of breast cancers, has improved over the last 20 years primarily due to the development of efficient monoclonal antibodies such as trastuzumab, pertuzumab and TDM-1 [61]. The anti-tumor efficacy of these therapies demonstrates both the drastic success of antibody-based therapies and the importance of of identifying tumor antigens such as HER2. However, anti-tumor responses are variable across the HER2 population, where unfortunately some HER2-positive tumors are intrinsically resistant to the anti-HER2 therapies whereas others become resistant after an initial response. It now clear that after 20 years of using anti-HER2 therapies in oncology, more than half of HER2+ breast cancers do not exhibit substantial clinical benefit to the currently available therapies and new therapeutic strategies are necessary to improve patient benefit.

Many research efforts have successfully elucidated mechanisms of resistance to anti-HER2 therapies in tissue culture based conditions, which are typically acquired during prolonged drug exposures. While some of these mechanisms also appear to occur in the clinical setting, it is unclear whether additional resistance mechanisms are intrinsic to the type of HER2 amplification that occurs in patient tumors or whether the complex tumor micro-environment immune cells are fully active in breast tumors or not. Therefore, continued investigation into clinically relevant resistance mechanisms to the anti-HER2 therapy and the identification of biomarkers aid in patient selection is a priority in breast oncology. In addition, alternative therapeutic options for non-responding patients are imperative to eradicating this disease.

In this thesis, we address the above-mentioned points. In Section 1, we present our studies evaluating a novel resistance mechanism for anti-HER2 therapy mediated by the loss of the Double Minute HER2 amplicon. We also examine whether the amplification pattern of each tumor predicts anti-HER2 therapy response. In Section 2, we demonstrate that p95HER2, a truncated form of HER2 expressed in 30% of HER2+ breast tumors, is a novel target for immune therapy using a bispecific antibody against p95-HER2 that recruits T cells (p95-TCB). Importantly, we prove that since p95HER2 is a tumor-specific target, p95-TCB is

able to spare normal tissues from tumoral one.

Various types of genomic alteration have been detected in tumors, of which gene amplification has a commonly been identified as a mechanism supporting to oncogene dependence. Amplifications are observed in two distinctive patters depending on whether the amplification happens within the chromosome (Homogenous Stained Regions) or extra chromosomally (Double Minutes). We present here the first study on the patterns of amplification of HER2 in breast cancers. Although in most breast tumors the majority of the cells exhibit one of the amplification types DM or HSR preferentially, the existence of tumors with a mixed pattern of amplification indicates that different mechanisms of HER2 gene amplification co-exist within some tumors.

Evidence indicating that the amplification of genes in DM may result in a dynamic regulation of gene expression through the reversible gain or lose of gene copies has slowly but steadily accumulated [70] [69] [68]. Since resistance to anti-HER2 therapies may be caused by downmodulation of HER2 expression [103], see also Figs 19 and 21), and intratumoral heterogeneity of HER2 gene amplification is associated with shorter disease free survival [104], it was reasonable to hypothesize that amplification of HER2 in DM would endow breast cancers with the ability to modulate HER2 protein expression and, thus, sensitivity to anti-HER2 therapies by dynamically regulating HER2 copy number. We tested this hypothesis in different settings. We performed analysis in clinical samples from patients treaded in neo-adjuvance and adjuvance with anti-HER2 therapy and we generated *in vivo* trastuzumab and TDM-1 resistant PDXs and *in vitro* resistant models to TDM-1 and Lapatinib. All of the results obtained by this study disproved our original hypothesis. Of clinical importance, our study demonstrated for the first time that breast cancer tumors with HER2 amplification in DM respond in a similar fashion to neoadjuvant or adjuvant trastuzumab (Fig 13 and 15). This observation was further corroborated in later studies [105]. Also, in children with neuroblastomas, the pattern of amplification of MYCN did not affect the overall survival [106]. In contrast, a different study later argued that breast cancer patients with cluster amplifications of HER2 that were treated with trastuzumab-based

therapies had shorter survival than those with non-cluster amplification [107]. Since cluster amplification likely corresponds to amplification in HSR, this result does not support that tumors with DM amplification are more likely to develop resistance against trastuzumab. Nonetheless, in the mentioned work, it was not detailed which criteria they used to differentiate between cluster amplification or non-cluster amplification. We cannot assume that with our criteria we would arrive to this same conclusion.

We also showed that resistance against different anti-HER2 therapies (trastuzumab, T-DM1 and lapatinib) could be acquired without modifying DM content, even if it is concomitant with the loss of HER2 protein expression. Nuciforo and colleagues report that quantitative HER2 protein analysis may identify a subset of HER2 tumors amplified in DM with low HER2 expression that are less sensitive to anti-HER2 treatment [105]. This observation was not statistically significant but went in line with our pre-clinical observation in which tumors with DM down modulated HER2 protein levels (Fig. 19 and 21). It would be interesting to evaluate in a larger study with pre- a post- treatment samples whether DM tumors have higher chances of loosing HER2 expression.

Our results suggest that in addition to HER2 the amplicon carried by breast cancer cells includes other critical loci. Meaning that cancer cells cannot “afford” to loose the amplicon. The strongest indication of this point is the maintenance of the amplified DNA even in resistant cells that have lost HER2 protein expression. These results point to the presence of additional sequences in the amplicon of HER2 that contribute to the growth of breast cancer cells. In agreement with this conclusion, it has been shown that the co-silencing of HER2 with other genes included in the HER2 amplicon such as STARD3, GRB7, PSMD3 and PERLD1, leads to an additive impairment of cell viability [108].

The mechanisms why our HER2 patient-derived xenograft and their derived cells in culture stop responding to the anti-HER2 therapy is still under investigation. Even though resistant PDX tumors down-modulated HER2 protein, they still expressed considerable levels of HER2. Whether these levels are enough for

trastuzumab and T-MD1 to be effective is not known. On the other hand, we observed that in the PDX derived cell line the loss of HER2 protein is even more profound and may indicate that cells in culture can support the loss of HER2. Understanding the mechanisms leading to sustain HER2 downmodulation and allowing cells to “hide” from the anti-HER2 therapy is pertinent to restoring therapeutic sensitivity. Due to the clinical importance of this finding, further expanding this observation to additional models is currently underway and will allow us to determine the exact mechanism regulating HER2 levels and the mechanisms that provide cells the advantage of surviving in the absence of their driver oncogene.

Since the PDX models were grown in NOD/SCID animals that only have monocytes and macrophages with impaired function, we assume that the initial effect of trastuzumab observed in these tumors is due to blockade of HER2 signaling and not ADCC recruitment. This is confirmed by the anti-proliferative effect of T-DM1 and Lapatinib on the cells *in vitro*, where no immune component is present. However, we cannot discard that in an immunocomptenet mouse this effect is reverted, meaning that the combinatorial effect of both the inhibition of signaling plus the immune system can work together in eliminating the tumor cells despite the downmodulation of the target. Therefore, we propose that testing the effect of trastuzumab and TDM-1 on these tumors in humanized mouse models will help explain this point.

Once we had confirmed that the amplification pattern did not play a role in anti-HER2 therapy resistance, we aimed to further characterize these models to see if we could depict the cause of resistance. The most distinctive alteration we detected in one of the resistant models compared with the parental tumor was the amplification of CCND1. Unfortunately, western blot and quantitative PCR showed that the amplification was not concomitant with an increase in protein. It would be interesting to evaluate whether other genes in the CCND1 amplicon were involved in tumor resistance. Furthermore, since membrane HER2 levels were reduced, it would be interesting to evaluate whether the trafficking of HER2 to the membrane

was being altered.

In section two of this thesis we propose p95HER2, a truncated version of HER2, as target form immunotherapy for p95HER2/HER2+ tumors, which account for 30% of HER2+ tumors. There is accumulating evidence suggesting that therapies that boost the immune system and release immune suppression present in the tumor microenvironment are successful strategies to treat different types of cancer. [22] [12]. The clearest examples of this is demonstrated in studies using monoclonal antibodies targeting PD-1/PDL-1 and CTLA-1 for the treatment of melanoma and NSCLC. Breast cancer itself is not proposed malignancy for this type of therapies since compared with other tumors it has a low mutational load which is a characteristic correlated with response to these immunotherapies [9] [109] [110]. Despite breast cancers not having a high mutational load, there is now accumulating evidence suggesting the important role of the immune system in the evolution and progression of breast cancer. We here propose the use of a bispecific antibody, directed against p95HER2 and CD3ε, an invariant member of the T cell receptor, for the treatment of p95HER2/HER2+ tumors. The choice of T cells, as target for our antibody is due to the crucial role T cells, in particular CD8+ cell, play in anti-tumor immunity. Immunosuppression of CD8+ cells has been suggested to be the major limiting factor repressing clearance of aberrant tissues. Therefore, we chose to try to activate these cells directly at target cancer cells. This is an advantage against monoclonal antibodies that are not able to activate directly T cells. We demonstrate here that simultaneous binding of p95-TCB to T cells and to p95HER2+ cells promotes the activation of T cells, the secretion of activating cytokines and the killing of the tumor cell, both *in vitro* and *in vivo*.

We believe that the design chosen for the p95-TCB has a number of positive points compared with other bispecific antibody formats. It has an IgG like format that confers a good half life (4 days) (Fig. 35) compared with other bispecific molecules such as the BiTes that have to be continuously administered by drug pumps due to the short half life (2,5 hours). Despite having an IgG like format, the Fc domain of the p95TCB is mutated; therefore it cannot interact with the Fc receptor in innate immune cells, which would give rise to toxicities. Furthermore,

the polymorphism of Fc receptor, something reported to have an impact on trastuzumab-based treatments, would not be a concern for this type of therapy [45].

Tumors have strategies to avoid the recognition by the immune system. In particular HER2+ tumors have been reported to “hide” from the immune system by downregulating MHC class I expression [65]. Since T cell bispecific antibodies act independently of MHC presentation, this mechanism of avoidance observed in HER2+ tumors would not interfere in the effect of p95-TCB. In addition, we have shown that binding of p95-TCB to T-cells cells induces the secretion of IFN-gamma (Fig. 31). This cytokine has been shown to restore MHC class I surface expression [111], therefore p95-TCB treatment can also overcome this immunosuppressive mechanism.

TCBs are efficient in engaging T cells even when the tumor antigen they bind is expressed at low levels [75]. This is in contrast to highly expressed antigens, which can lead to excess T-cell activation and increased toxicity. The expression of p95HER2 is restricted to tumor cells because it occurs as a truncation or alternative start mediated expression during HER2 overexpression. Indeed, p95HER2 expression is correlated with high levels of HER2 [41]. Therefore p95HER2 represents a better antigen for the development of TCBs, particularly compared to proteins that are normally expressed and found in healthy tissues. In this work we have shown that p95-TCB related toxicities are lower compared to the same type of molecule targeting HER2. We report that HER2-TCB but not p95-TCB kills cells expressing endogenous low levels of HER2 in normal epithelial breast cell line such as MCF10A (Fig. 33). In line with this, mutation of the alternate methionine start site in full-length HER2 from which p95HER2 is generated; we have demonstrated that p95-TCB exclusively binds this p95HER2 and not the full-length HER2. Importantly, we also report that p95-TCB does not kill human cardiomyocytes, which express considerable levels of endogenous HER2 [112]. The clinical limitations HER2 expression in cardiomyocytes underlies heart failure that occurs in approximately 4% of trastuzumab treated patients and is further limiting due to cardiac dysfunctions that range from 3 to 18% [82]. The

targeting of an antigen such as p95HER2, which is restricted to the tumoral tissue, would prevent anti-HER2 therapy induced cardiac conditions. Also, p95-TCB would be an alternative therapy for p95HER2/HER2+ breast cancer patients that have a cardiac pre-condition and cannot be treated with other anti-HER2 therapies.

To date, the p95HER2 antibody has been successfully used for the classification of p95HER2-positive tumors. It would therefore be useful to further determine which levels of p95HER2 are correlated with antibody efficacy.

T cell infiltration is variable within HER2+ tumors. It would be important to determine if p95-TCB effect in tumor growth differs depending on the basal level of TILs a tumor contains. Also, whether p95HER2 tumors are more or less infiltrated at baseline, compared to HER2 only expressing ones has not been studied in our investigations. Given that p95HER2 is only present in tumor cells, it may be possible that the immune system could have lowered immune-tolerance to the truncated form compared to HER2, leading to an increase immune recognition and higher infiltration. Retrospective analysis of samples from clinical studies could shed a light on this point.

The use of humanized mouse models has allowed us to test p95-TCB in a cell line xenografts and in a Patient Derived Xenografts. We have shown here that the PBMC transfer model is a suitable model to test the efficacy of p95-TCB. The short therapeutic window is a disadvantage of this mouse model. T cells expand exponentially in these models; therefore the effect of the p95-TCB is observed within the last days of the experiment before the GvHD takes place. This could represent a limitation in rapid growing tumors, where at these later stages the size of the tumor is too big and the effect and the possible effect of the TCB can be underestimated. Therefore, the use of CD34+ model, where you have a high number of T cells in circulation from the beginning of the experiment, would be the optimal for this type of fast-growing models. Studies in this model will also likely give a larger therapeutic window and allow for the examination of whether tumor resistance takes place after TCB induced tumor regression.

It is compelling to evaluate therapy combinations of p95-TCB with other immune enhancing agents. Due to the increase of T cell infiltration observed *in vivo* upon p95-TCB treatment, it is highly possible that there is also a concomitant activation of the immune checkpoints such as PD-1/PD-L1 axis that rise to restrict the activity of T cells. This has already been observed with other TCB [79, 81]. Therefore, we are currently testing the effect of and anti PD-L1 antibody in combination with p95-TCB in a fully humanized mouse model.

As a proof of principle, we have demonstrated that p95-TCB can eradicate p95HER2/HER2+ breast cancers. The PDX used in our proof-of-principal studies represents trastuzumab sensitive tumors (Fig. 16, Section 1). Therefore, it would be useful to next evaluate the effect of p95-TCB in trastuzumab-resistant tumors since patients that resist therapy lack many treatment options. Interestingly, the patient from which PDX173 was established recently relapsed to trastuzumab-based therapy and we were able to establish a PDX from a hepatic metastasis. It will be useful to test p95-TCB with this PDX to learn whether relapsing tumors can be sensitive to further therapeutic inhibition with p95-TCB. In our study on anti-HER2 resistance in patients we determined that p95HER2 does not appear during the down-modulation of HER2. We could think that restoring HER2 expression in these tumors, which maintain the HER2 amplification, may be accompanied with p95HER2 expression. Therefore, we speculate that continued investigation into the mechanism regulating HER2 expression during anti-HER2 therapies may lead to new therapeutic options using p95-TCB.

It would be also interesting to evaluate the combination of p95-TCB and trastuzumab. Since it has been reported that trastuzumab effect also depends on the adaptive immune cells, in particular CD8 T cells [46], the increased infiltration induced by p95-TCB in the tumor may also augment the effect of trastuzumab. The most suitable mouse model to test this combination would be one carrying both the innate and the adaptive immune system. Transgenic animals carrying cytokines that favor the engraftment of innate cells such as NK cells and macrophages would be optimal.

In summary, in this dissertation we have proven that the amplification pattern of HER2 does not predict the response to anti-HER2 therapy and that resistance to trastuzumab, T-DM1 and lapatinib occur without the loss of HER2 amplicon. Furthermore we have present p95-TCB as a new and safe therapeutic option for a subpopulation of HER2+ patients that boost the immune system to aid in the killing of tumor cells.

Conclusions

Section 1:

1- HER2 amplification pattern, DM, HSR or mixed, can be detected in breast tumor samples

2- Response of breast tumors with HER2 amplified in DM to anti-HER2 therapies is similar to that of tumors with HSR

3- Anti-HER2 therapy resistant occurs with loss HER2 protein levels but not of HER2 amplification

Section 2:

1- p95-TCB binds specifically p95HER2 expressing cells

2- p95-TCB binds and activates T cells only with simultaneous binding to p95HER2

3- p95-TCB promotes the lysis of p95HER2 expressing cells

4- p95-TCB effect is restricted to tumor cells

5- p95-TCB induces the regression of p95HER2+ breast tumors

References

1. Senkus E, Kyriakides S, Ohno S et al. Primary breast cancer: ESMO Clinical Practice Guidelines for diagnosis, treatment and follow-up. Ann Oncol 2015; 26 Suppl 5: v8-30.
2. Sonnenblick A, Fumagalli D, Sotiriou C, Piccart M. Is the differentiation into molecular subtypes of breast cancer important for staging, local and systemic therapy, and follow up? Cancer Treat Rev 2014; 40: 1089-1095.
3. Perou CM, Sorlie T, Eisen MB et al. Molecular portraits of human breast tumours. Nature 2000; 406: 747-752.
4. Cancer Genome Atlas N. Comprehensive molecular portraits of human breast tumours. Nature 2012; 490: 61-70.
5. Yerushalmi R, Woods R, Ravdin PM et al. Ki67 in breast cancer: prognostic and predictive potential. Lancet Oncol 2010; 11: 174-183.
6. Sorlie T, Perou CM, Tibshirani R et al. Gene expression patterns of breast carcinomas distinguish tumor subclasses with clinical implications. Proc Natl Acad Sci U S A 2001; 98: 10869-10874.
7. Weigelt B, Mackay A, A'Hern R et al. Breast cancer molecular profiling with single sample predictors: a retrospective analysis. Lancet Oncol 2010; 11: 339-349.
8. Budczies J, Bockmayr M, Denkert C et al. Classical pathology and mutational load of breast cancer - integration of two worlds. J Pathol Clin Res 2015; 1: 225-238.
9. Alexandrov LB, Nik-Zainal S, Wedge DC et al. Signatures of mutational processes in human cancer. Nature 2013; 500: 415-421.
10. de Azambuja E, Holmes AP, Piccart-Gebhart M et al. Lapatinib with trastuzumab for HER2-positive early breast cancer (NeoALTTO): survival outcomes of a randomised, open-label, multicentre, phase 3 trial and their association with pathological complete response. Lancet Oncol 2014; 15: 1137-1146.
11. Slamon DJ, Clark GM, Wong SG et al. Human breast cancer: correlation of relapse and survival with amplification of the HER-2/neu oncogene. Science 1987; 235: 177-182.
12. Kroemer G, Senovilla L, Galluzzi L et al. Natural and therapy-induced immunosurveillance in breast cancer. Nat Med 2015; 21: 1128-1138.
13. Staaf J, Ringner M, Vallon-Christersson J et al. Identification of subtypes in human epidermal growth factor receptor 2--positive breast cancer reveals a gene signature prognostic of outcome. J Clin Oncol 2010; 28: 1813-1820.
14. Salgado R, Denkert C, Demaria S et al. The evaluation of tumor-infiltrating lymphocytes (TILs) in breast cancer: recommendations by an International TILs Working Group 2014. Ann Oncol 2015; 26: 259-271.
15. Savas P, Salgado R, Denkert C et al. Clinical relevance of host immunity in breast cancer: from TILs to the clinic. Nat Rev Clin Oncol 2016; 13: 228-241.
16. Loi S, Michiels S, Salgado R et al. Tumor infiltrating lymphocytes are prognostic in triple negative breast cancer and predictive for trastuzumab benefit in early breast cancer: results from the FinHER trial. Ann Oncol 2014; 25: 1544-1550.
17. Denkert C, von Minckwitz G, Brase JC et al. Tumor-infiltrating lymphocytes

and response to neoadjuvant chemotherapy with or without carboplatin in human epidermal growth factor receptor 2-positive and triple-negative primary breast cancers. J Clin Oncol 2015; 33: 983-991.
18. Ingold Heppner B, Untch M, Denkert C et al. Tumor-infiltrating lymphocytes: a predictive and prognostic biomarker in neoadjuvant treated HER2-positive breast cancer. Clin Cancer Res 2016.
19. Chen DS, Mellman I. Oncology meets immunology: the cancer-immunity cycle. Immunity 2013; 39: 1-10.
20. Schumacher TN, Schreiber RD. Neoantigens in cancer immunotherapy. Science 2015; 348: 69-74.
21. Medler TR, Cotechini T, Coussens LM. Immune response to cancer therapy: mounting an effective antitumor response and mechanisms of resistance. Trends Cancer 2015; 1: 66-75.
22. Pardoll DM. The blockade of immune checkpoints in cancer immunotherapy. Nat Rev Cancer 2012; 12: 252-264.
23. Motz GT, Coukos G. Deciphering and reversing tumor immune suppression. Immunity 2013; 39: 61-73.
24. Joyce JA, Fearon DT. T cell exclusion, immune privilege, and the tumor microenvironment. Science 2015; 348: 74-80.
25. Walker LS, Sansom DM. The emerging role of CTLA4 as a cell-extrinsic regulator of T cell responses. Nat Rev Immunol 2011; 11: 852-863.
26. Yarden Y, Sliwkowski MX. Untangling the ErbB signalling network. Nat Rev Mol Cell Biol 2001; 2: 127-137.
27. Zhang X, Gureasko J, Shen K et al. An allosteric mechanism for activation of the kinase domain of epidermal growth factor receptor. Cell 2006; 125: 1137-1149.
28. Yarden Y, Pines G. The ERBB network: at last, cancer therapy meets systems biology. Nat Rev Cancer 2012; 12: 553-563.
29. Baselga J, Swain SM. Novel anticancer targets: revisiting ERBB2 and discovering ERBB3. Nat Rev Cancer 2009; 9: 463-475.
30. Jaiswal BS, Kljavin NM, Stawiski EW et al. Oncogenic ERBB3 mutations in human cancers. Cancer Cell 2013; 23: 603-617.
31. Albertson DG. Gene amplification in cancer. Trends Genet 2006; 22: 447-455.
32. Storlazzi CT, Lonoce A, Guastadisegni MC et al. Gene amplification as double minutes or homogeneously staining regions in solid tumors: origin and structure. Genome Res 2010; 20: 1198-1206.
33. Lundberg G, Rosengren AH, Hakanson U et al. Binomial mitotic segregation of MYCN-carrying double minutes in neuroblastoma illustrates the role of randomness in oncogene amplification. PLoS One 2008; 3: e3099.
34. Anido J, Scaltriti M, Bech Serra JJ et al. Biosynthesis of tumorigenic HER2 C-terminal fragments by alternative initiation of translation. EMBO J 2006; 25: 3234-3244.
35. Arribas J, Baselga J, Pedersen K, Parra-Palau JL. p95HER2 and breast cancer. Cancer Res 2011; 71: 1515-1519.
36. Pedersen K, Angelini PD, Laos S et al. A naturally occurring HER2 carboxy-terminal fragment promotes mammary tumor growth and metastasis. Mol Cell Biol

2009; 29: 3319-3331.
37. Angelini PD, Zacarias Fluck MF, Pedersen K et al. Constitutive HER2 signaling promotes breast cancer metastasis through cellular senescence. Cancer Res 2013; 73: 450-458.
38. Morancho B, Martinez-Barriocanal A, Villanueva J, Arribas J. Role of ADAM17 in the non-cell autonomous effects of oncogene-induced senescence. Breast Cancer Res 2015; 17: 106.
39. Parra-Palau JL, Pedersen K, Peg V et al. A major role of p95/611-CTF, a carboxy-terminal fragment of HER2, in the down-modulation of the estrogen receptor in HER2-positive breast cancers. Cancer Res 2010; 70: 8537-8546.
40. Sperinde J, Jin X, Banerjee J et al. Quantitation of p95HER2 in paraffin sections by using a p95-specific antibody and correlation with outcome in a cohort of trastuzumab-treated breast cancer patients. Clin Cancer Res 2010; 16: 4226-4235.
41. Parra-Palau JL, Morancho B, Peg V et al. Effect of p95HER2/611CTF on the response to trastuzumab and chemotherapy. J Natl Cancer Inst 2014; 106.
42. Saez R, Molina MA, Ramsey EE et al. p95HER-2 predicts worse outcome in patients with HER-2-positive breast cancer. Clin Cancer Res 2006; 12: 424-431.
43. Molina MA, Saez R, Ramsey EE et al. NH(2)-terminal truncated HER-2 protein but not full-length receptor is associated with nodal metastasis in human breast cancer. Clin Cancer Res 2002; 8: 347-353.
44. Clynes RA, Towers TL, Presta LG, Ravetch JV. Inhibitory Fc receptors modulate in vivo cytotoxicity against tumor targets. Nat Med 2000; 6: 443-446.
45. Musolino A, Naldi N, Bortesi B et al. Immunoglobulin G fragment C receptor polymorphisms and clinical efficacy of trastuzumab-based therapy in patients with HER-2/neu-positive metastatic breast cancer. J Clin Oncol 2008; 26: 1789-1796.
46. Park S, Jiang Z, Mortenson ED et al. The therapeutic effect of anti-HER2/neu antibody depends on both innate and adaptive immunity. Cancer Cell 2010; 18: 160-170.
47. Perez EA, Thompson EA, Ballman KV et al. Genomic analysis reveals that immune function genes are strongly linked to clinical outcome in the North Central Cancer Treatment Group n9831 Adjuvant Trastuzumab Trial. J Clin Oncol 2015; 33: 701-708.
48. Coussens PM, Coussens MJ, Tooker BC, Nobis W. Structure of the bovine natural resistance associated macrophage protein (NRAMP 1) gene and identification of a novel polymorphism. DNA Seq 2004; 15: 15-25.
49. Baselga J. Treatment of HER2-overexpressing breast cancer. Ann Oncol 2010; 21 Suppl 7: vii36-40.
50. Lewis Phillips GD, Li G, Dugger DL et al. Targeting HER2-positive breast cancer with trastuzumab-DM1, an antibody-cytotoxic drug conjugate. Cancer Res 2008; 68: 9280-9290.
51. Junttila TT, Li G, Parsons K et al. Trastuzumab-DM1 (T-DM1) retains all the mechanisms of action of trastuzumab and efficiently inhibits growth of lapatinib insensitive breast cancer. Breast Cancer Res Treat 2011; 128: 347-356.
52. Agus DB, Akita RW, Fox WD et al. Targeting ligand-activated ErbB2 signaling inhibits breast and prostate tumor growth. Cancer Cell 2002; 2: 127-137.
53. Baselga J, Cortes J, Kim SB et al. Pertuzumab plus trastuzumab plus

docetaxel for metastatic breast cancer. N Engl J Med 2012; 366: 109-119.
54. Spector NL, Xia W, Burris H, 3rd et al. Study of the biologic effects of lapatinib, a reversible inhibitor of ErbB1 and ErbB2 tyrosine kinases, on tumor growth and survival pathways in patients with advanced malignancies. J Clin Oncol 2005; 23: 2502-2512.
55. Scaltriti M, Verma C, Guzman M et al. Lapatinib, a HER2 tyrosine kinase inhibitor, induces stabilization and accumulation of HER2 and potentiates trastuzumab-dependent cell cytotoxicity. Oncogene 2009; 28: 803-814.
56. Gradishar WJ. HER2 therapy--an abundance of riches. N Engl J Med 2012; 366: 176-178.
57. Eichhorn PJ, Gili M, Scaltriti M et al. Phosphatidylinositol 3-kinase hyperactivation results in lapatinib resistance that is reversed by the mTOR/phosphatidylinositol 3-kinase inhibitor NVP-BEZ235. Cancer Res 2008; 68: 9221-9230.
58. Majewski IJ, Nuciforo P, Mittempergher L et al. PIK3CA mutations are associated with decreased benefit to neoadjuvant human epidermal growth factor receptor 2-targeted therapies in breast cancer. J Clin Oncol 2015; 33: 1334-1339.
59. Ritter CA, Perez-Torres M, Rinehart C et al. Human breast cancer cells selected for resistance to trastuzumab in vivo overexpress epidermal growth factor receptor and ErbB ligands and remain dependent on the ErbB receptor network. Clin Cancer Res 2007; 13: 4909-4919.
60. Garrett JT, Olivares MG, Rinehart C et al. Transcriptional and posttranslational up-regulation of HER3 (ErbB3) compensates for inhibition of the HER2 tyrosine kinase. Proc Natl Acad Sci U S A 2011; 108: 5021-5026.
61. Arteaga CL, Engelman JA. ERBB receptors: from oncogene discovery to basic science to mechanism-based cancer therapeutics. Cancer Cell 2014; 25: 282-303.
62. Minuti G, Cappuzzo F, Duchnowska R et al. Increased MET and HGF gene copy numbers are associated with trastuzumab failure in HER2-positive metastatic breast cancer. Br J Cancer 2012; 107: 793-799.
63. Huang X, Gao L, Wang S et al. Heterotrimerization of the growth factor receptors erbB2, erbB3, and insulin-like growth factor-i receptor in breast cancer cells resistant to herceptin. Cancer Res 2010; 70: 1204-1214.
64. Scaltriti M, Eichhorn PJ, Cortes J et al. Cyclin E amplification/overexpression is a mechanism of trastuzumab resistance in HER2+ breast cancer patients. Proc Natl Acad Sci U S A 2011; 108: 3761-3766.
65. Inoue M, Mimura K, Izawa S et al. Expression of MHC Class I on breast cancer cells correlates inversely with HER2 expression. Oncoimmunology 2012; 1: 1104-1110.
66. Seliger B, Kiessling R. The two sides of HER2/neu: immune escape versus surveillance. Trends Mol Med 2013; 19: 677-684.
67. Bonavia R, Inda MM, Cavenee WK, Furnari FB. Heterogeneity maintenance in glioblastoma: a social network. Cancer Res 2011; 71: 4055-4060.
68. Nathanson DA, Gini B, Mottahedeh J et al. Targeted therapy resistance mediated by dynamic regulation of extrachromosomal mutant EGFR DNA. Science 2014; 343: 72-76.
69. Von Hoff DD, McGill JR, Forseth BJ et al. Elimination of

extrachromosomally amplified MYC genes from human tumor cells reduces their tumorigenicity. Proc Natl Acad Sci U S A 1992; 89: 8165-8169.
70. Kaufman RJ, Brown PC, Schimke RT. Loss and stabilization of amplified dihydrofolate reductase genes in mouse sarcoma S-180 cell lines. Mol Cell Biol 1981; 1: 1084-1093.
71. Mittendorf EA, Wu Y, Scaltriti M et al. Loss of HER2 amplification following trastuzumab-based neoadjuvant systemic therapy and survival outcomes. Clin Cancer Res 2009; 15: 7381-7388.
72. Scaltriti M, Rojo F, Ocana A et al. Expression of p95HER2, a truncated form of the HER2 receptor, and response to anti-HER2 therapies in breast cancer. J Natl Cancer Inst 2007; 99: 628-638.
73. Kontermann RE, Brinkmann U. Bispecific antibodies. Drug Discov Today 2015; 20: 838-847.
74. Garber K. Bispecific antibodies rise again. Nat Rev Drug Discov 2014; 13: 799-801.
75. Zhukovsky EA, Morse RJ, Maus MV. Bispecific antibodies and CARs: generalized immunotherapeutics harnessing T cell redirection. Curr Opin Immunol 2016; 40: 24-35.
76. Weidle UH, Kontermann RE, Brinkmann U. Tumor-antigen-binding bispecific antibodies for cancer treatment. Semin Oncol 2014; 41: 653-660.
77. Nagorsen D, Baeuerle PA. Immunomodulatory therapy of cancer with T cell-engaging BiTE antibody blinatumomab. Exp Cell Res 2011; 317: 1255-1260.
78. Linke R, Klein A, Seimetz D. Catumaxomab: clinical development and future directions. MAbs 2010; 2: 129-136.
79. Bacac M, Fauti T, Sam J et al. A Novel Carcinoembryonic Antigen T-Cell Bispecific Antibody (CEA TCB) for the Treatment of Solid Tumors. Clin Cancer Res 2016; 22: 3286-3297.
80. Kiewe P, Thiel E. Ertumaxomab: a trifunctional antibody for breast cancer treatment. Expert Opin Investig Drugs 2008; 17: 1553-1558.
81. Junttila TT, Li J, Johnston J et al. Antitumor efficacy of a bispecific antibody that targets HER2 and activates T cells. Cancer Res 2014; 74: 5561-5571.
82. Zagar TM, Cardinale DM, Marks LB. Breast cancer therapy-associated cardiovascular disease. Nat Rev Clin Oncol 2016; 13: 172-184.
83. Stagg J, Loi S, Divisekera U et al. Anti-ErbB-2 mAb therapy requires type I and II interferons and synergizes with anti-PD-1 or anti-CD137 mAb therapy. Proc Natl Acad Sci U S A 2011; 108: 7142-7147.
84. Schreiner J, Thommen DS, Herzig P et al. Expression of inhibitory receptors on intratumoral T cells modulates the activity of a T cell-bispecific antibody targeting folate receptor. Oncoimmunology 2016; 5: e1062969.
85. Lacroix M, Leclercq G. Relevance of breast cancer cell lines as models for breast tumours: an update. Breast Cancer Res Treat 2004; 83: 249-289.
86. Barretina J, Caponigro G, Stransky N et al. The Cancer Cell Line Encyclopedia enables predictive modelling of anticancer drug sensitivity. Nature 2012; 483: 603-607.
87. Vargo-Gogola T, Rosen JM. Modelling breast cancer: one size does not fit all. Nat Rev Cancer 2007; 7: 659-672.
88. DeRose YS, Wang G, Lin YC et al. Tumor grafts derived from women with

breast cancer authentically reflect tumor pathology, growth, metastasis and disease outcomes. Nat Med 2011; 17: 1514-1520.
89. Hidalgo M, Amant F, Biankin AV et al. Patient-derived xenograft models: an emerging platform for translational cancer research. Cancer Discov 2014; 4: 998-1013.
90. Brehm MA, Shultz LD, Greiner DL. Humanized mouse models to study human diseases. Curr Opin Endocrinol Diabetes Obes 2010; 17: 120-125.
91. Ito R, Takahashi T, Katano I, Ito M. Current advances in humanized mouse models. Cell Mol Immunol 2012; 9: 208-214.
92. Shultz LD, Brehm MA, Garcia-Martinez JV, Greiner DL. Humanized mice for immune system investigation: progress, promise and challenges. Nat Rev Immunol 2012; 12: 786-798.
93. Pearson T, Greiner DL, Shultz LD. Humanized SCID mouse models for biomedical research. Curr Top Microbiol Immunol 2008; 324: 25-51.
94. Weigelt P, Kissling WD, Kisel Y et al. Global patterns and drivers of phylogenetic structure in island floras. Sci Rep 2015; 5: 12213.
95. Swain SM, Clark E, Baselga J. Treatment of HER2-positive metastatic breast cancer. N Engl J Med 2015; 372: 1964-1965.
96. Wolff AC, Hammond ME, Hicks DG et al. Recommendations for human epidermal growth factor receptor 2 testing in breast cancer: American Society of Clinical Oncology/College of American Pathologists clinical practice guideline update. J Clin Oncol 2013; 31: 3997-4013.
97. Marcelin LH, Vivian J, DiClemente R et al. Trends in alcohol, drug and cigarette use among Haitian youth in Miami-Dade county, Florida. J Ethn Subst Abuse 2005; 4: 105-131.
98. Serra V, Vivancos A, Puente XS et al. Clinical response to a lapatinib-based therapy for a Li-Fraumeni syndrome patient with a novel HER2V659E mutation. Cancer Discov 2013; 3: 1238-1244.
99. Soule HD, Maloney TM, Wolman SR et al. Isolation and characterization of a spontaneously immortalized human breast epithelial cell line, MCF-10. Cancer Res 1990; 50: 6075-6086.
100. Herting F, Herter S, Friess T et al. Antitumour activity of the glycoengineered type II anti-CD20 antibody obinutuzumab (GA101) in combination with the MDM2 selective antagonist idasanutlin (RG7388). Eur J Haematol 2016.
101. Nelson BH. IL-2, regulatory T cells, and tolerance. J Immunol 2004; 172: 3983-3988.
102. Junttila TT, Akita RW, Parsons K et al. Ligand-independent HER2/HER3/PI3K complex is disrupted by trastuzumab and is effectively inhibited by the PI3K inhibitor GDC-0941. Cancer Cell 2009; 15: 429-440.
103. Niikura N, Liu J, Hayashi N et al. Loss of human epidermal growth factor receptor 2 (HER2) expression in metastatic sites of HER2-overexpressing primary breast tumors. J Clin Oncol 2012; 30: 593-599.
104. Seol H, Lee HJ, Choi Y et al. Intratumoral heterogeneity of HER2 gene amplification in breast cancer: its clinicopathological significance. Mod Pathol 2012; 25: 938-948.
105. Nuciforo P, Thyparambil S, Aura C et al. High HER2 protein levels correlate with increased survival in breast cancer patients treated with anti-HER2 therapy.

Mol Oncol 2016; 10: 138-147.
106. Moreau LA, McGrady P, London WB et al. Does MYCN amplification manifested as homogeneously staining regions at diagnosis predict a worse outcome in children with neuroblastoma? A Children's Oncology Group study. Clin Cancer Res 2006; 12: 5693-5697.
107. Xuan Q, Ji H, Tao X et al. Quantitative assessment of HER2 amplification in HER2-positive breast cancer: its association with clinical outcomes. Breast Cancer Res Treat 2015; 150: 581-588.
108. Sahlberg KK, Hongisto V, Edgren H et al. The HER2 amplicon includes several genes required for the growth and survival of HER2 positive breast cancer cells. Mol Oncol 2013; 7: 392-401.
109. McGranahan N, Furness AJ, Rosenthal R et al. Clonal neoantigens elicit T cell immunoreactivity and sensitivity to immune checkpoint blockade. Science 2016; 351: 1463-1469.
110. Van Allen EM, Miao D, Schilling B et al. Genomic correlates of response to CTLA-4 blockade in metastatic melanoma. Science 2015; 350: 207-211.
111. Epperson DE, Arnold D, Spies T et al. Cytokines increase transporter in antigen processing-1 expression more rapidly than HLA class I expression in endothelial cells. J Immunol 1992; 149: 3297-3301.
112. Eldridge S, Guo L, Mussio J et al. Examining the protective role of ErbB2 modulation in human-induced pluripotent stem cell-derived cardiomyocytes. Toxicol Sci 2014; 141: 547-559.

Appendix

Appendix Table 1: Baseline characteristics of the cohort treated with neoadjuvant trastuzumab

Parameter	DM		HSR		Mixed	
	No.	%	No.	%	No.	%
Age						
media	51.35		49.47		57.71	
range	36-81		22-79		39-93	
Histological subtype						
Ductal	19	95	30	93.8	6	85.7
Lobular	0	0	0	0	0	0
Other	1	5	2	6.3	0	0
Missing	0	0	0	0	1	14.3
Histological grade						
G1	0	0	1	3.1	0	0
G2	7	35	15	46.9	2	28.6
G3	12	60	14	43.8	4	57.1
Missing	1	5	2	6.3	1	14.3
HR status						
ER						
positive	17	85	20	62.5	3	42.9
negative	3	15	12	37.5	3	42.9
Missing	0	0	0	0	1	14.3
PR						
positive	12	60	17	53.1	1	14.3
negative	8	40	15	46.9	5	71.4
Missing	0	0	0	0	1	14.3
Ki67						
<20%	3	15	10	31.3	0	0
>20%	17	85	21	65.6	6	85.7
Missing	0	0	1	3.1	1	14.3

Appendix Table 2. Baseline characteristics of the cohort treated with adjuvant trastuzumab

Parameter	DM		HSR		Mixed	
	No.	%	No.	%	No.	%
Age						
media	56,4		54,2		46,7	
range	35-81		33-86		32-73	
Histological subtype						
Ductal	14	100	32	91.4	7	100
Lobular	0	0	2	5.7	0	0
Other	0	0	1	2.9	0	0
Missing	0	0	0	0	0	0
Histological grade						
G1	1	7.1	1	2.9	0	0
G2	4	28.6	12	34.3	1	14.3
G3	9	64.3	20	57.1	6	85.7
Missing	0	0	2	5.7	0	0
HR status						
ER						
positive	9	64.3	25	71.4	5	71.4
negative	5	35.7	10	28.6	2	28.6
Missing	0	0	0	0	0	0
PR						
positive	6	42.86	17	48.57	3	42.86
negative	8	57.14	18	51.43	4	57.14
Missing	0	0	0	0	0	0
Ki67						
<20%	4	28.6	11	31.4	0	0
>20%	10	71.4	23	65.7	7	100
Missing	0	0	1	2,9	0	0